ISSN 1608-5043 (Print)
ISSN 1608-5078 (Online)

SCIENTIFIC AND TECHNICAL JOURNAL

GEORESOURCES

www.georesjournal.ru

V. 22. No. 1. 2020

20 YEARS AMONG THE ACADEMY

SCIENTIFIC AND TECHNICAL JOURNAL
GEORESURSY
www.geors.ru
e-mail: mail@geors.ru
ISSN 1608-5043 (Print)
ISSN 1608-5078 (Online)
V. 22. Is. 1. 2020
Key title: «Georesursy». Parallel title: «Georesources»

Publisher: Georesursy LLC
Editorial and Publisher's address:
1-10, Mayakovsky st., Kazan, 420012, Russian Federation
Phone: +7 843 2390530, e-mail: mail@geors.ru

Georesursy (Georesources) is a peer-reviewed scientific and technical journal published since 1999.

The journal is included/indexed in:
- **Scopus;**
- **Web of Science (ESCI);**
- **Directory of Open Access Journals (DOAJ);**
- **CAS (Chemical Abstracts Service) databases;**
- **GeoRef database;**
- **EBSCOhost™ databases;**
- **Ulrich's Periodicals Directory.**

The full-text e-versions of the articles are available on: **www.geors.ru**

Registered by the Federal Service for Supervision of Communications and Mass Media No. PI FS77-38832

The Journal is issued 4 times a year. Circulation: 1000 copies
Issue date: March 30, 2020

Table of Contents

EDITORIAL

DOI: https://doi.org/10.18599/grs.2020.1.2-3

Journal Georesursy (Georesources) – XX years among the academy

V.G. Izotov[1], L.M. Sitdikova[1], D.A. Khristoforova[2]
[1]Kazan Federal University, Kazan, Russian Federation
[2]Georesursy LLC, Kazan, Russian Federation

Each fundamental and applied scientific direction can develop only in conditions of close scientific communication and publication of the results. Therefore, scientific journals in the scientific development are of great importance.

In this regard, a special role belongs to the scientific and technical journal Georesursy (Georesources). Georesursy is the leading peer-reviewed open access journal of the Republic of Tatarstan in the field of Earth sciences, indexed in Scopus and Web of Science (ESCI).

2019 marks 20 years since the publication of the first issue of the journal. By now, for more than 10 years, the journal has been living and developing without its founder and ideological inspirer, doctor of geological and mineralogical sciences Natalya N. Khristoforova. She worked for 36 years at the Department of Radio Electronics of Kazan State University (KSU), and was a leading researcher at the Laboratory of Physical Dynamics of Heterogeneous Media. Natalya was known as a talented and versatile scientist, a strict but friendly editor-in-chief, an indefatigable hard worker and an unsurpassed lecturer, a decent and very enthusiastic person.

N.N. Khristoforova was the permanent scientific leader of geothermal expeditions organized by the Department of Radio Electronics of KSU for more than 25 years. In these expeditions experimental studies were conducted to measure temperature and heat flow in the Earth's interior, and methods for their analysis and processing were developed. The studies were carried out using original equipment developed by a team of authors under the guidance of the famous physicist at KSU, professor, doctor of physical and mathematical sciences N.N. Neprimerov. The results of these studies were used to create the Geothermal Atlas of Europe (E Hurtig, V Čermák, R Haenel, V.I Zui (Eds.), Geothermal Atlas of Europe, Goth. Publ. House, Potsdam (1991)). Based on geothermal measurements N.N. Khristoforova studied the thermal regime of the crystalline basement, the geothermics of oil and gas accumulation areas, and subsequently developed a technique for the search and exploration of hydrocarbon deposits.

The results obtained required extensive discussion at conferences, seminars and in the open press, which contributed to the initiation of a scientific and technical journal.

As a result, in 1999 Natalya Khristoforova founded the scientific and technical journal Georesursy (Georesources) and independently brought it to such a level that other academic scientific journals could envy. Natalya with small editorial team of three carried out work for ten years that in other the editorial offices was done by dozens of people.

The creation of the journal was immediately supported by Nikolai N. Neprimerov and the leader in the field of petroleum geology, doctor of geological and mineralogical sciences, professor Renat Kh. Muslimov.

The journal is supported by the Ministry of Ecology and Natural Resources of the Republic of Tatarstan, cooperates with Tatneft PJSC, Lomonosov Moscow State University, Academy of Sciences of the Republic of Tatarstan and other research and production organizations, as well as with foreign geological schools, such as the Catholic University of Leuven (Belgium),

1999. N.N. Neprimerov, N.N. Khristoforova (bottom row). I.N. Kitiashvilli, A.V. Nikolaev, M.A. Khristoforova – Editorial office of the journal (top row).

Sedimentological School of France, the Geological Survey of India, etc.

Georesursy (Georesources) is a widely known journal at present time. Developing a wide range of basic geological studies, it reflects a complex of modern scientific and practical directions related to the development of the mineral resource base of Russia.

The journal provides distribution and growth of scientific knowledge in the field of research and conservation of the Earth's interior, exploration and development of natural resources, support for high standards of scientific publications, patent protection, and enables specialists from universities, research centers, and industry to bring their scientific ideas, developments, technologies to a wide range of readers, implement their ideas in life and production.

The aim of the Editorial Board is to develop scientific interaction with increasing availability exchange of the accumulated knowledge and professional experience, creating a scientific and information environment, prompt and reliable distribution of information about research conducted by specialists in Russia, near and far abroad, and their fruitful cooperation.

The journal pays great attention to publication of results not only in the field of petroleum geology, but also to the problems of mineralogy, petrography, fields of solid minerals, etc.

The authors and readers of the journal are scientists and industrial workers, graduate students and researchers from universities, research centers, industry and government agencies in Russia, near and far abroad.

The journal is published in Russian and English, which is important for the experience exchange in order to increase the efficiency of studying the Earth's interior. Full-text electronic versions of the translated articles are freely available to the public on Journal's website over the next few months since date of publication (delay is due to needed time for translation).

Thanks to support of the government and many people who are interested in publishing the journal, the journal has been a platform for free publications for more than 20 years, creating a comfortable environment for achieving results in scientific and technical activities, defending dissertations, receiving grants and government orders, successful reports on them and etc. Moreover, the journal ensures the proper selection of incoming materials and helps to improve the quality of published materials, bringing them to the level of convincing scientific work.

The editors of the journal set a goal to strengthen reviewing and checking of incoming manuscripts. Peer review plays a key role in a scientific publication environment. Otherwise, positive evaluations of unfair works give the right to the authors to go further, and, for example, to receive funding in competitive events, leaving promising projects without support.

The question arises: how did a small independent journal, without the steady continuous support of academic centers or industry, reach such a level among Russian scientific journals? The clue is in people who are not indifferent to such an important and responsible matter, who love their work and science.

Let us recall the words of Natalya Khristoforova in the first issue of the journal back in 1999, "*Georesources are something immeasurably greater than the totality of individual minerals. Georesources are all the diversity of the world around us, from the simplest minerals to complex biological systems. It is a worldview that comprises a complex gamut of aspects of a person's relationship with the outside world in the mechanical process of production and consumption. It includes people themselves, representing the main, most important resource of the planet - the resource of a single human civilization on planet Earth, and a resource of intelligence*".

Natalya N. Khristoforova passed away too soon, but her cause continues to live and develop thanks to her many friends and colleagues.

In times of great challenges, the Editorial Board of the journal is in great need of the support and understanding of authors, reviewers and readers. Understanding the complexity of the task, Natalya wrote, "*We are facing difficult problems. But we will make every effort to ensure that the true traditions of selfless science, serving the benefit of the Fatherland, reign and dominate the pages of our journal*".

The present members of the Editorial Board of the Georesursy (Georesources) journal, headed by the Chief Editor Lyalya M. Sitdikova, will strive to implement this order.

Izotov V.G., Khristoforova N.N., 2008

Sitdikova L.M., Khristoforova D.A., 2017

ORIGINAL ARTICLE
DOI: https://doi.org/10.18599/grs.2020.1.4-12

Pore-scale investigation of the displacement fluid mechanics during two-phase flows in natural porous media under the dominance of capillary forces

T.R. Zakirov[1], M.G. Khramchenkov[1,2]*
[1]*Kazan Federal University, Kazan, Russian Federation*
[2]*Scientific Research Institute for System Analysis of the Russian Academy of Sciences, Moscow, Russian Federation*

Abstract. This paper presents the results of numerical simulations of two-phase flows in porous media under capillary forces dominance. For modeling of immiscible two-phase flow, the lattice Boltzmann equations with multi relaxation time operator were applied, and the interface phenomena was described with the color-gradient method. The objective of study is to establish direct links between quantitative characteristics of the flow and invasion events, using high temporal resolution when detecting simulation results. This is one of the few works where Haines jumps (rapid invasion event which occurs at meniscus displacing from narrow pore throat to its wide body) are considered in three-dimensional natural pore space, but the focus is also on the displacement mechanics after jumps. It was revealed the sequence of pore scale events which can be considered as a period of drainage process: rapid invasion event during Haines jump; finish of jump and continuation of uniform invasion in current pore; switching of mobile interfaces and displacement in new region. The detected interface change, along with Haines jump, is another distinctive feature of the capillary forces action. The change of the mobile interfaces is manifested in step-like behavior of the front movement. It was obtained that statistical distributions of pressure drops during Haines jumps obey lognormal law. When investigating the flow rate and surface tension effect on the pressure drop statistics it was revealed that these parameters practically don't affect on the statistical distribution and influence only on the magnitude of pressure drops and the number of individual Haines jumps.

Keywords: two-phase flow, Haines jumps, capillary forces, lattice Boltzmann equations, color-gradient method, X-ray computed tomography

Recommended citation: Zakirov T.R., Khramchenkov M.G. (2020). Pore-scale investigation of the displacement fluid mechanics during two-phase flows in natural porous media under the dominance of capillary forces. *Georesursy = Georesources*, 22(2), pp. 4-12. DOI: https://doi.org/10.18599/grs.2020.1.4-12

1. Introduction

Understanding of two-phase flow processes in porous media plays an important role in wide range of scientific and engineering disciplines, such as hydrogeology, oil- and gas-field development, soil science, underground hydromechanics, cardiology, etc. With the development of computing and experimental technique, many modern papers, studying the multiphase flows in porous media, have appeared (Liu et al., 2016; Chen et al., 2018; Zakirov et al., 2018a; Aursjø et al., 2011; Tsuji et al., 2016). These papers are united by the investigation of one phenomenon – the development of instabilities during two-phase drainage flow in porous media. Depending on the mechanics of the instabilities development, three displacement patterns of two-phase flows are distinguished: viscous fingering, capillary fingering and flow with stable front. It was shown in that the instability type is controlled by capillary number (*Ca*) and viscous ratio between non-wetting and wetting fluids (*M*).

The pattern with stable front is observed at simultaneously high *Ca* and $M \geq 1$. This flow is characterized by ideal flat interface in 2D homogeneous models (Liu et al., 2016), but, as shown in (Tsuji et al., 2016), the front geometry in natural heterogeneous porous media is far from stable. The flow with viscous fingering is formed at $M \leq 0.1$ and high *Ca* (typically more than 10^{-3}). In this regime, viscous forces strongly exceed capillary forces. This flow pattern is characterized by unstable front displacement, the formation of dominant displacement channels directed along the pressure drop, and tree-like structure of the instabilities (Zakirov et al., 2018b; Tsuji et al., 2016).

[*]*Corresponding authors: Timur R. Zakirov*
E-mail: tirzakirov@kpfu.ru

At low *Ca* (typically less than 10^{-5}), capillary forces dominate and the capillary fingering is observed. Some characteristics of such flow type are described in (Zakirov et al., 2018b; Tsuji et al., 2016; Yamabe et al., 2015). However, most of the modern works studying the mechanics of displacement in the regime of dominance of capillary forces are aimed at studying the Haines jumps. This event was first discovered in (Haines et al., 1930) and is characterized by burst-like the meniscus displacement from narrow pore throat to wide pore body, which is accompanied by sharp capillary pressure drop. Hines jumps are a bright example of the capillary forces manifestation in a porous medium.

In (Moebius, Or, 2012, 2014), Haines jumps investigation was performed at controlling of the pressure difference between fluids. Pressure fluctuations were detected during drainage displacement and Haines jumps were associated with sharp pressure drop, but the displacement mechanics after jumps wasn't investigated in detail. The measurement of interfacial velocities during Haines jumps was performed in (Moebius, Or, 2012; Zacharoudiou, Boek, 2016; Armstrong, Berg, 2013; Armstrong et al., 2015). It was shown that the velocity of meniscus displacement many times exceeds bulk flow rate and affect the fluids distribution in adjacent pores. Reynolds number is not negligibly small in that cases. Thus, the inertial forces should not be ignored and, as shown in (Armstrong et al., 2015), the *Ca* and *M* values are not enough for controlling the capillary fingering pattern. The Ohnesorge number which relates the viscous, inertial and capillary forces was offered to use in (Zacharoudiou, Boek, 2016).

In present paper, the displacement mechanics is studied using the mathematical modeling. In recent years, the lattice Boltzmann equations (LBM) is a widely used tool for pore-scale simulations of the two-flow processes (Liu et al., 2016; Zakirov et al., 2018b; Aursjø et al., 2011; Tsuji et al., 2016; Yamabe et al., 2015). In our study, we use the most modern version of the color-gradient method. LBM using the MRT collision operator (MRT – Multi relaxation time) with color gradient model for 3D lattices (D3Q15, D3Q19, and D3Q27) is formulated in (Leclaire et al., 2017)

The objective of this paper is to study the mechanics of two-phase drainage flow under the capillary forces dominance. The originality of the work is the study of events occurring in the porous space after Haines jump as well as the natural character of the pore structure.

We focus on establishing a direct links between quantitative dynamic characteristics of two-phase flow and invasion events, using high temporal resolution when detecting the results.

A special attention is paid to exploration of the statistical distributions of pressure drops which occur during Haines jumps in 3D natural sandstone. The influence of flow rate and surface tension on statistical properties of pressure drops is especially studied.

2. Materials and methods

2.1. LBE formulation

In the LBE, the fluid flow is considered as dynamics of particles ensemble with a given finite number of possible velocities. The flow domain in standard case is a grid with square or cubic cells. The set of these cells forms a lattice with step Δl. During a time step Δt, particles without interaction with each other can make one act of displacement between adjacent nodes. One-particle distribution functions $f(\mathbf{r}, \boldsymbol{u}, t)$ are used to describe the state of the system at each grid node. This function shows the part of particles at time t located in the vicinity of point $\mathbf{r}(x, y, z)$ with coordinates from x to $x+\Delta x$, from y to $y+\Delta y$, from z to $z+\Delta z$ and with velocity range from $\mathbf{u}(u_x, u_y, u_z)$ to $\mathbf{u}(u_x+\Delta u_x, u_y+\Delta u_y, u_z+\Delta u_z)$ (Leclaire et al., 2017).

In this paper, we consider two-dimensional case. Possible directions for particles moving are described using D3Q19 model. Since a detailed description of this model already cited in (Leclaire et al., 2017, Zakirov et al., 2018b), we restrict ourselves to a brief presentation of basic formulas and steps.

The dynamics of the particles ensemble for each fluid is described in several stages. The first is a streaming step. At this stage, during Δt the particles move to neighboring nodes in possible for D3Q19 directions. The second stage deals with the particles collision, as a result of which the distribution function tends to an equilibrium state. At the third stage, the phenomena on fluids interface are considered. Evolution of f_i^k in time and space is described by Eq. (1):

$$f_i^k(\mathbf{r}+\mathbf{e}_i\Delta t, t+\Delta t) = f_i^k(\mathbf{r},t) + (\Omega_i^k(\mathbf{r},t))^1 \\ (\Omega_i^k(\mathbf{r},t))^2 \quad (1)$$

where $k = 1, 2$ and indicates fluid type, i.e. wetting and non-wetting phases; $i = (1\text{-}19)$ characterizes the direction of particles movement in D3Q19; $(\Omega_i^k)^1$ is a collision operator, and $(\Omega_i^k)^2$ describes interactions between two fluids.

The macroscopic densities of each fluid and their total velocity are obtained by Eq. (2) and (3):

$$\rho^k(\mathbf{r},t) = \sum_{i=1}^{19} f_i^k(\mathbf{r},t) \quad (2)$$

$$\mathbf{u}(\mathbf{r},t) = \frac{1}{\rho}\sum_{k=1}^{2}\sum_{i=1}^{19}\mathbf{e}_i f_i^k(\mathbf{r},t) \quad (3)$$

Due to more accurate results when using the MRT model (Zakirov et. al, 2018a), in comparison with SRT-model (SRT – Single relaxation time), the first approach is applied in present paper:

$$(\Omega_i^k)^1 = -M^{-1}S(m_i^k - m_i^{k\,eq}) \quad (4)$$

In Eq. (4), $m_i^k = \sum_{j=1}^{19} M_{ij} \cdot f_j^k$. The view of matrix M and formulas for calculation of $m_i^{k\,eq}$, and the components of the diagonal matrix S are described in (Zakirov et. al, 2018a). Set B for matrix S in also shown (Zakirov et. al, 2018a)

Pressure P^k is associated with density by following relation: $P^k = \rho^k c^2/3$, where $c = \Delta l / \Delta t$ – the lattice speed, Δl – grid spacing.

The relaxation parameter τ^k controls the kinematic viscosity μ^k (Eq. (5)):

$$\mu^k = \left(\frac{2\tau^k - 1}{6}\right)\frac{\Delta l^2}{\Delta t} \quad (5)$$

To describe the phenomena between fluids as well as between fluid and solid phase, the color-gradient method is applied (Leclaire et al., 2017). First, the color-gradient vector **g** is defined as (Leclaire et al., 2017):

$$\mathbf{g}(\mathbf{r},t) = \sum_{i=1}^{19} \mathbf{e}_i(\rho^2(\mathbf{r}+\mathbf{e}_i\Delta t,t) - \rho^1(\mathbf{r}+\mathbf{e}_i\Delta t,t)) \quad (6)$$

The contact wetting angle θ is simulated in color-gradient method by giving the values of densities to the solid cells.

Next, the perturbation operator $(\Omega_i^k)^2$ is calculated by:

$$(\Omega_i^k)^2 = \frac{A^k}{2}|\mathbf{g}|\left(w_i \cdot \frac{(\mathbf{e}_i \cdot \mathbf{g})}{|\mathbf{g}|} - B_i\right) \quad (7)$$

In Eq. (7), $|\mathbf{g}|$ is a module of color-gradient vector; A^k is a numerical parameter which controls a magnitude of surface tension, and it's assumed that $A^1 = A^2 = A$; B_i takes the following values: $B_1 = -2/9$; $B_{2-7} = 1/27$; $B_{8-19} = 1/54$; $w_1 = 1/3$; $w_{2-7} = 1/18$; $w_{8-19} = 1/36$ – the weights coefficients.

Perturbation operator in Eq. (7) models surface tension, but doesn't provide an immiscibility of fluids. For avoidance their mixing, the recoloring operator is used. This step is performed after solving the Eq. (1) with MRT-operator $(\Omega_i^k)^1$ and perturbation operator $(\Omega_i^k)^2$ applying, and consists in modifying of f_i^k (Leclaire et al., 2017):

$$(f_i^1)^* = \frac{\rho^1}{\rho} f_i - \beta \frac{\rho^1 \cdot \rho^2}{\rho} f_i^{eq} \cdot \cos(\alpha_i) \quad (8)$$

$$(f_i^2)^* = \frac{\rho^2}{\rho} f_i + \beta \frac{\rho^2 \cdot \rho^1}{\rho} f_i^{eq} \cdot \cos(\alpha_i) \quad (9)$$

where $f_i = f_i^1 + f_i^2$, $\rho = \rho^1 + \rho^2$; f_i^{eq} is an equilibrium function calculated at $\mathbf{u} = 0$ and ρ by Eq. (10) (Zakirov et. al., 2018b):

$$f_i^{eq}(\rho,\mathbf{u}) = w_i\rho \cdot \left(1 + 3\frac{(\mathbf{e}_i \cdot \mathbf{u})}{c^2} + 4.5\frac{(\mathbf{e}_i \cdot \mathbf{u})^2}{c^4} - 1.5\frac{\mathbf{u}^2}{c^2}\right) \quad (10)$$

β is a free parameter which controls a thickness of interface. It takes values from 0 to 1 and is equal to 0.8 in our study; α_i is an angle between **g** and $\mathbf{e}_i$ directions. Contact wetting angle is simulated using the approach described in (Akai et al., 2018).

2.2. Boundary and initial conditions

At the initial time, the pore space of flow domain on which the computational experiments are carried out is filled with a wetting fluid which has zero flow velocity. Both fluids have similar viscosity and density 1 m²/s and 1 g/cm³, respectively. A non-wetting phase is injected through the conventional left side of the region, perpendicular to the *OX* axis, and is selected through the right side; the flow is occurred when the non-wetting fluid injected through the input boundary at known constant velocity. The pressure the output section is known and constant. Other external sides of the flow region are impermeable. In the LBE framework, the boundary conditions on the input and output boundaries are given by Zou and He relations (Zou, He, 1997). The boundary conditions on the impermeable obstacles are realized by "bounce-back" rule (Zakirov et. al, 2018b).

The implementation of mathematical model was in the form of software codes in Microsoft Visual Studio 2017 development environment using Intel Fortran programming language. The numerical validations of the algorithm on the layered flow in channel as well as on drainage displacement were preformed in (Zakirov et al., 2018a, 2018b).

2.3. Image processing and samples description

In this paper, sandstone from Ashalchinskoe oil field (Tatarstan, Russia) was used. The digital model of the pore space was formed on the base of X-ray computed tomography. The scans of cores were made on a micro-/nanofocus X-ray monitoring system for computed tomography and 2D inspection GE Phoenix v|tome|x s 240. We selected a cubic core with size of 3.7 millimeters for which X-ray tomographic scanning was performed. The resolution of digital model was 4.0 μm. Fig. 1 shows the X-ray CT 3D image with size of 350³ voxels.

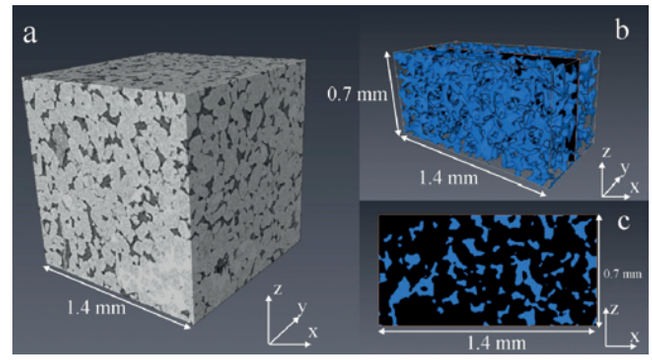

Fig. 1. 3D Digital X-ray CT model of sandstone with resolution of 4 μm: a – 3D-image with size of 350³ voxels; b – 3D-pore space of subsample No. 1 with size of 350×175×175 voxels; c – 2D-slice perpendicular to OY direction

The gray color scale in Fig. 1a characterizes the X-ray radiation attenuation intensity by different areas of the sample: light gray regions are the granules of sandstone, and black represents the pore space. Imaging of invasion processes, reported in sections 3.1, was carried out on subsample with smaller size of 250×125×125 voxels. Its porosity is 0.272 and k_{XX} = 0.612 μm^2.

The statistical investigations of Haines jumps, reported in section 3.2, were conducted on four subsamples, cut from big model, with dimensions of 350×175×175 voxels. Their properties are given in Table 1. A porous structure of subsample No.1, which was extracted after binarization, is shown in Figs. 1b and 1c.

Subsample number	Porosity, rel. units	Absolute permeability component k_{XX}, μm^2
1	0.270	0.645
2	0.263	0.456
3	0.277	0.621
4	0.276	0.541

Table 1. The porosities and absolute permeability components k_{XX} of four subsamples

3. Results and discussion

3.1. Pore-scale invasion events and dynamic characteristics of the flow

The focus of this is to establish links between numerical dynamic characteristics of the flow. The computational experiment was carried out on subsample with dimension of 250×125×125 voxels at flow wate u_0 = 0.2×10^{-3} m/s, surface tension σ = 20 mN/m and contact wetting angle θ = 10°. Firstly, in Fig. 2, we show the pressure difference evolution in time between inlet and outlet boundaries of the flow domain (further, the pressure difference between boundaries will be denoted as P, and pressure drops which occur during Haines jumps will be indicated as ΔP). The pressure measurement was made every 500 time steps which is equal to 0.08 ms. The blue curve in Fig. 2 shows the dynamics of P in the absence of capillary forces (σ (mN/m) = 0).

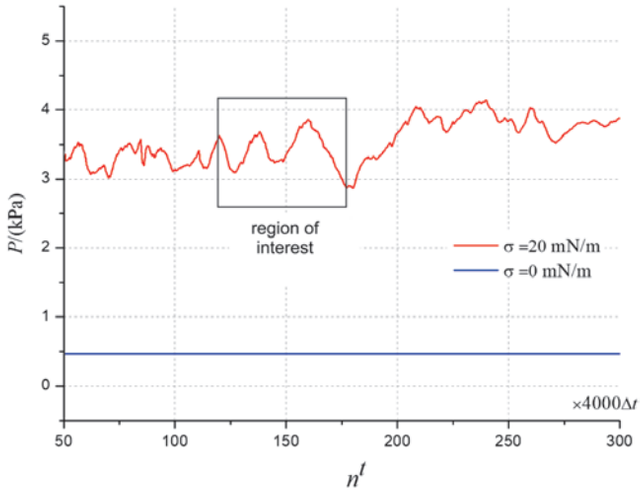

Fig. 2. The dynamics of pressure difference between input and output boundaries of the sample during drainage displacement

According to red curve in Fig. 2, the fluctuations of P are observed and the dynamics has wavy behavior (see also Fig. 7). In addition, to determine the cause of pressure fluctuation and to strengthen the link between numerical dynamics characteristics and invasion events, the specific surface area of pore space S_V, occupied by invaded non-wetting fluid, was calculated. This characteristic is defined as the ratio between surface area of non-wetting fluid and its volume. Further, we will accent on a period from 115 to 175 of n^t (the area of interest in Figs. 2 and 3). Fig. 3b shows the dynamics of change of the pore space specific surface area ΔS_V, where $\Delta S_V(n^t+1) = S_V(n^t+1) - S_V(n^t)$.

Step-by-step imaging of pore-filling events is shown in Figs. 4-6. Fig. 4a illustrates the distribution of injected non-wetting phase, which corresponds to position "a" and to "event 1" in Fig. 3. The blue

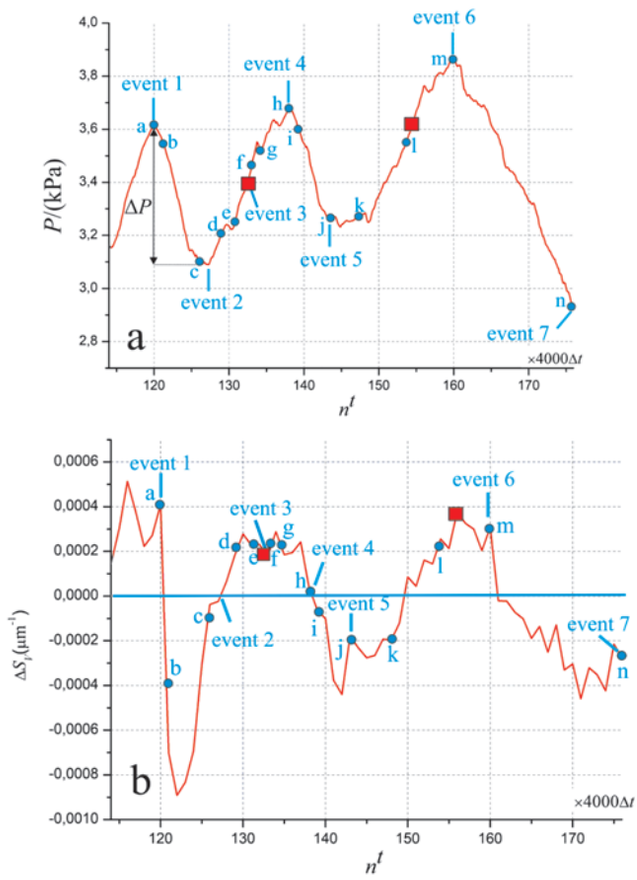

Fig. 3. The dynamics of the flow characteristics in the interval n^t = [115,175]: a – fluctuations of pressure difference; b – fluctuations of the change of the porous space specific surface area, which is occupied by non-wetting fluid. The "events" and positions "a" – "n", marked in graphs, are associated with Figs. 4-6. Red squares indicate the appearance of new mobile interfaces.

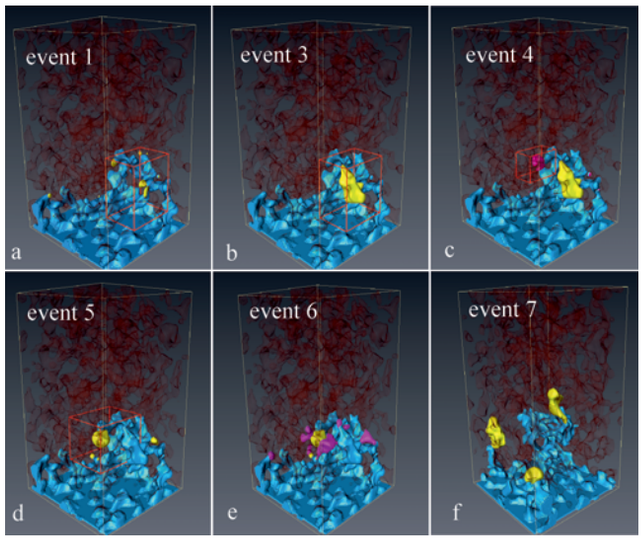

Fig. 4. The distributions of non-wetting phase during displacement between "event 1" and "event 7" (Fig. 3). The invaded regions between current and previous events are shown in yellow and pink. Blue, yellow and pink – the non-wetting phase, dark red – pore space occupied by wetting fluid.

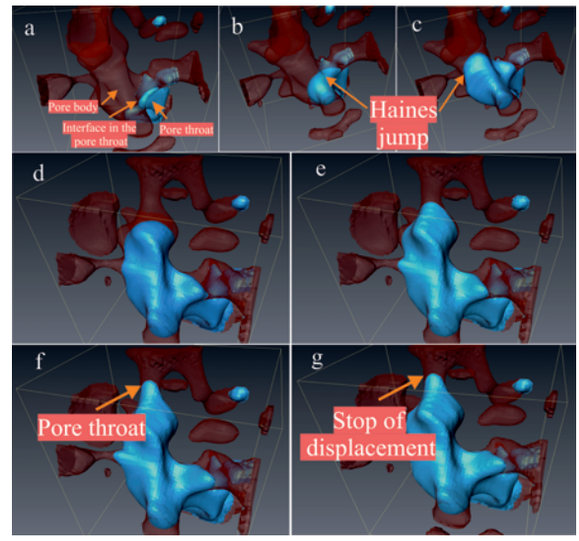

Fig. 5. The dynamics of non-wetting phase displacement between "event 1" and "event 4" (Fig. 3) in red box shown in Fig. 6a: a – the meniscus location in the connection of the pore throat and its body, position "a"; b, c – the rapid invasion of non-wetting phase to the pore body (Haines jump), positions "b" and "c"; d, e – the finish of rapid invasion, the displacement of interface at narrowing of the pore size, positions "d" and "e"; f, g – the meniscus location in new pore throat and the stop of interface displacement in current pore channel, positions "f" and "g". Positions "a" – "g" are associated with Fig. 3. Blue – the non-wetting phase, dark red – pore space occupied by wetting fluid.

color in Fig. 3a is a distribution of non-wetting phase at n^t = 115, and yellow shows the non-wetting phase invaded during n^t = [115, 120]. According to Fig. 3, the capillary pressure growth is accompanied by increase in the specific surface area because $\Delta S_V > 0$. Such relationship of the characteristics is explained by the inverse dependences of the specific surface and capillary pressure on the radius of the pore channel.

Next, after "event 1" in Fig. 3a, a pressure drop ΔP was detected. Drainage events in the interval between "event 1" and "event 3" will occur in a region of red box shown in Figs. 4a and 4b. Fig. 5 illustrates these events in larger view. The location of liquids interface in narrow pore throat, which will move in next snapshot to wide pore body, is shown in Fig. 5a (position "a" in Fig. 3). The reason of drainage event in this region is the pressure difference exceeding of the capillary pressure of this meniscus. Figs. 5b and 5c illustrate the invasion for positions "b" and "c" (Fig. 3). According to them, an observed event, when drainage front displaced, occurs rapidly and looks as a burst-like flow. Rapid invasion process is due to the sharp growth of pore channel size during meniscus displacement from pore throat to its body. This observation is also in agreement with variation of the specific surface area. According to Fig. 3b, the rapid increase in the interface surface between positions "a" and "c" is detected. Such character of the interface displacement is reflected and associated with quick drop of capillary pressure. The described phenomenon is a Haines jump.

Figs. 5d and 5e show meniscus displacement in positions "d" and "e". The drainage process continues in the same pore-channel and absent in the other regions of the pore space. It can be noted that after finish of rapid invasion from pore throat to its body, we detected the growth in capillary pressure in Fig. 3a after "event 2". According to Figs. 5d and 5e, the reason of such increase is the decrease in meniscus radius due to narrowing of the pore size on its pathway, which is also supported by Fig. 3b ($\Delta S_V > 0$ in interval between positions "c" and "e"). Fig. 4b shows the distribution of non-wetting phase in "event 3". The region occupied by non-wetting phase between "event 1" and "event 3" is shown in yellow.

Due to decrease in mobile interface radius, the probability of new invaded regions appearance is growing. Drainage process will continue in pore channel where capillary resistance, produced by meniscus, is lower than in current mobile interface. Figs. 5f and 5g (positions "f" and "g" in Fig. 5) illustrate finish of invasion event in this pore channel. The switching of mobile interface occurs between positions "e" and "f" and corresponds to "event 3". Fig. 3 shows that in this time interval, the increase in capillary pressure and specific surface area is observed. The new invaded region in "event 4" is shown in Fig. 4c. The area occupied by non-wetting phase between "event 3" and "event 4" is shown in pink in new red box.

Next, new drainage displacement between "event 4" and "event 5" (Fig. 3), as can be seen in Fig. 4d, will occur in a region of red box. Fig. 6 illustrates the invasion events in this time interval in a larger view.

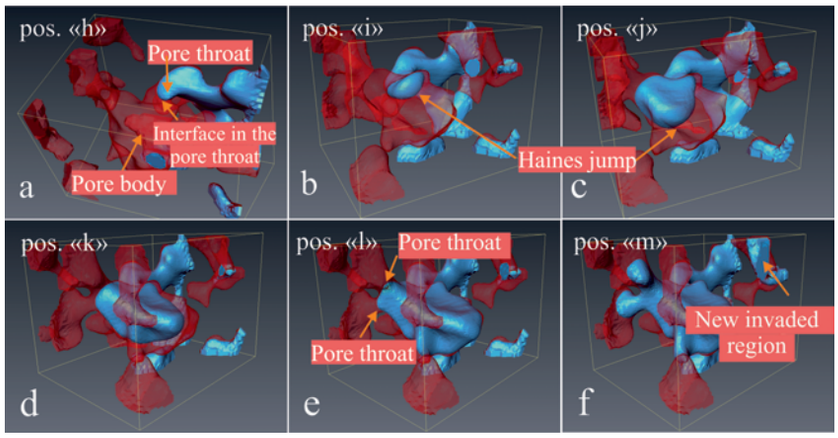

Fig. 6. The dynamics of non-wetting phase displacement between "event 4" and "event 6" (Fig. 3) in red box shown in Fig. 4d: a – the meniscus location in the connection of the pore throat and its body, position "h"; b, c – Haines jump, positions "i" and "j"; d – f – the finish of rapid invasion, the following uniform displacement at narrowing of the pore size and the appearing of new mobile interface, positions "k" – "m". Positions "h" – "m" are associated with Fig. 3. Blue – the non-wetting phase, dark red – pore space occupied by wetting fluid.

In position "h" (Fig. 3), shown in Fig. 6a, the interface is located in pore throat, and the pressure difference, evidently, exceeds capillary resistance of meniscus because followed event, which is illustrated in Figs. 6b and 6c, will occur in this pore channel. Haines jump is observed in positions "i" and "j" and associated with sharp decrease in capillary pressure and specific surface area (Fig. 3). The region occupied by non-wetting fluid between "event 4" and "event 5" is shown in yellow in Fig. 4d.

"Event 5" in Fig. 3 corresponds to the finish of Haines jump and appearance of new mobile interfaces. Invasion events, as shown in Figs. 6d and 6e (positions "k" and "l" in Fig. 3), will continue in current pore, but at narrowing of meniscus size. The displacement after position "j" and before "m" occurs uniformly and at growth of capillary pressure and specific surface area (Fig. 3). The pore space filled by non-wetting phase between "event 5" and "event 6" is shown in pink in Fig. 4e.

Next, we detected a sharp drop of capillary pressure and specific surface area after "event 6" (Fig. 3), again. According to established association between invasion events and dynamics of capillary pressure and specific surface area, Haines jumps were expected after "event 6" and they really were observed between positions "m" and "n" (Fig. 3). The regions invaded between "event 6" and "event 7" are shown in yellow in Fig. 4f.

It should be stressed that, in general case, the switching of mobile interfaces and/or the continuation of displacement in current pore after Haines jump is a result of the "competition" of capillary pressures produced by current mobile interface and other static meniscus. Thus, the revealed change of the mobile interfaces, along with Haines jump, is another new distinctive feature of the capillary forces dominance.

So, based on obtained in this section results, we can note that the scenario of drainage displacement with the dominance of capillary forces consists of following stages: 1 – uniform invasion in narrow pore channels at growth of capillary pressure and specific surface area; 2 – rapid invasion event during Haines jump and sharp drop of capillary pressure and specific surface area; 3 – finish of Haines jump and continuation of uniform invasion in current pore, where Haines jump occurred, the resumption of increase in capillary pressure and specific surface area; 4 – appearance of new mobile interfaces in other regions of pore space or continuation of uniform invasion in current pore in general case; 5 – Haines jump in new region of pore space. The sequence of stages 2-4 can be considered as a period of drainage events which, according to Figs. 2 and 7, will be repeated with variation of the time duration and amplitude of the pressure fluctuations.

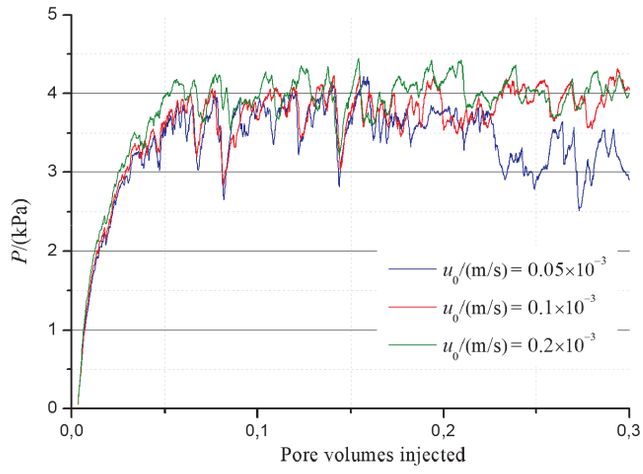

Fig. 7. The dynamics of pressure difference during drainage displacement for different injected fluid velocities

3.2. Haines jumps statistics

In this section, we investigate the impact of flow rate and surface tension on statistical distributions of pressure

drops at Haines jumps. It should be noted that, despite 2D micromodels, the statistical investigations on 3D X-ray CT images are limited and hampered. One of the reasons is a high resolution of digital model and, consequently, its small pore volume and large grid dimension, which is also accompanied by big computational costs. Thus, the number of pore-scale events in 3D models is less than in 2D micromodels (more than 500 (Furuberg et al., 1996; Soto et al., 2017)). Also, the investigation on big pore volumes is hampered with simultaneous invasion events, whereas it's necessary to observe the individual processes for statistical interpretation. That is why, for decreasing the frequency of simultaneous Haines jump and to obtain the sufficient number of pressure drops, the numerical experiments were conducted on four subsamples, which properties are given in Table 1.

3.2.1. Effect of flow rate

For the flow rate affect investigation, the series of numerical experiments at wide range of the injected fluid velocity was carried out: $[0.05 \div 1.5] \times 10^{-3}$ m/s. The surface tension in all simulations was 20 mN/m. The *Ca* numbers and average estimations of the relations between capillary pressure (P^{cap}) and pressure difference between input and output sections of the subsamples, conditioned by viscous forces action (P^{visc}), are given in Table 2. All simulations were carried till injection of 0.3 pore volumes.

The dynamics of pressure difference for subsample No.2, plotted for three cases of flow rate, is shown in Fig. 7. According to shown in column 5 (Table 2) data, the number of detected pressure drops (N^{drop}) is strongly affected by the flow rate. This feature is clearly visible on Fig. 7. We must note that N^{drop} is not equal to the number of individual Haines jumps. It was revealed that increase in injected fluid velocity leads to the growth of the mobile interfaces number. Thus, the number of simultaneous Haines jumps will increase with the magnitude of the flow rate and most individual jumps, especially at high velocities, cannot be separated and distinguished during a single pressure drop.

When imaging of invasion processes, it was found that for $u_0 \geq 0.4 \times 10^{-3}$ m/s, three and more simultaneous jumps occur during single pressure drop, whereas for $u_0 \leq 0.2 \times 10^{-3}$ m/s, the number of simultaneous jumps during single pressure drop doesn't exceed two. Such feature makes impossible strict statistical investigation for $u_0/(\text{m/s}) \geq 0.4 \times 10^{-3}$.

For $u_0 = 0.2 \times 10^{-3}$ m/s, the proportion of simultaneous paired jumps during single pressure drop is about 30 % and decreases to 5 % for $u_0 = 0.05 \times 10^{-3}$ m/s. Therefore, the influence of flow rate on the individual jumps number exists but insignificant. This observation is also reinforced with calculated pore volume filled during pressure drops (PV^{jump} in column 7, Table 2). According to shown in column 7 data, PV^{jump} values for $u_0 \leq 0.2 \times 10^{-3}$ m/s are almost the same.

The statistical distributions of pressure drops for $u_0 \leq 0.2 \times 10^{-3}$ m/s are shown in Fig. 8. It was revealed that obtained distributions obey lognormal law with R-squared equal to 0.93, 0.96 and 0.94 in the order of increasing u_0. According to Fig. 8, the flow rate affect on statistical distribution is insignificant, but influences on the mean value of pressure drop $\Delta\overline{P}$.

According to numerous experiments on 2D and 3D micromodels in (Moebius, Or, 2012; Furuberg et al., 1996; Soto et al., 2017), the cumulative distribution *N* of pressure drops obeys following relation:

$$\ln(N) = \beta \cdot \Delta P / \Delta\overline{P} \qquad (11)$$

where β is the linear coefficient. Fig. 8b shows the cumulative distribution *N*. The solid lines in Fig. 8b are the approximating curves using Eq. (11) with R-squared exceeding 0.98. Thus, the pressure drops statistics in 3D heterogeneous models of porous media, in 2D granular homogenous models (Moebius, Or, 2012; Furuberg et al., 1996) and in macroporous soils (Soto et al., 2017) obey the same law. When approximating the cumulative distribution, it was calculated that the β coefficients are –0.970, –0.983, –0.969 in the order of increasing u_0. Such close values indicate on the weak influence of flow rate on the statistical distributions of pressure drops.

3.2.2. Effect of surface tension

For the investigation of the surface tension affect, a series of numerical experiments at σ = 13, 20 and 28 mN/m was carried out. $u_0 = 0.1 \times 10^{-3}$ m/s in all simulations. All simulations were carried till injection of 0.3 pore volumes.

No.	$u_0 \times 10^{-3}$, m/s	$log_{10}Ca$	P^{cap}/P^{visc}	N^{drop}	Mean value $\Delta\overline{P}$, kPa	PV^{jump}
1	0.05	-5.6	67	360	0.206	0.265
2	0.1	-5.3	33.5	307	0.173	0.252
3	0.2	-4.9	16.7	271	0.165	0.257
4	0.4	-4.7	8.3	193	0.152	0.266
5	0.8	-4.4	4.2	159	0.129	0.256
6	1.5	-4.1	2.0	119	0.111	0.247

Table 2. The numerical values of computational simulations and the results of the flow rate affect on pressure drops statistics

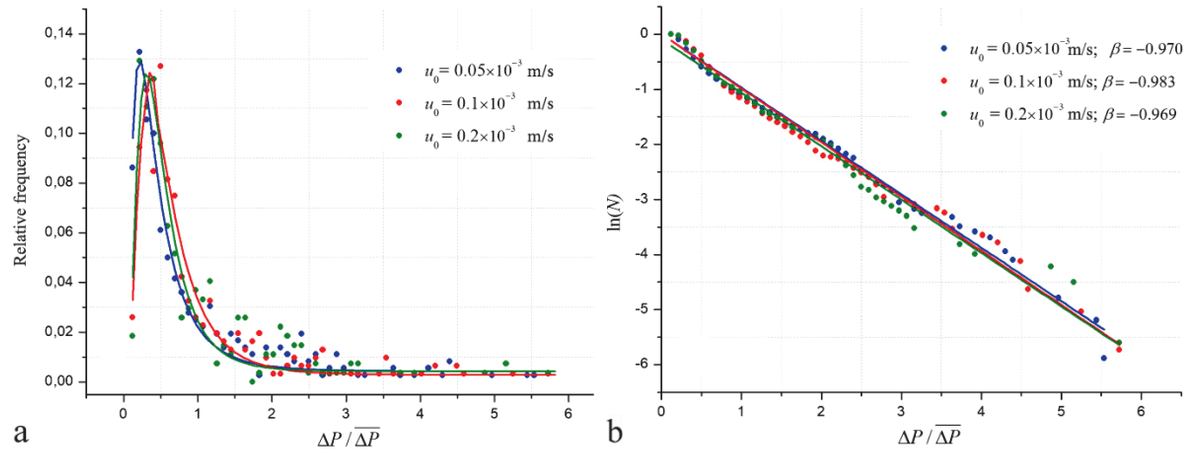

Fig. 8. The statistical distributions of the dimensionless parameter $\Delta P / \Delta \overline{P}$, calculated for different injected fluid velocities: a – distributions in form of the relative frequency; b – the cumulative distributions N. The circle symbols show measured data, and the solid lines are the result of approximation.

The characteristics of numerical simulations are given in Table 3. According to shown data, the value of interfacial interaction practically does not influence on the number of pressure drops (column 5, Table 3), but affects on its magnitude (column 6, Table 3). The close values of PV^{jump} (column 7, Table 3) indicate on the weak influence on the number of individual Haines jumps.

Fig. 9 illustrates the distributions of pressure drops at various surface tensions. Solid lines in Fig. 9 are the result of approximation by lognormal law. The R-squared for each curve exceed 0.93. The character of solid lines in Fig. 9 indicates a weak surface tension influence on the statistical distributions.

Thus, taking to account that $\beta \approx -1$ regardless of the injected fluid velocity and surface tension, it can be supposed that the statistical distribution of $\Delta P / \Delta \overline{P}$ is determined only by the geometry of porous structure. For example: $\beta = -1.3$ and -1.5 for two types of 2D mircomodels and $\beta = -1.7$ for 3D granular model in (Moebius, Or, 2012); $\beta = -1.31$ for 2D model in (Furuberg et al., 1996); $\beta \approx -3$ for soils in (Soto et al., 2017). This assumption requires special investigations in future.

No.	σ mN/m	$log_{10}Ca$	P^{cap}/P^{visc}	N^{drop}	Mean value $\Delta \overline{P}$, kPa	PV^{jump}
1	13	-5.1	21.7	289	0.115	0.268
2	20	-5.3	33.5	307	0.173	0.252
3	28	-5.45	47	300	0.241	0.278

Table 3. The numerical values of computational simulations and the results of the surface tension affect on pressure drops statistics

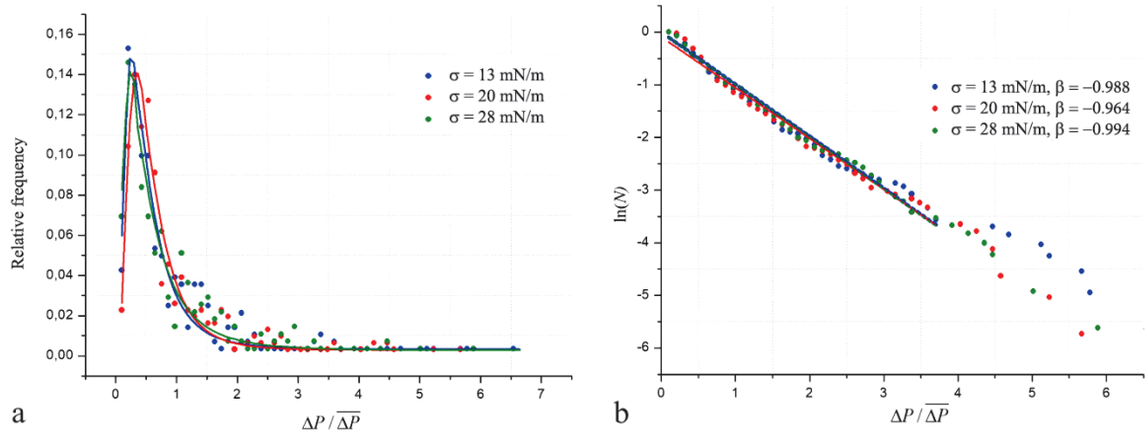

Fig. 9. The statistical distributions of the dimensionless parameter $\Delta P / \Delta \overline{P}$ calculated for different surface tensions: a – distributions in form of relative frequency; b – the cumulative distributions N. The circle symbols show measured data, and the solid lines are the result of approximation.

Conclusion

In this paper, we investigated the effects which occur during two-phase flow in natural 3D model of porous media with the dominance of capillary forces. A sequence of events has been identified that can be considered a period of drainage displacement. It consists of the following steps: Haines jump; continuation of the displacement in this channel, where a jump occurred; the appearance of new mobile menisci and subsequent displacement in new regions of the pore space. Periodic switching of moving interfaces is a new distinctive feature of the capillary forces manifestation in a porous medium.

The statistical investigations of pressure drops, which occur at Haines jumps, show that their distribution obeys lognormal law. It was found that the parameters of two-phase flow don't influence on the statistical distribution of pressure drops and affect only on its magnitude.

Acknowledgements

The work is performed according to the Russian Government Program of Competitive Growth of Kazan Federal University and by RFBR according to the research project No. 18-31-00134.

The authors are grateful to the reviewer for valuable comments that contributed to the improvement of the article.

References

Akai T., Bijeljic B., Blunt M.J. (2018). Wetting boundary condition for the color-gradient lattice Boltzmann method: Validation with analytical and experimental data. *Advances in Water Resources*, 116, pp. 56-66. https://doi.org/10.1016/j.advwatres.2018.03.014

Armstrong R.T., Berg S. (2013). Interfacial velocities and capillary pressure gradients during Haines jumps. *Physical Review E*, 88, 043010. https://doi.org/10.1103/PhysRevE.88.043010

Armstrong R.T., Evseev N., Koroteev D., Berg S. (2015). Modeling the velocity field during Haines jumps in porous media. *Advances in Water Resources*, 77, pp. 57-68. https://doi.org/10.1016/j.advwatres.2015.01.008

Aursjø O., Løvoll G., Knudsen H.A., Flekkøy E.G., Måløy K.J. (2011). A Direct Comparison Between a Slow Pore Scale Drainage Experiment and a 2D Lattice Boltzmann Simulation. *Transport in Porous Media*, 86(1), pp. 125-134. https://doi.org/10.1007/s11242-010-9611-y

Chen Y.-F., Wu D.-S., Fang Sh., Hu R (2018). Experimental study on two-phase flow in rough fracture: Phase diagram and localized flow channel. *International Journal of Heat and Mass Transfer.* 122, pp. 1298-1307. https://doi.org/10.1016/j.ijheatmasstransfer.2018.02.031

Furuberg L., Maløy K.J., Feder J. (1996). Intermittent behavior in slow drainage. *Physical Review E*, 53, pp. 966-977. https://doi.org/10.1016/0378-4371(92)90542-X

Haines W.B. (1930). Studies in the physical properties of soil. *Journal of Agricultural Science*, 20, pp. 98-116. https://doi.org/10.1017/S002185960008864X

Leclaire S., Parmigiani A., Malaspinas O., Chopard B., Latt J. (2017). Generalized three-dimensional lattice Boltzmann color-gradient method for immiscible two-phase pore-scale imbibition and drainage in porous media. *Physical Review E*, 95, 033306. https://doi.org/10.1103/PhysRevE.95.033306

Liu H., Kang Q., Leonardi C.R., Schmieschek S., Narváez A., Jones B.D., Williams J.R., Valocchi A.J., Harting J. (2016). Multiphase lattice Boltzmann simulations for porous media applications. *Computational Geosciences*, 20(4). pp. 777-805. https://doi.org/10.1007/s10596-015-9542-3

Moebius F., Or D. (2012). Interfacial jumps and pressure bursts during fluid displacement in interacting irregular capillaries. *Journal of Colloid and Interface Science*, 377, pp. 406-415. https://doi.org/10.1016/j.jcis.2012.03.070

Moebius F., Or D. (2014). Pore scale dynamics underlying the motion of drainage fronts in porous media. *Water Resources Research*, 50, pp. 8441-8457. https://doi.org/10.1002/2014WR015916

Soto D., Paradelo M., Corral Á., López Periago J.E. (2017) Pressure jumps during drainage in macroporous soils. *Vadose Zone Journal*, 16. https://doi.org/10.2136/vzj2017.04.0088

Tsuji T., Jiang F., Christensen K.T. (2016). Characterization of immiscible fluid displacement processes with various capillary numbers and viscosity ratios in 3D natural sandstone. *Advances in Water Recourses*. 95, pp. 3-15. https://doi.org/10.1016/j.advwatres.2016.03.005

Yamabe H., Tsuji T., Liang Y., Matsuoka T. (2015). Lattice Boltzmann Simulations of Supercritical CO2−Water Drainage Displacement in Porous Media: CO2 Saturation and Displacement Mechanism. *Environmental Science and Technology*, 49, pp. 537-543. https://doi.org/10.1021/es504510y

Zacharoudiou I., Boek E.S. (2016). Capillary filling and Haines jump dynamics using free energy Lattice Boltzmann simulations. *Advances in Water Resources*, 92, pp. 43-56. https://doi.org/10.1016/j.advwatres.2016.03.013

Zakirov T.R., Galeev A.A., Statsenko E.O., Khaidarova L.I. (2018a). Calculation of filtration characteristics of porous media by their digitized images. *Journal of Engineering Physics and Thermophysics*, 91(4), pp. 1069-1078. https://doi.org/10.1007/s10891-018-1833-9

Zakirov T.R., Galeev A.A., Khramchenkov M.G (2018b). Pore-scale Investigation of Two-Phase Flows in Three-Dimensional Digital Models of Natural Sandstones. *Fluid Dynamics*. 53(5), pp. 76-91. https://doi.org/10.1134/S0015462818050087

Zou Q., He X. (1997). On pressure and velocity boundary conditions for the lattice Boltzmann BGK model. *Phys. Fluids*, 9, pp. 1591-1598. https://doi.org/10.1063/1.869307

About the Authors

Timur R. Zakirov – Cand. Sci. (Physics and Mathematics), Associate Professor, Institute of Geology and Oil and Gas Technologies, Kazan Federal University

18, Kremlevskaya st., Kazan, 420008, Russian Federation

E-mail: tirzakirov@kpfu.ru

Maxim G. Khramchenkov – Dr. Sci. (Physics and Mathematics), Professor, Head of the Department of Mathematical Methods in Geology, Kazan Federal University; Leading Researcher, Scientific Research Institute for System Analysis of the Russian Academy of Sciences

18, Kremlevskaya st., Kazan, 420008, Russian Federation

Manuscript received 16 August 2019;
Accepted 25 October 2019;
Published 30 March 2020

ORIGINAL ARTICLE
DOI: https://doi.org/10.18599/grs.2020.1.13-21

Modeling the effect of dynamic adsorption on the phase behavior of hydrocarbons in shale and tight reservoirs

*O.A. Lobanova, I.M. Indrupskiy**
Oil and Gas Research Institute of the Russian Academy of Sciences, Moscow, Russian Federation

Abstract. It is known that in shale and tight reservoirs, adsorption significantly affects hydrocarbon reserves and the processes of their production. This fact is reflected in the methods for calculating reserves and evaluating the production potential of shale and tight deposits. To calculate the initial content of the components, multi-component adsorption models are used. The impact on hydrocarbon production is taken into account through special dynamic permeability models for shale reservoirs. According to laboratory studies, adsorption can lead to significant changes not only in volume, but also in the composition of the produced fluids and their phase behavior. Previously, this effect could not be reproduced on the basis of mathematical models. The method proposed in this article allows modeling the phase behavior of a hydrocarbon mixture taking into account the dynamic adsorption/desorption of components in the process of pressure change. The method is applicable in the simulations of multi-component (compositional) flow and PVT-modeling of real reservoirs. The phase behavior of hydrocarbons with pressure depletion in shale reservoirs has been simulated. It is shown that neglecting the dynamic effect of adsorption/desorption leads to significant errors in predicting the saturation pressure, as well as the dynamics of changes in the composition of the produced fluid and of hydrocarbon component recovery.

Keywords: phase behavior, oil, gas, multicomponent hydrocarbon mixture, multicomponent adsorption, shale reservoir, numerical algorithm

Recommended citation: Lobanova O.A., Indrupskiy I.M. (2020). Modeling the effect of dynamic adsorption on the phase behavior of hydrocarbons in shale and tight reservoirs. *Georesursy = Georesources*, 22(1), pp. 13-21. DOI: https://doi.org/10.18599/grs.2020.1.13-21

Introduction

Studies of the phase behavior of multicomponent hydrocarbon mixtures are an integral part of the theory and practice of modeling, designing and analyzing the development of oil and gas condensate deposits. In theoretical terms, their most important element is the calculation of phase equilibrium – the problem of determining the number, fractions and compositions of the phases into which the hydrocarbon mixture is divided under given thermobaric conditions. Phase equilibrium calculations are of particular importance in multicomponent (compositional) flow simulations used to design and evaluate technological solutions in the development of oil and gas condensate deposits with intensive interfacial mass transfer (Aziz, Wong, 1989; Coats, 1998). They are also the basis for PVT-modeling (PVT – pressure-volume-temperature) used for creating reservoir fluid models (Whitson, Brule, 2000) and their matching to data of laboratory experiments on fluid samples in bulk (PVT cells) (Pedersen, Christensen, 2006).

In oil and gas deposits, a number of factors can lead to significant deviations of the actual phase behavior of the reservoir hydrocarbon mixture from that observed in the study of samples in bulk. As a result, during the development of the field there is a discrepancy between the measured and predicted data. Such factors include the influence of water (Buleiko et al., 2007), trapped hydrocarbons (Brusilovskii, 2002), rock surfaces (Buleiko et al., 2007; Pang et al., 2013), capillary pressure (Nojabaei et al., 2013; Shapiro, Stenby, 2001), etc.

It is well known that in shale and tight reservoirs a great influence on hydrocarbon reserves and the dynamics of their production is exerted by the adsorption/desorption of the components of formation fluids (Zendehboudi, Bahadori, 2015). Experimental studies show that adsorption can also have a significant impact on the composition of the hydrocarbon mixture and its phase envelope (Buleiko et al., 2007).

Experimental determination of the amount of adsorbed substance (adsorption isotherms) for methane,

*Corresponding author: Ilya M. Indrupskiy
E-mail: i-ind@ipng.ru

ethane, nitrogen and other components, as well as binary and multicomponent mixtures, on various adsorbents in a wide range of temperature and pressure conditions has been studied by many authors. Choi et al. (2003) studied the pure component adsorption of methane, ethane, ethylene, nitrogen, and oxygen on activated carbon. However, the pressure in the experiments did not exceed 2 MPa, which is significantly lower than the typical reservoir pressures. The adsorption isotherms presented by (Song et al., 2007) for pure components on zeolite indicate that the pore structure of even the same adsorbent can have a significant effect on the adsorption behavior, especially for hydrocarbons heavier than C_5. Luo et al. (2015) considered adsorption of not only pure components, but also their mixtures, and Wang et al. (2015) studied adsorption of methane-ethane mixtures in different proportions. It was shown that the ratio of the components of the mixture significantly affects the intensity of their adsorption. Yun et al. (2002) also studied methane, ethane, and their binary mixtures, but on the MCM-41 adsorbent, which is characterized by a chemically homogeneous pore surface and simple pore structure. In (Matsumoto et al., 1997) it was shown that Langmuir model provides a good approximation for the adsorption isotherms of the heavy components on activated carbon for pressures up to 0.1 MPa. However, this is not true for higher pressures (Dong et al., 2016).

Despite the fact that the adsorption of hydrocarbons in shales has been intensively studied in the last decade, considerable attention has not been paid to modeling the influence of adsorption on the dynamic changes in the composition of hydrocarbon mixture and its phase behavior. The study (Ambrose et al., 2011) provides an example of calculating the geological reserves (volumes-in-place) of shale gas, taking into account the difference in the composition of free gas and adsorbed fluid for a five-component model of a hydrocarbon mixture in a shale reservoir. Dong et al. (2016) and Sandoval et al. (2016) developed similar methods of taking into account multicomponent adsorption in calculations of the phase behavior of hydrocarbons. It is assumed that adsorption affects phase equilibrium by changing the effective radii of pores due to the formation of thin adsorption films on the surface of rocks, which leads to minor changes in capillary pressure. The work (Dong et al., 2016) also considers the shift of the critical point of mixture caused by adsorption. The results of both studies showed a practically insignificant effect of taking adsorption into account, despite the fact that the effect of capillary pressure in a porous medium on the phase behavior of fluids was significant. In both papers, the effect of dynamic adsorption/desorption on the fluid composition in pores with a change in pressure was not studied.

The article (Sandoval et al., 2018) presents an alternative algorithm for calculating the phase equilibrium of a hydrocarbon mixture (the so-called flash-algorithm), taking into account multicomponent adsorption and capillary pressure in pores. The authors established a significant impact of these factors on the phase envelope and the calculated compositions of hydrocarbon phases. They introduce a hypothetical "excess adsorbed phase" in phase behavior calculations which is not a real thermodynamic object. It reflects compositional difference of the real adsorbed phase from the bulk part of the mixture, for which the equilibrium calculation of fractions and compositions of the vapor and liquid phases is performed. Integral compositional balance includes the bulk part of the mixture in the total pore volume and the "excess adsorbed phase" in the volume occupied by the adsorbed substance. The results obtained are in qualitative agreement with known field and experimental data. However, the use of the proposed model for practical applications is highly complicated by the need to obtain a large amount of initial data for a multicomponent adsorption model in a real reservoir, which is heterogeneous in lithology, pore structure, physico-chemical characteristics, etc.

This article also presents a method for taking into account dynamic changes in the composition due to the adsorption/desorption of components when modeling the phase behavior of hydrocarbon mixtures in tight and shale reservoirs. The iterative algorithm differs from the one presented in (Sandoval et al., 2018), but also uses a multicomponent adsorption model to obtain the adsorbed amount of each component, and further use of the current composition of the "free fluid" in phase behavior calculations under given temperature and pressure conditions. To take into account the heterogeneity of real reservoir properties, such as porosity, specific surface area of pores, etc., a special control parameter has been introduced in the model. It has a certain physical meaning and can be measured experimentally for a real heterogeneous reservoir. On the other hand, if laboratory data for a specific heterogeneous reservoir are insufficient, adjustment of this parameter (e.g., by matching of the adsorbed fraction of fluid at initial reservoir conditions) provides an equivalent model which can be used in phase behavior calculations. This makes the method much more convenient in practical calculation for real deposits.

The developed method is illustrated by calculations of the phase behavior of a hydrocarbon mixture during the dynamic desorption of components caused by a decrease in pressure during the depletion of a deposit. A significant effect is shown of adsorption/desorption processes on the saturation pressure, as well as on the dynamics of the phases' composition.

In subsequent sections of the article, the model and computational algorithm are first described. Then their application is illustrated by the example of a multicomponent hydrocarbon mixture and the results obtained are discussed.

Mathematical model

In this section, we describe a model and a general computational algorithm that includes blocks for calculating phase equilibrium and dynamic multicomponent adsorption.

Phase equilibrium

The key assumption of the model is that the phase behavior of the hydrocarbon mixture during component adsorption by the reservoir surface can be described in the same way as in bulk. But it is necessary to take into account the change in the total composition of the "free part" of the mixture due to the adsorption/desorption of individual components. This assumption arose from the analysis of experimental data (Buleiko et al., 2007). Other possible effects of a porous medium, such as pressure differences between phases (capillary pressure in pore channels with regard to adsorption films) and the shift of a critical point, can be included in the model by analogy with the works (Dong et al., 2016; Sandoval et al., 2016; Sandoval et al., 2018). In this paper, they are not taken into account in order to emphasize the effect on the phase behavior of the dynamic change in the total composition of the mixture due to the adsorption/desorption of components.

The equilibrium of the vapor and liquid phases at a given pressure, temperature and total mixture composition is determined by the equality of chemical potentials for each component between the phases (Brusilovskii, 2002; Whitson, Brule, 2000):

$$\mu_{i,L} = \mu_{i,V}, \quad i = 1,..,N, \tag{1}$$

where i is the component index of the mixture; N is the total number of components in the mixture; μ_i is the chemical potential of component i; the subscripts L and V denote the liquid and vapor phases, respectively.

In terms of fugacities, equation (1) takes the form:

$$lnf_{i,L} = lnf_{i,V}, \quad i = 1,..,N \tag{2}$$

The fugacities of the components in the vapor and liquid phases can be found by the known thermodynamic relations based on the solution of the equation of state (EOS). In oil and gas applications, the Peng-Robinson cubic equation of state (Peng, Robinson, 1976) with the three-parameter modification (Jhavery, Youngren, 1988) has received the most distribution:

$$p = \frac{RT}{v-b} - \frac{a}{(v+c)(v+d)}, \tag{3}$$

where v is the molar volume of the phase; a is a coefficient depending on temperature T; b, c and d are constant coefficients. Usually, equation (3) is rewritten to the cubic form:

$$v^3 + \left(c + d - b - \frac{RT}{p}\right)v^2 + \left(\frac{a}{p} - bc + cd - bd - \frac{RTd}{p} - \frac{RTc}{p}\right)v - \left(bcd + \frac{RTcd}{p} + \frac{ab}{p}\right) = 0. \tag{4}$$

The acentric factor ω_i, critical pressure P_{ci} and temperature T_{ci} for each component i, as well as the binary interaction coefficients of the components, are used to calculate the coefficients a, b, c and d in equation (4) for a given phase composition. Further, equation (4) is solved with respect to the z-factor $z = \frac{pv}{RT}$. The z-factor of the phase is then used to calculate the component fugacities (Brusilovskii, 2002).

Equations (2) must be supplemented by normalization constraints. The final system of algebraic equations for determining the fractions and compositions of the equilibrium phases is:

$$\begin{cases} lnf_{i,L} - lnf_{i,V} = 0, \quad i = 1,..,N \\ x_i L + y_i V - z_i = 0, \ i = 1,..,N \\ \sum_{i=1}^{N} y_i - 1 = 0 \\ L + V = 1 \end{cases} \tag{5}$$

Determination of the equilibrium molar fractions of L and V and the compositions (molar concentrations of the components) y_i and x_i of the vapor and liquid phases based on system (5) given the total composition of the mixture z_i, pressure p and temperature T is called the phase equilibrium problem, or the "flash" problem. To solve it, a number of methods are used, among which the method of successive substitutions, the Newton method and their modifications are most common (Michelsen, 1982 (a); Brusilovskii, 2002). These iterative procedures include solving the Rachford-Rice equation for V (Whitson, Brule, 2000):

$$F(V) = \sum_{i=1}^{N} \frac{z_i(K_i-1)}{V(K_i-1)+1} = 0, \tag{6}$$

where $K_i = \frac{y_i}{x_i}$ are the K-values (equilibrium constants). Initial estimates for K_i can be found from the Wilson correlation

$$K_i = \frac{P_{ci}}{P} exp\left[5{,}373(1+\omega_i)(1-\frac{T_{ci}}{T})\right] \tag{7}$$

or obtained using phase stability analysis (Michelsen, 1982 (b)). If the phase equilibrium calculations are repeated for varying temperature and pressure conditions, then initial approximations for K_i can be obtained from the solution found at previous pressure/temperature values.

The described procedure is widely used in calculations of the phase behavior of hydrocarbon mixtures as applied to the modeling and design of field development. Nonessential changes can be introduced to the system of equations (5) to take into account capillary pressure (Brusilovskii, 2002; Sandoval et al., 2016) and some other features of the porous medium (Dong et al., 2016).

In the proposed method, taking into account the adsorption of components, the novelty in the described procedure is that z_i in system (5) is not the total composition of the hydrocarbon mixture in the element of the porous medium, but the composition of free (not adsorbed) part of it. As compared to (Sandoval etc., 2018), only the composition z_i of the free part of the mixture is used in calculations, while its volume and density are not involved, and "excess adsorbed phase" is not required. We describe these differences in more detail below.

One more feature is also important to be noted. Using the composition z_i of the free part of the mixture in phase equilibrium calculations is not equivalent to adopting a constant composition of the mixture in accordance with the ideally collected sample of the initially free formation fluid and performing further calculations using standard procedures. The proposed method takes into account that in the conditions of field development the composition of free part of the hydrocarbon mixture changes continuously due to dynamic adsorption/desorption of components.

Multicomponent adsorption

In publications, one can find a rather large amount of experimental data on the adsorption of individual hydrocarbons on various adsorbents. However, most of these results were obtained either at too low pressures or on industrial adsorbents, and therefore are not suitable for direct application to oil and gas reservoirs. The exception is methane, due to worldwide interest in its reserves in coal beds and shale gas deposits.

In addition to problems with experimental data, there is the question of choosing adequate adsorption models. For alkanes up to C_4H_{10}, as well as for CO_2 and some other non-hydrocarbon components, the monolayer Langmuir adsorption model (Langmuir, 1918) was found to be satisfactory in most studies:

$$n = n_{max}(T)\frac{b(T)\cdot P}{1+b(T)\cdot P}, \quad (8)$$

where n_{max} is the maximum amount of the substance (adsorbate) that can be adsorbed at given temperature T on the surface of the adsorbent; b is the adsorption equilibrium constant.

Higher alkanes require more complex models, such as the Toth model (Toth, 1971) and its modifications, or the BET model (Brunauer et al., 1938). Some examples of the application of these models for the adsorption of hydrocarbons are given in (Dong et al., 2016).

For multicomponent adsorption, the Langmuir model can be expanded by introducing fugacities instead of partial pressures, which leads to the following expression for the adsorption isotherm of an individual component of the mixture:

$$n_i = n_{max,i}\frac{b_i(T)f_i(P,T)}{1+\sum_{i=1}^{N} b_i(T)f_i(P,T)}. \quad (9)$$

It is assumed that $n_{max,i}$ and b_i can be obtained using standard Langmuir analysis of experimental data on single-component adsorption.

Although the multi-component Langmuir model (MLM) (9) for alkanes up to C_4H_{10} gives satisfactory results in predicting the total amount of adsorbed mixture, it does not always adequately describe the adsorption selectivity, i.e. the adsorbed amount of each component. More complex models of multicomponent adsorption of hydrocarbons are presented and studied in the literature (Gusev et al., 1996), but none of them has been recognized as universally suitable for predicting adsorption at high pressures typical for oil and gas reservoirs (Sandoval et al., 2016).

Like the authors of (Sandoval et al., 2018), for the purposes of this work we limit ourselves to using the MLM model. Along with the reasons mentioned above, this choice is related to the input data of a shale reservoir adopted for test calculations, which we describe below. Nevertheless, it is important to emphasize that the proposed method allows the use of any model of multicomponent adsorption, which is of special importance for hydrocarbons higher than C_4H_{10} at pressures and temperatures typical for real reservoirs.

The choice of input data for following calculations was dictated, as mentioned, by practical absence of suitable experimental data for modelling of multicomponent adsorption of hydrocarbons at high pressures. As can be seen from the review in (Dong et al., 2016), there are no experimental data in the literature obtained at least for alkanes from methane to butane on the same adsorbent, at the same temperature and in a suitable pressure range. In the following examples, we use the data of (Ambrose et al., 2011) on the parameters of the Langmuir adsorption isotherms for hydrocarbons from methane to butane on shale rock at a temperature of 355°K (180°F) and pressures up to 310 bar (4500 psi) (Table 1). It should be noted that the data for butane in the (Ambrose et al., 2011) are obtained based on correlations of adsorption parameters with the number of carbon atoms in the alkane molecule.

Using the model of multi-component adsorption, one can calculate the adsorbed amount of each component. However, this is not enough to determine the composition of the adsorbed and free parts of the mixture in a porous medium for the following reasons.

• Although the adsorption process is associated with the pore surface, experimental data are usually available

Parameter	C1	C2	C3	C4
n_{max}, mmol/g	0.0670	0.109	0.214	0.277
b, 1/bar	0.009285	0.0179	0.0172	0.0409

Table 1. Langmuir coefficients for adsorption of pure alkanes on shale rock at 355 °K (according to (Ambrose et al., 2011), 1 bar = 10^5 Pa)

per unit mass of the adsorbent. This means that they cannot be transferred to adsorbents (reservoir zones) with different porosity, specific surface area of pores, mineral composition, content of bound water, etc., while in reality these characteristics are changed significantly even within the same deposit.

• The fraction of the adsorbed part of the mixture is a relative value. It depends not only on the adsorbed amount of mixture, but also on the total amount of the mixture per unit volume of pores (or specific surface area of pores) of the reservoir, which also varies significantly in actual conditions.

To overcome these two problems, we introduce into the model a single control parameter υ, which is expressed in mmol/g and corresponds to the total amount of the mixture per unit mass of the adsorbent (reservoir rock). Total amount of the mixture included in υ corresponds to hydrocarbons both in the adsorbed and free state.

The parameter υ can be treated as the total amount of hydrocarbons which "came" into the pores of a separate reservoir element, after which some part of it was adsorbed on the rock surface at current thermobaric conditions. Experimentally υ can be determined by extraction of all hydrocarbons from isolated rock element (sealed core specimen) of the reservoir. To account for reservoir heterogeneity, direct petrophysical dependencies of υ on reservoir parameters determined from well logs can be established and used. Note that to get the value of υ, one doesn't need to know free and adsorbed amounts of the mixture separately.

For an isolated reservoir element, value of υ remains constant under changes of pressure and temperature, while fractions, densities and other characteristics of the adsorbed and free parts of the mixture, as well as the number and properties of free (bulk) phases and even pore volume would change. Treating υ as constant is appropriate in the same bounds as total mixture composition $z_{bulk,i}$ in conventional PVT calculations. If simulated process assumes mass transfer between the element and the environment (e.g., constant volume depletion (CVD) or compositional simulation of fluid flow), then changes in υ are computed simultaneously with changes in $z_{bulk,i}$ by the balance of inflow/outflow to/from the reservoir element for each mixture component.

With a lack of direct experimental data, υ can be determined using information on the fraction of adsorbed hydrocarbons for a particular section of the reservoir or reservoir type at initial reservoir pressure p_0 and temperature T. For example, for the Barnett shale formation (USA), this fraction varies from 20 to 40 %. Given a certain value of the adsorbed fraction of hydrocarbons, initial approximation for υ can be calculated by determining the adsorbed amount of mixture at p_0 and T in a unit reservoir element from the Langmuir equation (8) applied to the component with the largest concentration in the mixture. Then, phase equilibrium calculations are performed with multicomponent adsorption at p_0, T and given total mixture composition, as described in the next subsection. The total fraction of adsorbed hydrocarbons obtained using the model is compared with the actual one, and υ is adjusted accordingly. It may take several iterations. As soon as υ is adjusted by actual data, the model is ready for dynamic calculations, for example, with varying pressure.

Computational procedure

Since we consider the equilibrium phase behavior and adsorption, simulation of the process with dynamic changes in pressure (or/and temperature) can be performed in a sequence of independent calculations for each step in p (and T), as in conventional PVT simulations. The computational procedure for a given pressure and temperature is as follows.

An iterative loop is implemented. At each iteration, the phase equilibrium (flash) problem (5) is solved first for the total composition of the free part of the mixture z_i. Then, using the obtained fugacity values, the adsorbed amounts of each component n_{adsi} are determined with the multicomponent adsorption model (for example, the MLM model (9)). After that, the composition of the free part of the mixture is adjusted as follows:

$$z_i = \left(\nu \cdot z_{bulk,i} - n_{ads,i}\right) / \left(\nu - \sum_{j=1}^{N} n_{ads,j}\right), \quad i = 1,..,N, \tag{10}$$

or equivalently

$$z_i = \left(z_{bulk,i} - n_{ads,i}/\nu\right) / \left(1 - \sum_{j=1}^{N} n_{ads,j}/\nu\right), \quad i = 1,..,N, \tag{11}$$

where $z_{bulk,i}$ corresponds to the full total composition of the mixture (free + adsorbed part), and $z_i = z_{bulk,i}$ at the initial iteration.

A flowchart of the computational procedure in the case of calculating phase equilibria by the method of successive substitutions is shown in Fig. 1. According to the experience of the performed calculations, no more than 3-5 external iterations are usually required to find a solution (q-iterations in Fig. 1).

The following feature of the method is meaningful for practical applications.

The adsorbed amount of hydrocarbons in a reservoir element is determined by the fluid composition, pressure, temperature, and rock properties. Since reservoir rocks are highly inhomogeneous, application of, e.g., the method of (Sandoval et al., 2018) requires obtaining enough experimental data on multicomponent adsorption isotherms for different combinations of reservoir parameters – mineral composition, specific pore surface, pore size distribution, water content, etc., which is practically almost impossible.

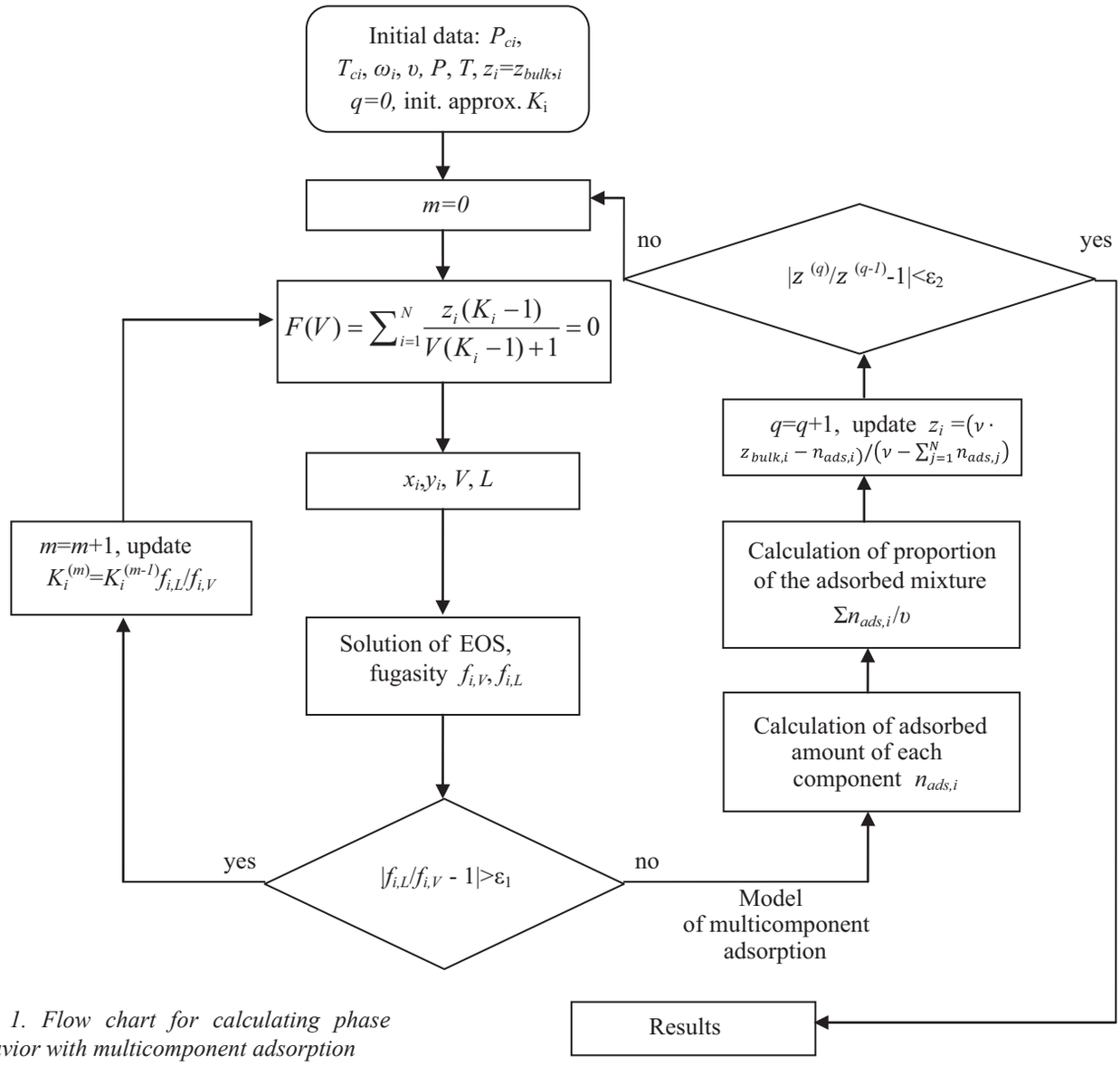

Fig. 1. Flow chart for calculating phase behavior with multicomponent adsorption

Within the framework of our method, in a lack of input data, the following approach can be used. Adjustment of υ allows to "scale" multicomponent adsorption isotherms obtained in a limited number of experiments (or taken from similar rocks), so that the shape of the isotherm and relative adsorption of components (selectivity) are maintained, while the total adsorption intensity is matched according to variations in rock mineral composition and properties.

Specifically, for fixed thermobaric conditions and given parameters of the adsorption model, change in υ would not influence the values of n_{adsi}. But as formula (11) shows, the effect of changing υ on relative parameters – fraction of the free part of the mixture and its composition z_i – is equivalent to the effect of proportional change in n_{adsi}, i.e. "scaling" of adsorption isotherms. Thus, adjusting υ (e.g., by matching initial fraction of the adsorbed mixture, as described above) allows to perform phase behavior calculations with account for adsorption in a lack of experimental data.

Example calculations

To illustrate the features of the model and evaluate the effect of dynamic adsorption/desorption on phase behavior, test calculations were performed for a three-component methane-ethane-butane mixture. The total mixture composition and thermobaric conditions are given in Table 2. Three cases with different values of υ, also presented in Table 2, are considered. These values correspond to specified fractions of the adsorbed part of the mixture at initial pressure – 10, 25, or 40 %. The

Parameter	**Value**		
Total composition $z_{bulk,i}$, mol.%	C1 – 25, C2 –15, C4 – 60		
Temperature , °K	355		
Initial pressure, bar	276		
υ, mmol/g	0.99	0.39	0.238
Initial fraction of adsorbed part of the mixture, mol.%	10	25	40

Table 2. Data for test calculations

parameters for the multicomponent MLM adsorption model are listed in Table 1.

The process of isothermal pressure depletion is simulated while maintaining the total composition of the mixture. In conventional PVT simulations, this corresponds to the process of constant composition expansion (CCE). However, in our case, the phase behavior cannot be described using the traditional calculation of CCE due to the dynamic changes in the composition of free part of the mixture.

Fig. 2 shows the free and adsorbed fractions of the components of the mixture at initial conditions (p = 276 bar) for the three cases with different υ. All values are normalized by the total amount of the mixture. Note that due to the most intense adsorption of butane, its adsorbed fraction is larger than the adsorbed fraction of the mixture as a whole, whereas the opposite situation is observed for other components. The composition of free part of the mixture corresponds to the single-phase liquid state.

At p = 100 bar, the free part of the mixture remains single phase, but its composition is slightly different from the initial one due to the different relative desorption of the components. Table 3 shows how the total composition of the free part of the mixture changes with a decrease in pressure for υ = 0.238 mmol/g.

For the accepted total composition of the mixture, the saturation pressure in bulk (no adsorption) is estimated at 68 bar. When calculated with adsorption for the free

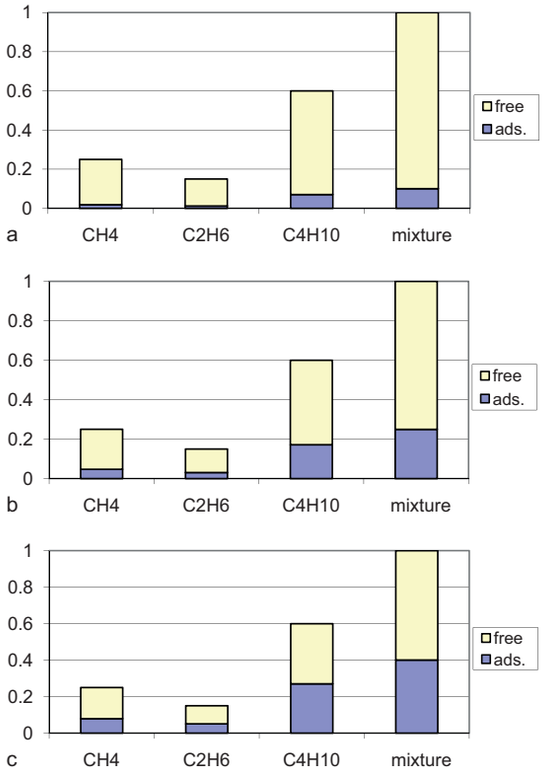

Fig. 2. Free and adsorbed fractions of the mixture components at initial pressure of 276 bar: a – υ = 0.99, b – υ = 0.39, c – υ = 0.238 mmol/g

Pressure, bar	Composition of the free part of the mixture z_i, mol. %		
	C1	C2	C4
276	0.2845	0.1652	0.5503
100	0.2949	0.1643	0.5408
70	0.2942	0.1635	0.5423
40	0.3397	0.1807	0.4797

Table 3. Composition of the free part of the mixture at various pressures and υ = 0,238 mmol/g

part of the mixture, it increases by up to 5 bar (Table 4).

Fig. 3 shows the dynamics of the mole fraction of the vapor phase V versus pressure. Desorption of components leads to quite significant changes in phase behavior. For example, at p = 50 bar in bulk (without adsorption) the mole fraction of the vapor phase is V = 0.38, and for υ = 0.238 mmol/g – V = 0.56.

In Fig. 3 the dotted line is of the greatest interest. It corresponds to the dynamics of the vapor phase fraction calculated using standard (in bulk) phase equilibrium algorithms. But here the mixture composition is taken to be equal to the composition of the free part of the mixture obtained at the initial pressure for the case υ = 0.238 mmol/g. This corresponds to the situation when a sample of reservoir fluid is collected under initial reservoir conditions, and conventional PVT experiments and simulations are carried out on it. Despite the fact that the saturation pressure in this case turns out to be the same as when taking into account dynamic desorption, the dynamics of the phase behavior in the two-phase region are significantly different, and the fraction of the vapor phase is greatly underestimated. This clearly demonstrates the effect of dynamic adsorption/desorption on phase behavior, in contrast to static adsorption which affects only the initial composition of the mixture.

No adsorption	υ, mmol/g		
	0.99	0.39	0.238
68	69	71	73

Table 4. Calculated saturation pressure, bar

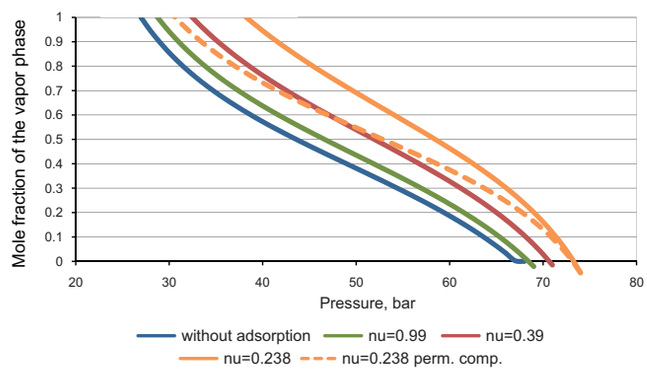

Fig. 3. Dynamics of the mole fraction of the vapor phase versus pressure at various values of υ, mmol/g

It should also be noted that the most pronounced effect of different relative dynamics of the desorption of components is observed in the two-phase region (Table 3, Fig. 3). Fig. 4a and 4b show the dynamics of the mole fraction of methane and butane in the free part of the mixture for different values of υ to illustrate this effect. Fig. 5 and 6 show the adsorbed and free fraction of each component in the vapor and liquid phases for two

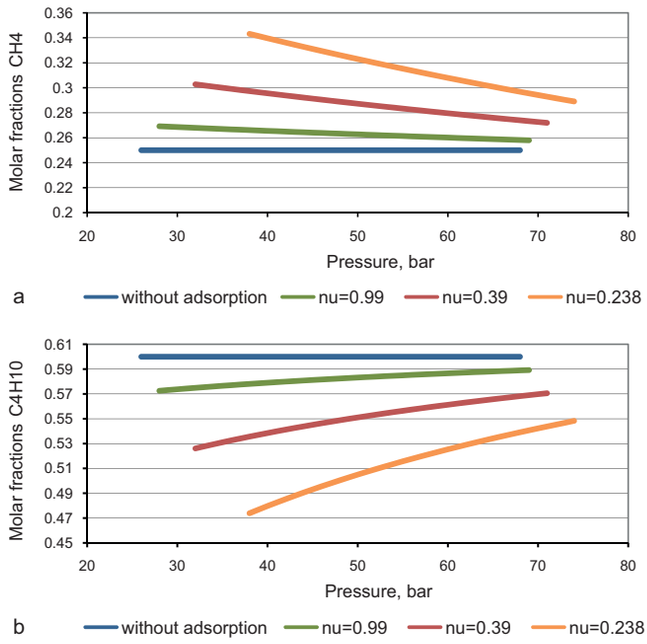

Fig. 4. Molar fractions of methane (a) and butane (b) versus pressure at various values of υ, mmol/g

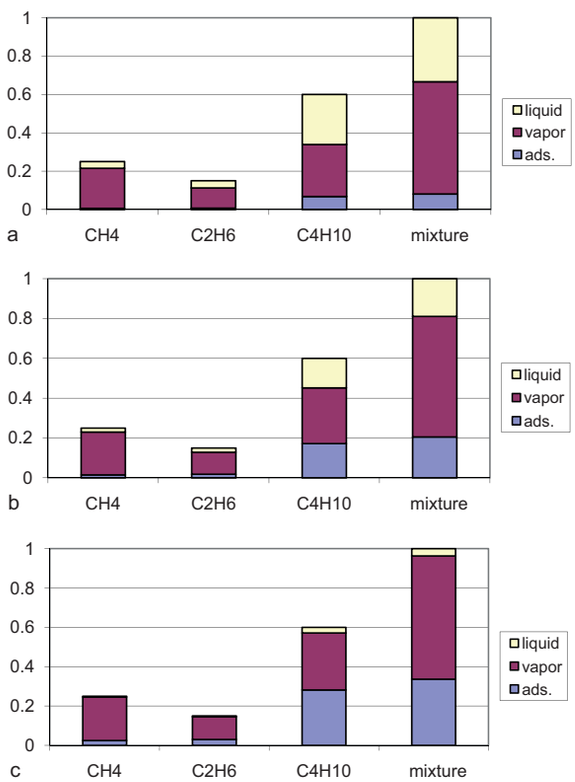

Fig. 5. Fractions of the mixture components in the adsorbed part, vapor and liquid phases at P = 65 bar: a – υ = 0.99, b – υ = 0.39, c – υ = 0.238 mmol/g

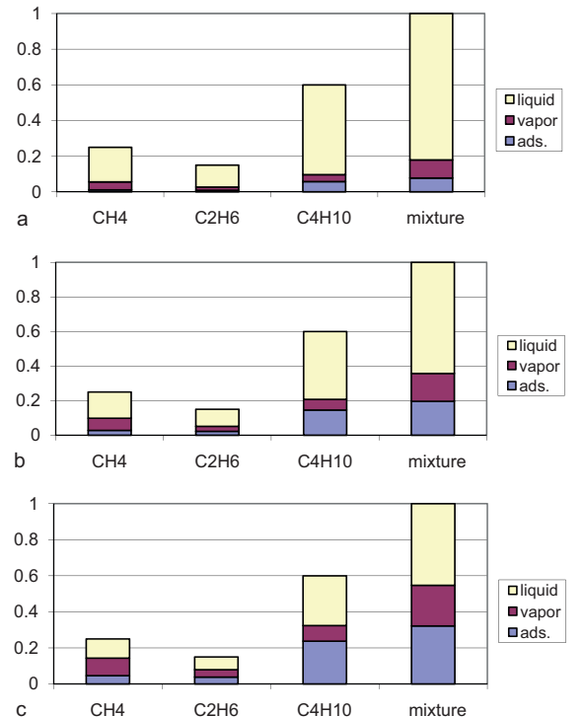

Fig. 6. Fractions of the mixture components in the adsorbed part, vapor and liquid phases at P = 40 bar: a – υ = 0.99, b – υ = 0.39, c – υ = 0.238 mmol/g

values of pressure in the two-phase region. Here again, the significant effect of multicomponent adsorption on the equilibrium fractions and compositions of the phases is evident.

Conclusions

In the paper, we presented a new method for phase behavior simulation of hydrocarbon mixtures under adsorption conditions. Dynamic multicomponent adsorption/desorption is considered as a key factor affecting the composition of the free part of the mixture and phase equilibrium. For calculations of the phase behavior in the presence of multicomponent adsorption, we presented a mathematical model, developed a computational algorithm and proposed a control parameter that takes into account variations in properties of the reservoir and the total adsorption intensity.

Test calculations were carried out for a three-component hydrocarbon mixture with adsorption and thermobaric parameters corresponding to the example of a real shale reservoir. The simulation results clearly demonstrate the significant effect of dynamic multicomponent adsorption/desorption on phase behavior.

The mechanism described in the model can be critical in shale and tight reservoirs where a decrease in pressure leads to different relative desorption of components. This significantly affects the composition of the free part of the mixture, as well as the fracttions and compositions of the phases in the two-phase region. Therefore, the effect of multicomponent adsorption is to be considered dynamically.

Acknowledgements

The study was carried out in the framework of the OGRI RAS State Research Contract on the topic "Justification of innovative environmentally responsible technologies for the development of hydrocarbon deposits in difficult geological conditions based on 3D computer simulations, laboratory experiments and field research" No. AAAA-A19-119022090096-5.

References

Ambrose R.J., Hartman R.C., Labs W., Akkutlu I.Y. (2011). SPE 141416. Multi-component Sorbed-phase Considerations for Shale Gas-in-place Calculations. *SPE Production and Operations Symp.*, pp. 1-10. https://doi.org/10.2118/141416-MS

Aziz K., Wong T. (1989). Considerations in the development of multipurpose reservoir simulation models. *First and Second Forum on Reservoir Simulation*, pp. 77-208.

Brunauer S., Emmett P.H., Teller E. (1938). Adsorption of Gases in Multimolecular Layers. *Journal of the American Chemical Society*, 60(2), pp. 309-319. https://doi.org/10.1021/ja01269a023

Brusilovskii A.I. (2002). Phase transformations in the development of oil and gas fields. Moscow: Graal, 575 p.

Buleiko V.M., Voronov V.P., Zakirov S.N., Zakirov E.S., Indrupskii I.M. (2007). Regularities in the behavior of hydrocarbon systems of oil and gas pools. *Doklady Earth Sciences*, 415(1), pp. 686-689. https://doi.org/10.1134/S1028334X07050054

Choi B.U., Choi D.K., Lee Y.W., Lee B.K. (2003). Adsorption Equilibria of Methane, Ethane, Ethylene, Nitrogen, and Hydrogen onto Activated Carbon. *J. Chem. Eng.*, 48, pp. 603-607. https://doi.org/10.1021/je020161d

Coats K.H. (1998). Implicit Compositional Simulation of Single-Porosity and Dual-Porosity Reservoirs. *SPE Symp. on Reservoir Simulation,* SPE 18427

Dong X., Liu H., Hou J., Wu K. Chen Z. (2016). Phase Equilibria of Confined Fluids in Nanopores of Tight and Shale Rocks Considering the Effect of Capillary Pressure and Adsorption Film. *Industrial & Engineering Chemistry Research*, 55(3), pp. 798-811. https://doi.org/10.1021/acs.iecr.5b04276

Gusev V., O'Brien J.A., Jensen C.R.C., Seaton N.A. (1996). Theory for Multicomponent Adsorption Equilibrium: Multispace Adsorption Model. *AIChE Journal*, 42(10), pp. 2773-2783. https://doi.org/10.1002/aic.690421009

Jhavery B.S., Youngren G.K. (1988). Three-Parameter Modification of the Peng-Robinson Equation of State to Improve Volumetric Predictions. *SPE Reservoir Engineering*, 3, p. 1033. https://doi.org/10.2118/13118-PA

Langmuir I. (1918). The Adsorption of Gases on Plane Surface of Glass, Mica and Platinum. *The Research Laboratory of the General Electric Company*, 40, pp. 1361-1402. https://doi.org/10.1021/ja02242a004

Luo X., Wang S., Wang Z., Jing Z., Le M., Zhai Z., Han T. (2015). Adsorption of Methane, Carbon Dioxide and Their Binary Mixtures on Jurassic Shale from the Qaidam Basin in China. *Int. J. Coal Geol.*, 150-151, pp. 210-223. https://doi.org/10.1016/j.coal.2015.09.004

Matsumoto A., Zhao J., Tsutsumi K. (1997). Adsorption Behavior of Hydrocarbons on Slit-Shaped Micropores. *Langmuir*, 13, pp. 496-501. https://doi.org/10.1021/la9509581

Michelsen M.L. (1982a). The Isothermal Flash Problem. Part II. Phase-Split Calculation. *Fluid Phase Equilibria*, 9, pp. 21-40. https://doi.org/10.1016/0378-3812(82)85002-4

Michelsen M.L. (1982b). The Isothermal Flash Problem. Part I. Stability. *Fluid Phase Equilibria*, 9, pp. 1-19. https://doi.org/10.1016/0378-3812(82)85001-2

Nojabaei B., Johns R.T., Chu L. (2013). Effect of Capillary Pressure on Phase Behavior in Tight Rocks and Shales. *SPE Reservoir Eval. Eng.*, 16, pp. 281-289. https://doi.org/10.2118/159258-PA

Pang J., Zuo J., Zhang D., Du L. (2013). Effect of Porous Media on Saturation Pressure of Shale Gas and Shale Oil. *Proc. Int. Petro. Techn. Conf.* Beijing, pp. 1-7, IPTC 16419. https://doi.org/10.2523/IPTC-16419-MS

Pedersen K.S., Christensen P.L. (2006). Phase Behavior of Petroleum Reservoir Fluids. Taylor & Francis, USA. https://doi.org/10.1201/9781420018257

Peng D.Y., Robinson D.B. (1976). A New Two-Constant Equation of State. *Ind. Eng. Chem. Fundam.*, 15, p. 59. https://doi.org/10.1021/i160057a011

Shapiro A., Stenby E.H. (2001). Thermodynamics of the Multicomponent Vapor-Liquid Equilibrium under Capillary Pressure Difference. *Fluid Phase Equilib.,* 178, pp. 17-32. https://doi.org/10.1016/S0378-3812(00)00403-9

Sandoval D., Yan W., Michelsen M., Stenby E. (2016). Model Comparison for High-pressure Adsorption in Shale and its Influence on Phase Equilibria. *ECMOR XV – 15th European Conference on the Mathematics of Oil Recovery*, Proc., Mo Efe 02. https://doi.org/10.3997/2214-4609.201601740

Sandoval D.R., Yan W., Michelsen M.L., Stenby E.H. (2018). Influence of Adsorption and Capillary Pressure on Phase Equilibria Inside Shale Reservoirs. *Energy & Fuels,* 32(3), pp. 2819-2833. https://doi.org/10.1021/acs.energyfuels.7b03274

Song L., Sun Z., Duan L., Gui J., McDougall G.S. (2007). Adsorption and Diffusion Properties of Hydrocarbons in Zeolites. *Microporous and Mesoporous Materials*, 104, pp. 115-128. https://doi.org/10.1016/j.micromeso.2007.01.015

Toth J. (1971). State Equations of the Solid Gas Interface Layer. *Act. Chim. Acad. Sci. Hung.*, 69, p. 311.

Wang Y., Tsotsis T.T., Jessen K. (2015). Competitive Sorption of Methane/Ethane Mixtures on Shale: Measurements and Modeling. *Ind. Eng. Chem. Res.,* 54, pp. 12187-12195. https://doi.org/10.1021/acs.iecr.5b02850

Whitson C.H., Brule M.R. (2000). Phase Behavior. SPE Monograph (Henry L. Doherty) Series, Vol. 20, SPE, Richardson, Texas USA.

Yun J.H., Duren T., Keil F.J., Seaton N.A. (2002). Adsorption of Methane, Ethane and Their Binary Mixtures on MCM-41: Experimental Evaluation of Methods for the Prediction of Adsorption Equilibrium. *Langmuir*, 18, pp. 2693-2701. https://doi.org/10.1021/la0155855

Zendehboudi S., Bahadori A. (2015). Shale Oil and Gas Handbook: Theory, Technologies, and Challenges. Gulf Professional Publ.

About the Authors

Olga A. Lobanova – Cand. Sci. (Engineering), Researcher, Oil and Gas Research Institute of the Russian Academy of Sciences

3, Gubkin st., Moscow, 119333, Russian Federation

Ilya M. Indrupskiy – Dr. Sci. (Engineering), Head of the Laboratory, Oil and Gas Research Institute of the Russian Academy of Sciences

3, Gubkin st., Moscow, 119333, Russian Federation

E-mail: i-ind@ipng.ru

Manuscript received 19 March 2019;
Accepted 5 December 2019; Published 30 March 2020

ORIGINAL ARTICLE
DOI: https://doi.org/10.18599/grs.2020.1.22-31

The chemical composition and age of monazite and kularite from titanium ore of Pizhemskoye and Yarega deposits (Middle and Southern Timan)

A.B. Makeyev[1], S.E. Borisovsky[1], A.O. Krasotkina[2]*
[1]*Institute of Ore Geology, Petrography, Mineralogy and Geochemistry of the Russian Academy of Sciences, Moscow, Russian Federation*
[2]*Institute of Precambrian Geology and Geochronology of the Russian Academy of Sciences, Saint-Petersburg, Russian Federation*

Abstract. A study on the typomorphic characteristics and age of the monazite the two giant titanium deposits of the Timan – Pizhemskoye and Yarega, which revealed differences in morphology in the species composition of the inclusions, the grain size, distribution of chemical types of a mineral associated with conditions of crystallization and different sources of the substance. The isochronous Th-Pb monazite age was calculated using the CHIME method. For Yarega monazite built three isochrone with age 1301, 1105 and 778 Ma; for Pizhemsky monazite-kularite one isochrone with age 782 Ma. Source of hith-Th monazite Yarega oil-titanium deposit could be ancient granite batholith and the origin Yarega less-Th monazite and Nd-Ce-monazite-kularite Pizhemskoye deposit with an age of ~ 780 Ma could be related to the hydrothermal conversion of the weathering crusts on lamprophyres close in age with lamprophyre (spessartite and kersantite) of Chetlassky Kamen.

Keywords: Pizhemskoye titanium, Yarega oil-titanium deposits, Timan, monazite, kularite, chemical composition, age

Recommended citation: Makeyev A.B., Borisovsky S.E., Krasotkina A.O. (2020). The chemical composition and age of monazite and kularite from titanium ore of Pizhemskoye and Yarega deposits (Middle and Southern Timan). *Georesursy = Georesources*, 22(1), pp. 22-31. DOI: https://doi.org/10.18599/grs.2020.1.22-31

Monazite is a phosphate of cerium-group light rare-earth elements. It is a rare but very informative compositionally variable mineral occurring in Timan titanium deposits and occurrences. Its typomorphic characteristics are studied to better understand the genesis, age and sources of the substance in titanium deposits (Makeyev, 2016; Makeyev, Dudar, 2001; Makeyev et al., 2008; Skublov et al., 2018). The goal of the present project is to study monazite from two Russia's giant titanium deposits: Pizhemskoye and Yarega. The deposits are similar in geological structure and possibly genesis but are different from other titanium deposits in the non-standard phase-mineral composition (ilmenite-pseudorutile-leucoxene-quartz and siderite-leucoxene-quartz) of titanium ores. The non-standard phase composition of titanium ores (Ignatiev, Burtsev, 1997; Kalyuzhny, 1982; Makeyev, 2016; Makeyev, Dudar, 2001) from these deposits would require a preliminary chemical stage to remove silicon from leucoxene and pseudorutile, to manufacture commercial products (artificial porous rutile, etc.) and to launch the economic mining of these deposits that are highly important for Russia. As monazite is a principal recoverable constituent of titaniferous sandstone (because it occurs in the ore as free grains), the economic profitability and cost price of the economic mining of the above deposits will undoubtedly increase.

The goal of the present study is to better understand the chemical composition pattern of monazite grains from the Yarega and Pizhemskoye deposits and to estimate the time of their formation using the CHIME – chemical Th-U-total Pb isochrone method (chemical isochrone method) proposed by K. Suzuki (Suzuki, Adachi, 1991; Suzuki, Kato, 2008).

Method for monazite grain analysis

Monazite was analyzed at the Institute of Ore Geology, Petrography, Mineralogy and Geochemistry of the Russian Academy of Sciences (IGEM RAS), on a JXA-8200 wave microprobe. Fifty-nine analyses of the composition of monazite grains from two industrial samples per 15 constituents: matrix (P_2O_5, La_2O_3, Ce_2O_3, Pr_2O_3, Nd_2O_3, Sm_2O_3, Y_2O_3, ThO_2) and trace constituents (CaO, SiO_2, UO_2, PbO, FeO, MnO, SO_3) were done.

*Corresponding author: Alexander B. Makeyev
E-mail: abmakeev@igem.ru

Special analytical conditions were as follows: ThO_2, UO_2, PbO: an accelerating voltage of 20 kV, a probe current of 150 nA and a PET analyzer crystal (Table 1). Age was calculated from the results of electron-probe X-ray spectral determination of ThO_2, UO_2 and PbO using the CHIME method. The positive results of our studies based on this method are described in (Votyakov et al., 2011; Makeyev, Viryus, 2013; Pilyugin, Mukhanova, 2008; Popova et al., 2010; Williams et al., 2007, etc).

Calculations of estimated **ThO_2*** concentration for constructing an isochrone were made using the formula:

$$\omega(ThO_2^*) = \omega(ThO_2) + \omega(UO_2)\cdot M(ThO_2)/M(UO_2)\cdot \{[(e^{\lambda 232t} + 137.88\cdot e^{\lambda 238t})/138.88] - 1\}/(e^{\lambda 232t} - 1),$$

where $\omega(ThO_2)$ and $\omega(UO_2)$ are the mass fraction of thorium oxide (IV) and uranium oxide (IV) in monazite; $M(ThO_2)$ and $M(UO_2)$ are the molar masses of thorium oxide (IV) and uranium oxide (IV); λ_{232} and λ_{238} are decay constants for thorium and uranium isotopes, respectively; it is the time taken by the decay.

Age calculation:

$$T = \{\ln(m\cdot[M(ThO_2)/M(PbO)] + 1)\}/\lambda_{232},$$

where m is the inclination of the isochrone.

Analytical results for monazite composition and age calculations are shown in Tables 2 and 3. U and Pb were not estimated in all the grains analyzed because of their low concentrations. Therefore, 52 monazite analyses out of 59 were used for age estimation and isochrones construction.

Materials

Yarega monazite. The grains and crystal fragments of Yarega monazite were extracted from an ultra-heavy fraction of a big (several tons) industrial sample. They are small in size (84×49 – 110×80, average size 93×63 μm) and display an isometric to mildly elongated irregular shape with a perfect cleavage; no other phases, except for scarce quartz inclusions, were found inside the grains (Fig. 1). Yarega monazite is concentrated to form a fine (< 0.125 μm) non-magnetic leucoxene fraction together with zircon and rutile. The chemical composition of monazite is shown in Table 2.

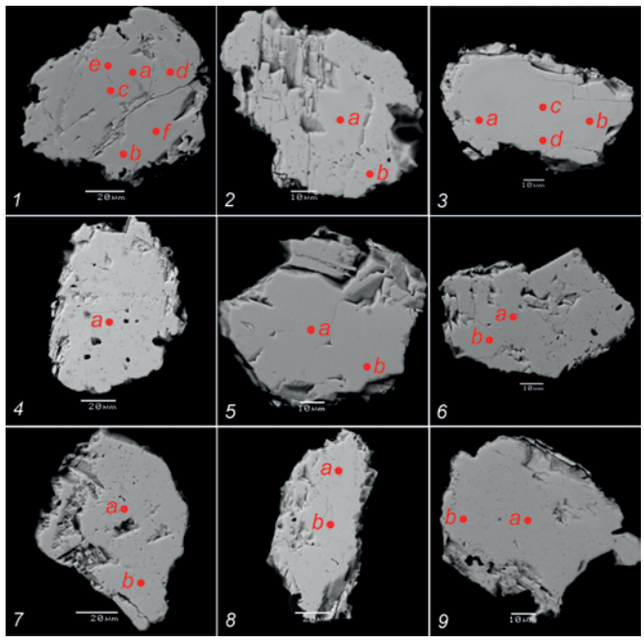

Fig. 1. Electron microscopy images (backscattered electron regime) of nine Yarega monazite grains. Ce-La-Th-monazite grains (1-3) are zonal. Thorium is more abundant in the cores than on the margins. Points indicate the location of microprobe analyses, whose symbols coincide with numbers in Table 2.

Elements in composition	Analytic line	Analyzer crystal	Exposure Line/background, s	Standard	Limit of deterction 3 σ (ppm)
Th	ThMα	PETJ	50/25	ThO_2	210
U	UMβ	PETH	100/50	UO_2	150
Pb	PbMα	PETH	150/75	$PbCrO_4$	120
La	LaLα	PETJ	10/5	$LaPO_4$	900
Ce	CeLα	PETJ	10/5	$CePO_4$	950
Pr	PrLβ	LiF	60/30	$PrPO_4$	725
Nd	NdLα	LiF	50/25	$NdPO_4$	500
Sm	SmLβ	LiF	60/30	$SmPO_4$	600
Y	YLα	TAP	30/15	YPO_4	200
P	PKα	TAP	10/5	Apatite	270
Ca	CaKα	PETH	10/5	$CaAl_2Si_2O_8$	120
Si	SiKα	TAP	10/5	$NaFeSi_2O_6$	200
Fe	FeKα	LiF	10/5	$NaFeSi_2O_6$	400
Mn	MnKα	LiF	10/5	$Mn_3Al_2[SiO_4]_3$	400
S	SKα	PETH	10/5	$BaSO_4$	180

Table 1. Analytical conditions for certain elements in monazite composition. The monazite samples were analyzed at IGEM RAS, on a JXA-8200 wave microanalyzer with five X-ray spectrometers at a voltage of 20 kV and a current of 150 mA. The probe diameter is 5 μm.

No	P_2O_5	La_2O_3	Ce_2O_3	Pr_2O_3	Nd_2O_3	Sm_2O_3	Y_2O_3	UO_2	ThO_2	PbO	CaO	SiO_2	FeO	MnO	SO_3	Total	ThO_2*	Age
1 a	30.84	12.11	25.84	2.99	11.75	2.05	2.68	0.305	6.496	0.353	1.52	0.16	0.01	0.03	0.01	97.13	7.553	1071.6
1 b	30.88	12.53	26.65	3.09	12.09	2.10	2.29	0.367	5.593	0.333	1.33	0.13	0.00	0.01	0.00	97.39	6.870	1111.6
1 c	31.25	12.12	25.68	2.97	11.63	2.11	2.80	0.425	6.422	0.384	1.60	0.15	0.02	0.04	0.00	97.61	7.901	1112.4
1 d	31.51	13.02	26.40	3.05	11.42	1.98	2.79	0.430	4.760	0.282	1.27	0.10	0.00	0.04	0.01	97.05	6.247	1047.6
1 e	31.20	12.06	25.74	3.00	11.74	2.06	2.82	0.357	6.299	0.369	1.47	0.17	0.00	0.03	0.00	97.31	7.544	1134.0
1 f	31.44	12.28	25.53	2.98	11.68	2.08	2.47	0.360	6.792	0.406	1.56	0.21	0.00	0.03	0.01	97.83	8.051	1166.8
2 a	31.27	13.01	26.67	3.23	12.36	2.23	2.57	0.305	4.078	0.266	0.98	0.14	0.01	0.04	0.00	97.15	5.147	1194.8
2 b	31.52	22.17	31.84	2.58	7.87	0.69	0.31	0.059	1.375	0.053	0.24	0.04	0.03	0.04	0.00	98.80	1.575	783.6
3 a	30.99	14.45	28.70	3.07	11.34	1.80	1.71	0.202	4.459	0.293	0.96	0.28	0.00	0.00	0.00	98.27	5.174	1294.0
3 b	31.10	13.82	28.20	3.09	11.57	1.95	1.82	0.216	4.937	0.325	0.96	0.34	0.00	0.01	0.00	98.34	5.701	1290.8
3 c	31.18	13.61	28.06	3.13	11.72	1.96	1.82	0.209	5.096	0.340	0.99	0.33	0.00	0.00	0.00	98.45	5.839	1341.2
3 d	31.16	13.79	28.09	3.02	11.68	1.91	1.80	0.217	5.028	0.324	1.00	0.35	0.02	0.00	0.02	98.39	5.796	1289.6
4 a	31.07	8.11	28.79	4.43	19.33	3.61	0.69	0.168	0.369	0.029	0.19	0.11	0.00	0.06	0.02	96.98	0.934	721.4
5 a	31.20	15.91	31.47	3.46	13.30	2.37	0.35	0.000	0.035	0.006	0.04	0.03	0.01	0.04	0.01	98.23		3593
5 b	31.44	15.70	31.01	3.43	13.36	2.37	0.38	0.012	0.126	0.000	0.08	0.04	0.02	0.03	0.01	98.02		no
6 a	31.03	15.61	31.88	3.58	13.42	1.81	0.61	0.003	0.577	0.016	0.17	0.05	0.02	0.03	0.01	98.82	0.587	797.0
6 b	31.25	16.25	32.16	3.47	12.86	1.63	0.51	0.013	0.418	0.008	0.17	0.05	0.00	0.04	0.01	98.84	0.461	608.2
7 a	31.33	10.09	32.40	4.39	16.91	2.38	0.54	0.055	0.227	0.001	0.19	0.00	0.01	0.04	0.02	98.59		no
7 b	31.52	15.70	34.72	3.53	11.49	1.35	0.50	0.070	0.219	0.020	0.12	0.00	0.02	0.01	0.02	99.28	0.466	997.4
8 a	31.23	13.46	34.97	3.74	12.73	1.54	0.50	0.066	0.000	0.004	0.16	0.08	0.01	0.03	0.00	98.52	no	no
8 b	31.00	12.77	34.88	3.90	13.52	1.61	0.50	0.070	0.024	0.004	0.13	0.17	0.00	0.06	0.01	98.65		no
9 a	31.37	10.52	32.90	4.26	16.33	2.24	0.49	0.072	0.218	0.018	0.16	0.05	0.02	0.01	0.00	98.67	0.460	997.4
9 b	31.45	17.92	33.64	3.10	10.16	1.38	0.39	0.069	0.430	0.015	0.13	0.00	0.00	0.04	0.00	98.71	0.655	351.0

Table 2. Chemical composition (wt. %) and age (Ma) of nine Yarega monazite grains. Lack of sum in the analyses of monazites is due to the absence of the estimation of the middle members of the REE series, Gd_2O_3 and Eu_2O_3, the presence of which in the same grains was confirmed earlier on a JSM-7300 electron microscope with a Link ED-spectrometer (Makeyev, Magazina, 2019).

No	P_2O_5	La_2O_3	Ce_2O_3	Pr_2O_3	Nd_2O_3	Sm_2O_3	Y_2O_3	UO_2	ThO_2	PbO	CaO	SiO_2	FeO	MnO	SO_3	Total	ThO_2*	Age
1	30.34	10.06	30.46	4.25	17.37	2.91	0.93	0.231	0.458	0.044	0.13	0.05	0.02	0.03	0.01	97.28	1.242	823.4
	30.43	14.32	32.57	3.73	13.67	1.86	0.68	0.143	0.153	0.019	0.12	0.02	0.02	0.01	0.00	97.71	0.633	695.0
2	30.19	8.84	30.28	4.44	18.09	2.74	0.71	0.034	0.291	0.015	0.24	0.23	0.43	0.06	0.01	96.59	0.407	848.2
	30.18	9.37	30.67	4.33	17.38	2.51	0.64	0.033	1.147	0.039	0.23	0.32	0.03	0.03	0.00	96.93	0.633	721.8
3	30.49	19.34	32.78	3.12	10.12	1.09	0.50	0.078	0.260	0.013	0.08	0.09	0.13	0.00	0.00	98.10	0.519	578.2
	30.43	14.93	32.78	3.71	13.20	1.67	0.52	0.095	0.247	0.019	0.11	0.05	0.03	0.02	0.00	97.81	0.568	777.0
4	30.18	5.68	23.62	4.50	23.40	6.92	0.57	0.114	0.266	0.023	0.14	0.05	0.01	0.06	0.00	95.51	0.653	815.4
	29.83	4.84	21.03	4.30	24.60	9.00	0.61	0.145	0.151	0.022	0.07	0.03	0.00	0.05	0.01	94.66	0.643	793.4
5	30.83	10.35	31.53	4.37	17.71	2.73	0.43	0.225	0.112	0.027	0.05	0.05	0.02	0.06	0.00	98.49	0.868	721.8
	30.47	9.53	29.97	4.37	18.05	3.04	0.69	0.151	0.552	0.040	0.13	0.02	0.06	0.04	0.00	97.10	1.066	870.2
6	30.35	6.46	24.92	4.64	23.13	5.39	0.60	0.103	0.865	0.039	0.16	0.01	0.04	0.06	0.01	96.77	1.212	748.6
	30.22	6.80	25.46	4.65	22.76	5.07	0.41	0.066	0.700	0.032	0.13	0.00	0.00	0.06	0.00	96.36	0.924	804.2
7	30.70	15.18	33.88	3.53	12.12	1.67	0.45	0.067	0.508	0.018	0.11	0.04	0.00	0.02	0.00	98.29	0.731	571.8
	30.46	14.39	33.81	3.63	12.16	1.60	0.50	0.071	1.031	0.039	0.17	0.02	0.01	0.01	0.00	97.90	1.270	715.4
8	30.44	12.77	32.64	3.88	14.17	1.80	0.35	0.048	1.565	0.054	0.15	0.00	0.12	0.02	0.01	98.01	1.727	729.4
9	30.32	17.14	33.20	3.29	11.05	1.23	0.33	0.039	0.776	0.000	0.08	0.10	0.24	0.05	0.59	98.44		Not det.
	30.65	19.93	33.02	2.99	9.82	0.94	0.27	0.065	0.670	0.031	0.08	0.00	0.03	0.00	0.00	98.49	0.890	807.8
10	30.40	12.59	32.26	3.94	14.83	2.09	0.61	0.108	0.631	0.033	0.14	0.10	0.06	0.04	0.00	97.82	0.996	769.0
	30.44	10.64	31.19	4.20	16.74	2.66	0.58	0.154	0.173	0.022	0.09	0.07	0.17	0.04	0.01	97.18	0.692	737.0
11	30.45	10.38	32.47	4.46	17.22	2.38	0.41	0.132	0.010	0.012	0.04	0.04	0.05	0.05	0.02	98.11	0.450	614.2
12	30.21	6.84	26.04	4.49	21.43	5.90	0.62	0.092	0.368	0.026	0.11	0.09	0.06	0.03	0.01	96.31	0.682	881.8
	28.73	8.10	26.60	3.94	16.38	3.18	0.61	0.159	0.274	0.020	0.32	1.48	0.39	0.05	0.01	90.23	0.803	579.0
13	30.02	5.76	24.18	4.57	23.47	6.20	0.70	0.210	0.124	0.031	0.05	0.02	0.02	0.05	0.01	95.41	0.838	856.6
	30.41	5.69	23.70	4.67	24.42	6.36	0.48	0.027	0.246	0.017	0.18	0.04	0.04	0.05	0.00	96.32	0.340	1142.6
14	30.35	18.09	32.84	3.23	10.86	1.25	0.60	0.149	0.600	0.038	0.08	0.04	0.11	0.00	0.00	98.24	1.105	799.4
	30.42	17.83	33.61	3.36	11.22	1.24	0.47	0.085	0.169	0.005	0.08	0.00	0.04	0.03	0.00	98.54	0.445	255.0
15	30.44	12.34	32.10	3.92	14.74	1.88	0.53	0.094	0.622	0.038	0.12	0.32	0.03	0.02	0.01	97.19	0.944	932.2
	30.40	8.94	30.76	4.62	18.97	2.81	0.40	0.118	0.382	0.035	0.06	0.01	0.00	0.03	0.00	97.52	0.789	1023.8
16	29.58	7.88	27.96	4.40	18.71	3.16	0.73	0.073	0.398	0.021	0.16	0.55	0.01	0.03	0.01	93.66	0.644	754.6
	29.92	8.55	29.74	4.59	19.43	3.27	0.49	0.068	0.408	0.023	0.13	0.04	0.07	0.04	0.01	96.76	0.639	832.6
17	30.08	10.42	30.60	4.35	17.66	2.48	0.54	0.235	0.650	0.058	0.10	0.01	0.01	0.06	0.01	97.26	1.454	925.4
	30.34	9.82	30.73	4.53	18.57	2.81	0.33	0.083	0.348	0.018	0.10	0.01	0.01	0.06	0.00	97.75	0.626	666.2
18	31.33	11.78	32.41	4.18	16.02	2.29	0.47	0.133	0.061	0.017	0.08	0.18	0.00	0.03	0.01	98.99	0.510	769.0
	30.27	12.23	33.29	4.28	15.80	1.96	0.28	0.072	0.044	0.008	0.03	0.01	0.00	0.02	0.00	98.29	0.285	641.0
19	30.27	7.73	29.05	4.68	20.67	3.80	0.42	0.024	0.393	0.019	0.15	0.09	0.02	0.05	0.00	97.37	0.475	920.6
	30.34	8.99	31.35	4.63	19.15	2.82	0.45	0.054	0.013	0.008	0.06	0.03	0.02	0.04	0.00	97.94	0.198	919.6

Table 3. Chemical composition (mas. %) and age (Ma) of Pizhemsky monazite-kularite. The first analytical result in the line is shown for the probe point in the centre of the grain and the second result – for the margin of the same grain.

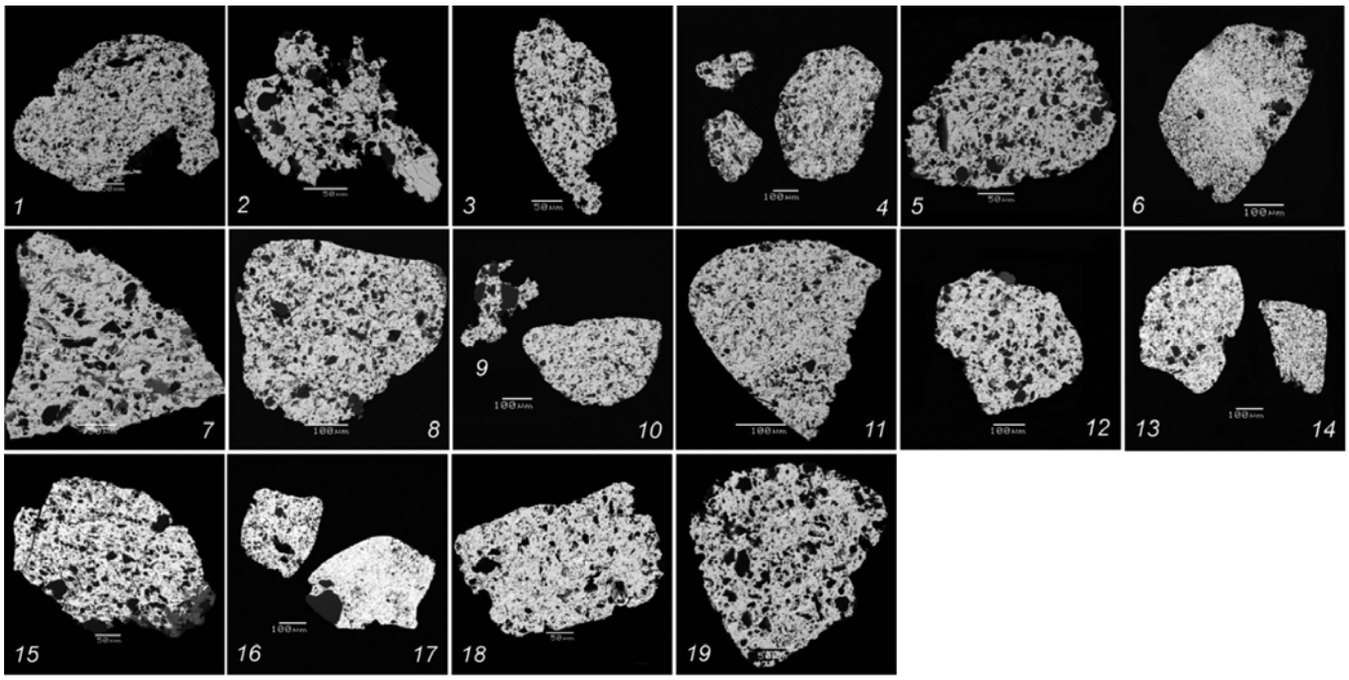

Fig. 2. Electron microscopy images (BSE regime) of 19 Pizhemsky monazite-kularite grains with quartz (black) and florencite (light-grey in grains 7 and 15) inclusions. Grain numbers coincide with analytical numbers in Table 3.

There are three chemical varieties of Yarega monazite: neodymium-cerium, lanthanum-thorium-cerium and lanthanum-cerium. The latter is the most common variety (over 60 % of cases). A high positive correlation between cerium, lanthanum, thorium, yttrium and calcium, on the one hand, and between neodymium, praseodymium, samarium, europium and gadolinium, on the other hand, is observed (Makeyev, Magazina, 2019). The tetrad rule in the chemical composition of Yarega high-thorium monazite is violated in both the first (La-Ce-Pr-Nd) and second (Sm-Eu-Gd-Tb) tetrads because of a negative cerium anomaly associated with the isomorphic replacement Th+Y+Ca → Ce and a negative Eu-anomaly in the second tetrad. The typochemical characteristics of Yarega high-thorium monazite with a distinctive Eu-anomaly are typical of monazite, which is genetically related to granitoids (Skublov et al., 2018; Schandl, Gorton, 2004; Williams et al., 2007).

Pizhemsky monazite-kularite. Pizhemsky monazite grains were extracted from the magnetic ilmenite-pseudorutile concentrate of the grey-coloured sandstone of an industrial sample weighing 250 kg. They are much bigger (521×446 ÷ 228×130, average size is 375×278 μm) than the grains and crystal fragments of Yarega monazite; they are often amoeba-shaped, rounded or ellipsoid and are grey or brown in color. Individual grains are filled with quartz inclusions (up to 10-15 %, Fig. 2) and are similar in shape, color and internal morphology to leucoxene grains. This morphological variety of monazite is called kularite. In addition to quartz, it contains florencite, muscovite and pseudorutile inclusions. Monazite-kularite grains are magnetized by pseudorutile and are concentrated to form an electromagnetic fraction together with ilmenite, pseudorutile and siderite (Lutoev, Makeyev, 2019). The chemical characteristics of monazite-kularite are shown in Table 3. There are three chemical varieties of Pizhemsky monazite: lanthanum-cerium, neodymium-samarium-cerium and neodymium-cerium. The latter is the most common (over 80 % of cases). There is a high positive correlation between cerium and lanthanum, on the one hand, and between praseodymium, neodymium, samarium, gadolinium and europium, on the other (Makeyev, Magazina, 2019). The tetrad rule in Pizhemsky monazite-kularite is violated: there is no bending between the first (La-Ce-Pr-Nd) and second (Sm-Eu-Gd-Tb) tetrads, which seems to be due to elevated Nd and Sm concentrations. This could have been provoked by the hydrothermal transformation of the mineral in the weathering crust of the primary source and the removal of some of the constituents.

The diagrams (Figs. 3 and 4) show the correlations of the constituents used to distinguish between the typochemical characteristics of the above two deposits. Pizhemsky monazite contains more neodymium and samarium, while Yarega monazite carries more lanthanum, thorium, yttrium, calcium, uranium and lead.

Results of monazite dating by the CHIME method

The results of monazite dating, based on 18 and 35 analyses, are shown in Tables 2 and 3. The average age of Yarega monazite, based on "point" determinations in three combinations, is: 1) 1304±22; 2) 1107±39;

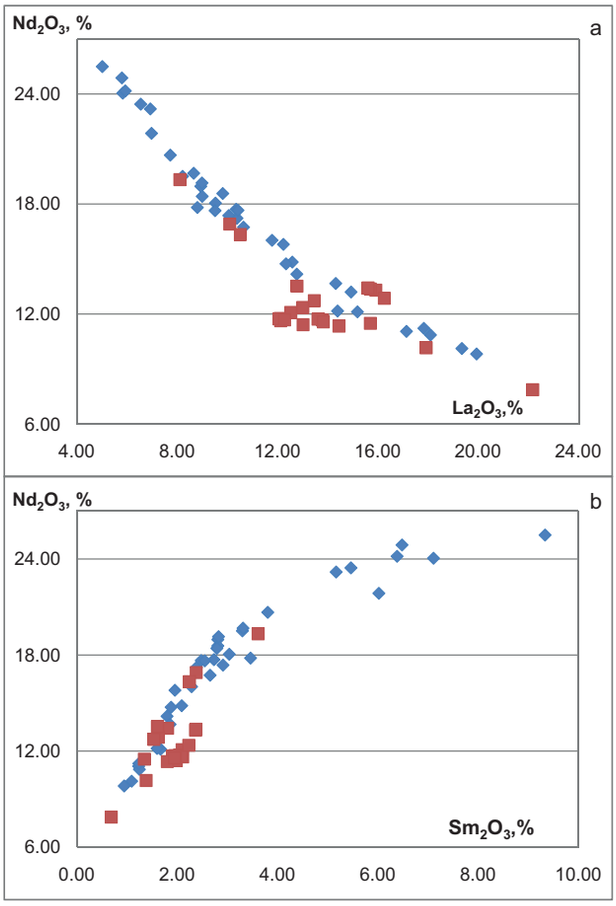

Fig. 3. Oxide ratios: a – La_2O_3-Nd_2O_3; b – Sm_2O_3-Nd_2O_3 in Yarega (squares) and Pizhemsky (rhombs) monazites.

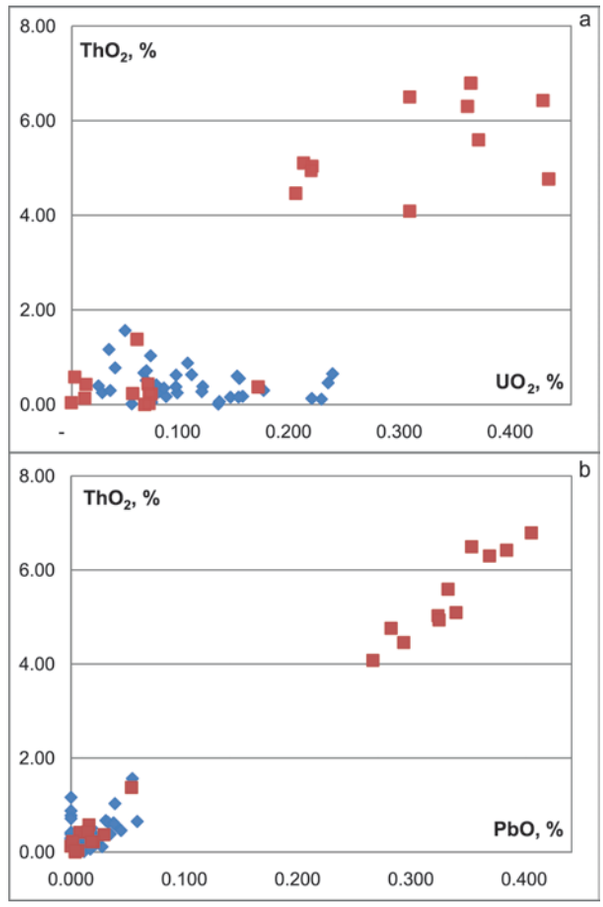

Fig. 4. Oxide ratios: a – UO_2-ThO_2; b – PbO-ThO_2 in Yarega (squares) and Pizhemsky (rhombs) monazites.

3) 837±147 Ma. The average age of Pizhemsky monazite-kularite from 33 points (if 2 marginal points on both sides, which are not in the 3 σ interval, are removed) T is 777±110 Ma. Figures 5 and 6 show the correlations of PbO and ThO_2* for samples from the two deposits. These data were used to calculate and construct corresponding isochrones. The three isochrones constructed for Yarega monazite are:

Isochrone I with parameters: T = 1301 Ma, $y = 0.0566x$, $R^2 = 0.906$;

Isochrone II with parameters: T = 1105 Ma, $y = 0.0481x$, $R^2 = 0.901$;

Isochrone III with parameters: T = 778 Ma, $y = 0.0335x$, $R^2 = 0.931$.

The first two isochrones were constructed for high-thorium monazite grains, while the last one for low-thorium grains. This evidence, together with data on the chemical composition of monazite, suggests that monazite grains from three primary sources, considerably differing in age by ~200 and ~320 Ma, occur together in the Yarega deposit.

Only one isochrone (Fig. 6), showing an age (T) of 782 Ma, can be constructed for the Pizhemsky deposit, based on the results obtained. Statistical analysis was done to calculate two isochrones similar in age: one with a free member $PbO = -0.007+0.0345 \cdot ThO_2$*, $R^2 = 0.908$; and the other which has no free member and approaches zero, – $PbO = 0.0337 \cdot ThO_2$*, $R^2 = 0.9084$. Let us choose the latter isochrone, as is accepted in this type of study. It should be noted that it is a perfect case, when the isochrones for Pizhemsky monazite closely coincide with the average "point" age of the entire combination. Another feature of the present study is that the age values in isochrone ***III*** for Yarega monazite coincide with the only isochrone for Pizhemsky monazite-kularite. This may indicate the close nature of the geological object of one of the indigenous primary sources of monazite of the two Timan deposits.

Discussion

The most similar object for discussion of the results obtained is the well-known and well-studied Ichetyu base mineral gold-diamond-rare earth-rare metal-titanium deposit. It is a 0.2-1.5 m thick breccio-conglomerate horizon resting directly on the Malorucheiskaya rock sequence of the Pizhemsky deposit (Makeyev, 2016; Makeyev, Dudar, 2001). Isotopic (Pb-Th and Pb-U) and chemical age estimations (CHIME method) for La-Ce-monazite and Nd-Ce-monazite-kularite from the horizon are known (Krasotkina, 2018; Makeyev, Viryus, 2013; Skublov et al., 2018). Local dating of monazite yielded two peaks of ^{206}Pb-^{238}U age values: a major peak with an

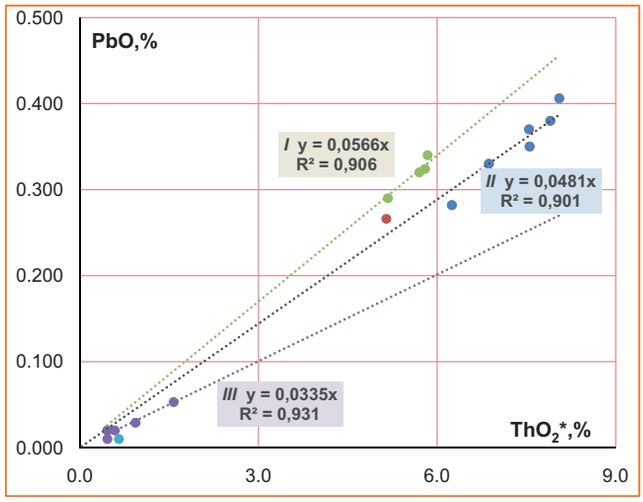

*Fig. 5. Isochrones for Yarega monazite: **I** – T = 1301 Ma, **II** – T = 1105 Ma (high-thorium); **III** – T = 778 Ma (low-thorium).*

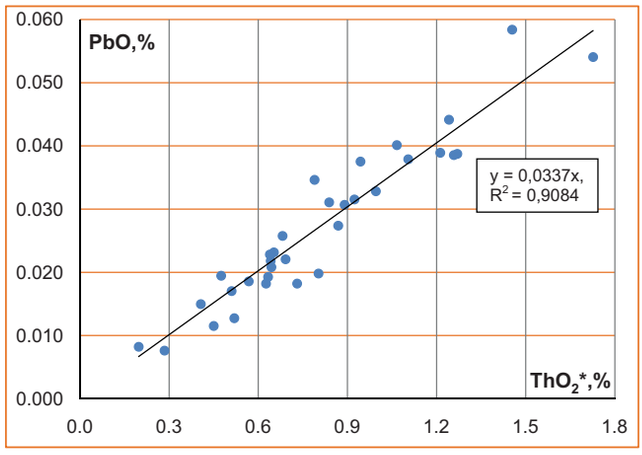

Fig. 6. Isochrone for Pizhemsky monazite-kularite: T = 782 Ma.

age of 1000-1060 Ma and a minor peak with a maximum of about 570 Ma. ^{208}Pb-^{232}Th age, estimated at the same points as ^{206}Pb-^{238}U age, yielded only one peak with an age of 500-700 Ma (Skublov et al., 2018). In addition to monazite, the isotope-geochemical characteristics of rutile and zircon were analyzed (Krasotkina, 2018). It has been shown that the isotope systems and trace element compositions of all the three mineral-chronometers studied (zircon, rutile and monazite) from the Ichetyu ore occurrence are indicative of a major hydrothermal event dated at ~600 Ma. The event does not manifest itself in the rocks that underlie titanium deposits, and is understood as an age similar to the age of formation of Middle Timan titanium deposits.

The distribution of data on individual age calculations (CHIME) for Ichetyu monazites at the «point» (Makeyev, Viryus, 2013) shows three modes. Hence, the samples can be divided into three groups and their average age can be calculated: **1)** 955±124 Ma, **2)** 706±76 Ma, **3)** 401±88 Ma. The isochrone method of calculation also yields three sets that are consistent with three isochrones:

- ***isochrone I*** with parameters: 967 Ma ($y = 0.0414x$, $R^2 = 0.9669$);
- ***isochrone II*** with parameters: 737 Ma ($y = 0.0314x$, $R^2 = 0.9434$);
- ***isochrone III*** with parameters: 522 Ma ($y = 0.0221x$, $R^2 = 0.9840$).

The results obtained were interpreted as follows. Consistent with isochrones ***I*** are mostly ellipsoidal grains of a neodymium-cerium variety (except for two thorium grains and two lanthanum-cerium monazite grains). Consistent with isochrone ***II*** are only grains of a neodymium-cerium variety (monazite-kularite). Consistent with isochrone ***III*** are all three monazite varieties, but thorium and lanthanum-cerium varieties prevail over a neodymium-cerium variety. The early isochrones (***I***) seem to indicate the time of formation of rare metal – rare earth high-temperature hydrothermal-metasomatic mineralization in Neoproterozoic shales, which are similar to the Bobrovskoye and Oktyabskoye Chetlassky Kamen deposits, Middle Timan.

The middle isochrones (***II***) can be correlated in age with Chetlassky lamprophyres, whose intrusion time was estimated by the Rb-Sr method at 815 Ma (Makeyev et al., 2009). Chetlassky carbonatites (600 Ma), in which monazite is one of the most common accessory minerals, were derived in the same period of time.

The latest isochrones for monazite (***III***) are consistent with the intrusion age of Devonian basalts and probably with the age of formation of the Ichetyu occurrence proper. During this phase monazite could have recrystallized and lost part of radiogenic lead. This assumption is consistent with the geological knowledge of the structure of a productive breccio-conglomerate horizon (in which basalt fragments occur) and shows that Ichetyu breccio-conglomerates are of volcanic-fluidisate origin and were formed simultaneously with the intrusion of basalt sills.

These data should be compared with new age dates for monazite and zircon from the Pizhemskoye and Yarega deposits to more precisely date the deposits themselves. Interestingly, the age values for Nd-Ce-monazite-kularite from the Ichetyu occurrence and the Pizhemskoye deposit are very similar and seem to indicate a common primary source.

With respect to Timan igneous rocks, only Chetlassky lamprophyres are the most similar in isotope age (Makeyev et al., 2008; 2009) to the chemical age of Yarega low-thorium monazite and Pizhemsky monazite-kularite. Rb-Sr-data show that the largest group of Chetlassky lamprophyre samples forms an isochrone with a Neoroterozoic age of 819±19 Ma (Makeyev et al., 2009). Hence, it is Neoroterozoic lamprophyres, most similar in age and the mineral composition of accessories (Makeyev, 2016; Makeyev et al., 2008;

2009; 2016), that could have provided a source of ore matter for the two titanium deposits. The prospecting and exploration of the northern Volsk-Vymskaya Ridge is likely to reveal Chetlassky-like lamprophyres beneath titaniferous sequences.

The species composition of micron-sized mineral inclusions in Yarega zircon (Makeyev, Zhilicheva, 2018), which is closely associated in titaniferous sandstone with the monazite studied, is: quartz, muscovite, F-REE-apatite, xenotime, chlorite, K-feldspar, biotite – PASE (phlogopite-annite-siderophyllite-eastonite) – series mica (according to a new nomenclature, International Mineralogical Association). This clearly shows that the entire association is bimica granite. Well-known criteria (Krasotkina, 2018; Skublov et al., 2018; Schandl, Gorton, 2004; Williams et al., 2007), such as extremely low Th concentration, U/Th ration and the absence of Eu-anomaly, the chemical compositions of Pizhemsky monazite-kularite and Yarega low-thorium monazite are indicative of their hydrothermal genesis. According to the same criteria, a bedrock source for Yarega high-thorium monazite could have been provided by old Timan granitic batholiths that seem to occur in Timan's crystalline basement and are not exposed on the day surface.

It was thought earlier that oil-saturated leucoxene sandstones from the Yarega deposit are of Middle Devonian age, as shown by spore-and-pollen analysis. However, O.P. Telnova of the Yushkin Institute of Geology of Komi Science Center of Ural Branch of Russian Academy of Sciences (personal communication), has recently conducted extensive studies of core samples from prospecting holes, which showed that the samples contain both Middle and Late Devonian microfossils. This ambiguity suggests that microfossils were carried to Yarega titaniferous sandstones and distributed there by migrating oil, which was squeezed out from Devonian parent rock and migrated to porous sandstones as the most favorable collector (an anticlinal trap formed by the Yarega tectonic structure). The mineral compositions of leucoxene sandstones of oil and water grades were identical. It means that oil later filled the upper anticlinal portion of the Yarega deposit and that it was not genetically related to the formation of the titaniferous sequence itself. Here, oil also fills the upper ore-free quartz sandstone bed in the anticlinal trap. It is safe to assume that oil carried a mixture of ***Middle and Late Devonian*** plant spores and pollen while migrating. So, the Middle Devonian age of the Yarega deposit is not proven. The question remains open. To correctly approach the problem, further isotope-geochemical studies, similar to those carried out earlier in the Pizhemsky deposit (Chernyshov et al., 2010), are needed.

The genesis and ages of the two deposits studied are problems of animated debate. It was assumed earlier that the deposits are old placers, but this point of view has not been generally accepted. According to the existing classification of Russia's titanium deposits, the Yarega is clearly a metamorphogenetic bedrock deposit. The two deposits are identical in geological structure and are similar in mineral composition (and possibly age and genesis). The titaniferous sequence of the Pizhemsky deposit is barren and contains no organic remains. Therefore, its Devonian age was tentatively accepted earlier. The Malorucheiskaya sequence is overlain by the Middle Devonian terrigenous rocks of the Pizhemsky suite (D_2pz) that contain Middle Devonian pollen. Many scholars estimate the age of the Malorucheiskaya titaniferous sequence of the Pizhemskoye deposit from indirect evidence in the Early Devonian − Neoroterozoic time span. Isotope methods were used to precisely date the titaniferous sequence of the Pizhemsky deposit from a Rb-Sr-isochrone as Neoroterozoic, T = 685±30 Ma (Chernyshov et al., 2010). Material for age determination was provided by ore-hosting rocks, such as siltstone and argillite-like clay, as well as leucoxene ore concentrate proper. Thus, the chemical age obtained for monazite supports our earlier data on the isotope age of zircon, monazite and leucoxene. Hence, the Pizhemsky titanium deposit is much older (most probably 600-700 Ma) and was formed in Neoroterozoic time (PR_3mr).

The authors of the publications that saw the light in the past few years tried to provide arguments in favor of the ***bedrock*** rather than other (not placer) genesis of the Pizhemsky deposit (Makeyev, 2016; Makeyev et al., 2008; 2009; 2016, etc). One of their arguments is the complete absence of the roundness of quartz (at both localities) a major mineral in terms of ore volume. It is sharply angular and clastic − a feature indicative of the short-distance transport of the entire material. Some of the mineral phases, e.g. leucoxene and monazite-kularite, may display the ***pseudo-rounded*** shape of grain produced by the hydrothermal reworking of the material and the vertical movement of the material in a vertical flow. Therefore, the rounded shape of grains is a ***convergent*** feature, which cannot be accepted as strong evidence for the placer origin of ore occurrences and the movement of the material in subhorizontal water flows. The sizes of quartz and other non-metallic and ore minerals (0.1-2.0 mm) are much greater than those of minerals from Riphean fine-grained (0.01-0.10 mm) shale (bedrock). Furthermore, the shale does not contain sufficient amounts of ore constituents. Therefore, the weathering crust after the shale could not have been a bedrock source of the matter that made up the overlying ore sequence. Calculations show that to create current TiO_2 concentration in the deposits, the volume of weathering crusts after shale should have been tens of times the volume and thickness of the titaniferous sequences. Thick weathering crusts

after Riphean shales have never formed on Timan, and nobody has ever seen them. The underlying shales of the Lunvozhskaya suite (PR_3ln) were dated by the Rb-Sr-method at T = 816.3±5.2 Ma (Makeyev et al., 2018). No other ore concentrations, which could be a source of ore matter, have been revealed on the day surface near the Pizhemsky deposit. Hence, the probable source (it could be weathering crusts after lamprophyre) was at some depth beneath the deposits, and the ore masses must have moved vertically. Another convincing evidence for the contribution of hydrothermal processes to the formation of both titanium deposits is the presence (3-15 % by volume) of porous and veined siderite with the endogenic isotope composition of carbon (Makeyev, Nosik, 2009). The decay of ilmenite as a primary ore mineral, which gave rise to leucoxene, took place in a hydrothermal process in the presence of endogenic CO_2. The reaction was as follows:

$$FeTiO_3 + H_2O + CO_2 + SiO_2 \rightarrow (2TiO_2 \cdot SiO_2) + TiO_2 + FeCO_3 \rightarrow Fe(OH)_3 + Fe_2O_3 + CO_2.$$

The aforementioned geological, geochemical and mineralogical features and proofs are convincing enough to argue that the Pizhemsky titanium deposit is of volcanic (phreato-magmatic) origin. Its formation of a mud volcano type was contributed to by water vapour and carbon dioxide. The deposit formed after the substrate of the weathering crusts of lamprophyres followed by the long (hundreds of millions of years) metamorphism of ore sequences (Makeyev, 2016).

Thus, two Timan's giant structurally similar titanium deposits, Yarega and Pizhemskoye, resting directly on Neoroterozoic shales, overlain by Middle and Upper Devonian sedimentary rocks and erroneously interpreted earlier as Middle Devonian, are indeed Neoroterozoic. One of the most probable sources of ore matter could have been provided by Chetlassky-like lamprophyres similar in the age, species composition and typomorphic characteristics of accessory indicator minerals.

Conclusions

The typomorphic characteristics and age of monazite samples from Timan's giant Pizhemsky and Yarega titanium deposits were studied. Differences in morphology (Yarega monazite occurs as crystal fragments, while Pizhemsky monazite is present as hydrothermally altered ellipsoid grains), the species composition of inclusions (quartz inclusions make up 10-15 % of Pizhemsky kularites), grain size (Pizhemsky monazite is 4 times bigger) and the distribution of the chemical characteristics of the mineral (a large portion of Yarega monazites occurs as high-thorium and lanthanum varieties, while Pizhemsky monazite-kularite occurs as neodymium and samarium varieties) were revealed. The isochrone Th-Pb age of monazite was estimated using the CHIME method. Three isochrones for Yarega monazite with the ages of 1301, 1105 and 778 Ma and one isochrone for Pizhemsky monazite-kularite with an age of 782 Ma were constructed. These differences are due to monazite crystallization conditions and a difference in the sources of the matter. A source for Yarega high-thorium monazite could have been provided by old granitic batholiths, and the origin of Yarega low-thorium monazite and ~780 Ma Pizhemsky Nd-Ce-monazite-kularite could have been associated with the hydrothermal alteration of weathering crusts after lamprophyres resting presumably beneath the deposits in the shale-quartzite sequence of the crystalline basement, which is similar in age to Chetlassky Kamen lamprophyres (spessartite and kersantite). The free form of monazite grains in both deposits allows us to develop technological methods for extracting the mineral from concentrates, which will certainly increase the profitability of their mining.

Acknowledgements

The authors are sincerely grateful to A.N. Konilov for help in calculating the age of monazite grains and constructing isochrones according to his own program and A.V. Lalomov for the useful discussion of the article and comments.

The study was carried out in the framework of budget theme No. 0136-2018-0020 and partially was funded by Russian Foundation for Basic Research, project number 19-35-60001.

References

Chernyshev I.V., Makeyev A.B., Goltsman Yu.V., and Bryanchaninova N.I. (2010). Age of Titanium Deposits of the Northeastern Part of the Eastern European Platform: Rb–Sr Data. *Doclady Earth Sciences*, 435(1). pp. 1524-1528. https://doi.org/10.1134/S1028334X10110255

Ignatiev D.V., Burtsev I.N. (1997). The leucoxene of Timan: Mineralogy and problems of technology. St.Petersburg: Nauka, 215 p. (In Russ).

Kalyuzhny V.A. (1982). Geology of new placeforming metamorphic formations. Moscow: Nauka, 264 p. (In Russ).

Krasotkina A.O. (2018). Isotopic-geochemical features and age of accessory minerals of the Ichetju occurrence and Pizhemsky deposit (Middle Timan). Abstract Cand. geol. and min. sci. diss. St. Petersburg, 20 p. (In Russ.)

Lyutoev V.P., Makeyev A.B. (2019). Assessment of the quality of the magnetic concentrates of the titanium ores at Pizhemsky deposit from the point of view of the technological mineralogy. *Proceedings of higher educational establishments. Geology and Exploration*, (3), pp. 31-41. (In Russ.) https://doi.org/10.32454/0016-7762-2019-3-31-42

Makeyev A.B. (2016). Typomorphic features of minerals of Ti ores from the Pizhemskoe deposit. *Mineralogiya = Mineralogy*, 1, pp. 24-49. (In Russ.)

Makeyev A.B., Andreichev V.L. and Bryanchaninova N.I. (2009). Age of Lamprophyres of the Middle Timan: First Rb-Sr Date. *Doklady Earth Sciences*, 426(4). pp. 584-587. https://doi.org/10.1134/S1028334X09040163

Makeyev A.B., Bryanchaninova N.I. (2009). Lamprophyres of Chetlassky Kamen (Middle Timan). *Regional Geol. Metallogeny*, 37, pp. 51-73. (In Russ)

Makeyev A.B., Dudar V.A. (2001). Diamond Mineralogy of the Timan. St. Petersburg: Nauka, 336 p. (In Russ.)

Makeyev A.B., Krasotkina A.O., Skublov S.G. (2016). Geochemistry and U-Pb-age of zircon from Pizhemskoe titanium deposit (Middle Timan). *Vestnik IG Komi SC UB RAS,* 5, pp. 38-52. https://doi.org/10.19110/2221-1381-2016-5-38-52 (In Russ.)

Makeyev A.B., Krasotkina A.O., Skublov S.G. (2018). Clay shales of the Lunvozhskojj suite of the Volsk-Vym ridge (Middle Timan): composition, age, accessory zircon. *Proc. Mineralogical seminar: Modern problems of theoretical, experimental and applied mineralogy (Yushkinsky readings – 2018)*. Syktyvkar, pp. 40-41. (In Russ.)

Makeev A.B., Lebedev V.A., Bryanchaninova N.I. (2008). Magmatites of Middle Timan. Ekaterinburg: UrO RAN, 348 p. (In Russ.)

Makeyev A.B., Magazina L.O. (2019). Typomorphic peculiarities of monazite and kularite from titanium ore of the Pizhemsky and Yaregsky deposites (Middle and South Timan). *XIV Int. sci.-pract. conf.: New ideas in Earth Sciences. Abstracts*. Vol. II. Moscow: MGRI-RSGPU, pp. 314-316. (In Russ.)

Makeyev A.B., Nosik L.P. (2009). Chemical and isotopic composition of siderite of the Pizhemsky deposit (Middle Timan)]. *Proc. XV Geological Congress of the Komi Republic: Geology and mineral resources of the European North-East of Russia*. Vol. II. Syktyvkar: IG Komi SC UB RAS. pp. 277-279. (In Russ.)

Makeyev A.B., Viryus A.A. (2013). Monazite of the Ichetju occurrence (composition, morphology, age). *Proceedings of higher educational establishments. Geology and Exploration*, 3, pp. 10-15. (In Russ.)

Makeyev A.B., Zhilicheva O.M. (2018). Color cathodoluminescence of zircon from Yarega oil-titanium deposite (South Timan). *Proc. XIX Int. Conf.: Physico-chemical and petrophysical studies in Earth Sciences*. Moscow: IGEM RAS, pp. 220-223. (In Russ.)

Popova V.I., Hiller V.V., Erohin V.V., Popov V.A. (2010). Monozites of late granite pegmatites of Ilmen mountains: chemical dating age of zonal-sectorial crystals. *Novye dannye o mineralakh = New Data on Minerals,* 45, pp. 72-78. (In Russ.)

Schandl E.S., Gorton M.P. (2004). A textural and geochemical guide to the identification of hydrothermal monazite: criteria for selection of samples for dating epigenetic hydrothermal ore deposits. *Economic Geology*, 99, pp. 1027-1035. https://doi.org/10.2113/gsecongeo.99.5.1027

Skublov S.G., Krasotkina A.O., Makeyev A.B., Tomsen T.B., Serre S.X., Abdrakhmanov I.A. (2018). Geochemistry of rare elements (LA-ICP-MS) in the monazite from Ichetju occurrence, Middle Timan. *Proc. Fersman Scientific session*, 15, pp. 338-341. https://doi.org/10.31241/FNS.2018.15.084 (In Russ.)

Skublov S.G., Makeyev A.B., Krasotkina A.O., Rizvanova N.G., Koiman E., Tomsen T.B., Serre S.X. (2018). New data on the age of the zircon, rutile and monazite from Ichetju occurrence, Middle Timan. *Proc. VII Russ. Conf. on isotope geochronology: Methods and geological results of the study of isotopic geochronological systems of minerals and rocks*. Moscow: IGEM RAS, pp. 326-328. (In Russ.)

Suzuki K., Adachi M. (1991).The chemical Th–U–total Pb isochron ages of zircon and monazite from the gray granite of the Hida Terrane, Japan. *The Journal of Earth and Planetary Sciences*, 38, pp. 11-38.

Suzuki K., Kato T. (2008). CHIME dating of monazite, xenotime, zircon and polycrase: Protocol, pitfalls and chemical criterion of possibly discordant age data. *Gondwana Research*, 14, pp. 569-586. https://doi.org/10.1016/j.gr.2008.01.005

Votyakov S.L., Shchapova U.V., Hiller V.V. (2011). Crystal chemistry and physics of radiation-thermal effects in a number of U-Th-containing minerals as a basis for their chemical microprobe Dating. Yekaterinburg: Institute of Geology and Geochemistry Urals Branch RAS, 336 p. (In Russ.)

Votyakov S.L., Hiller V.V., Shchapova U.V. (2012). Peculiarities of composition and chemical microprobe Dating of U-Th-bearing minerals. Part I. Monozites of a number of geological objects of the Urals and Siberia. *Zapiski RMO (Proceedings of the Russian Mineralogical Society)*, 1, pp. 45-60. (In Russ.)

Williams M.L., Jercinovic M.J., Hetherington C.J. (2007). Microprobe monazite geochronology: understanding geologic processes by integrating composition and chronology. *Annu. Rev. Earth Planet. Sci*., 35, pp. 137-175. https://doi.org/10.1146/annurev.earth.35.031306.140228

About the Authors

Alexander B. Makeyev – Dr. Sci. (Geology and Mineralogy), Professor, Leading Researcher, Laboratory of Ore Deposits Geology, Institute of Ore Geology, Petrography, Mineralogy and Geochemistry of the Russian Academy of Sciences

35, Staromonetny Lane, Moscow, 119017, Russian Federation

E-mail: abmakeev@igem.ru

Sergey E. Borisovsky – Cand. Sci. (Geology and Mineralogy), Researcher, Laboratory of the Analysis of Minerals, Institute of Ore Geology, Petrography, Mineralogy and Geochemistry of the Russian Academy of Sciences

35, Staromonetny Lane, Moscow, 119017, Russian Federation

Anna O. Krasotkina – Cand. Sci. (Geology and Mineralogy), Researcher, Head of the Project of Russian Foundation for Basic Research, Institute of Precambrian Geology and Geochronology of the Russian Academy of Sciences

2, Makarov emb., Saint-Petersburg, 199034, Russian Federation

Manuscript received 25 September 2019;
Accepted 15 November 2019;
Published 30 March 2020

ORIGINAL ARTICLE
DOI: https://doi.org/10.18599/grs.2020.1.32-38

New data on oil and gas potential of the Vychegda trough

T.V. Karaseva[1], Yu.A. Yakovlev[2], G.L. Belyaeva[2], S.E. Bashkova[2]*
[1]*Perm State University, Perm, Russian Federation*
[2]*Kama Research Institute for Integrated Research of Deep and Superdeep Wells (KamNIIKIGS JSC), Perm, Russian Federation*

Abstract. This article is devoted to the problem of studying the petroleum potential of the underexplored territories of the European part of Russia, in particular, the Vychegda trough. Taken a new approach to assessing the hydrocarbon potential of the Vychegda trough, based on the allocation of petroleum systems, widely used abroad. Based on a comprehensive analysis of the geological structure of the deflection and geological-geochemical results, including those obtained by the authors, two potential petroleum systems – "domanik" and "riphean" – were identified.

The potential domanik petroleum system dominates in the Eastern regions and is a peripheral fragment of the regional petroleum system covering the territory of the Volga-Ural and Timan-Pechora basins. The system is linked to development in the South-Eastern part of the trough and the neighbouring Solikamsk depression of bituminous domanik and domanikoid sediments as a source rock, which is confirmed by the genetic correlation of crude oils of Devonian-Carboniferous deposits of the Northern districts of Solikamsk depression with domanik biomarker. The stratigraphic range of the domanik system is upper Devonian-upper Permian; the formation time is late Devonian-Mesozoic.

The potential Riphean hydrocarbon system can be identified by the fact of oil-bitumen occurrences in the Proterozoic strata and the presence of the productive source rocks in the upper Riphean. The source rocks were at oil window. The Riphean system can cover the entire territory of the Vychegda trough, and the section from the Riphean to upper Permian sediments. The time of the system formation – Riphean-Mesozoic. Due to large thickness of the Riphean sediments, even with a large loss of hydrocarbon potential, the residual potential hydrocarbon resources of the Riphean petroleum system can be very significant.

Based on the research conducted, prioritized exploration studies are substantiated.

Keywords: Vychegda deflection, petroleum system, domanik sediments, source rocks, generation potential, oil and gas potential

Recommended citation: Karaseva T.V., Yakovlev Yu.A., Belyaeva G.L., Bashkova S.E. (2020). New data on oil and gas potential of the Vychegda trough. *Georesursy = Georesources*, 22(1), pp. 32-38. DOI: https://doi.org/10.18599/grs.2020.1.32-38

Introduction

Vychegda trough, located between the Timan ridge and the Volga-Ural anteclise and characterized by a significant thickness of a sedimentary cover, in recent years increasingly attracted the attention of geologists as perhaps a promising area for oil and gas exploration. Geological structure and petroleum potential of the Vychegda trough and adjacent areas is discussed in several summarizing published and unpublished works of P.E. Hoffman, A.V. Kuraev, B.P. Elokhina, N.A. Nikonov, T.I. Shilovskaya, A.P. Shilovsky, B.P. Bogdanova, O.V. Merkulov, R.Z. Chenborisova, N.T. Fortunatova, etc. Systematic and targeted regional seismic and geological-geochemical studies of the deflection were not carried out. Drilling is limited to a small number of wells, of which only three have opened Riphean formations. Individual details of the reservoirs parameters, the content of the C_{org} and bitumens in rocks and hydrocarbons presented in unpublished materials of the Timan-Pechora research centre (Uhta), Institute of Geology (Syktyvkar, Russia), KamNIIKIGS JSC) (Perm) and other organizations, as well as in the publications and dissertation work (Bazhenova et al., 2014; Kuzmin, 2006).

Methods

In this paper, a new approach to assessing the prospects of oil and gas potential of the the Vychegda trough, based on the allocation of petroleum systems, widely used abroad (Barnaby, 2006; Mancini, 2006; Albrandt et al., 2005, etc.). Oil (hydrocarbon) systems in oil and gas geology have been distinguished relatively recently. The classification was based on the study of their various elements. In foreign practice, for example,

*Corresponding author: Svetlana E. Bashkova
E-mail: sbashkova@mail.ru

the classification of US hydrocarbon systems (Magoon, 1989) was carried out taking into account the different composition of reservoirs (siliceous/carbonate), or by different types of kerogen, types of traps, types of migration, the size of oil and gas reserves in open fields, etc. In the Russian oil and gas literature, the term "oil and gas complex" is widely used, although unlike the term "hydrocarbon systems" it does not include a genetic model of their formation using geochemical data. According to V.V. Payrazyan, one of the important and new directions of studying hydrocarbon systems is the application of methods of reservoir geochemistry. The study of all types of fluids that saturate reservoirs and their mineral component is especially important, since the processes of formation of hydrocarbon systems are associated with the history of formation of the porous reservoir environment (Payrazyan, 2010). Hydrocarbon systems are clearly arranged in a hierarchical series: oil and gas basin – hydrocarbon systems – oil and gas accumulation zones – field – deposit, which is confirmed by the quantitative relationship between the generation potential of oil-and-gas source rock (OGSR) in the source of generation and the size of the deposits identified in them (Payrazyan, 2010). Petroleum (hydrocarbon, generation-accumulation) system is a complex of deposits in a certain area of development of the oil and gas basin associated with the processes of formation of oil and gas content. It includes oil and gas source rocks, hydrocarbon migration routes, reservoir rocks, fluid seals and traps (Magoon et al., 2000; Mancini et al., 2001). To identify the oil system, it is necessary to detect hydrocarbons in the form of deposits or oil and gas-bitumen occurrences. The systems are usually named after one of the key geographical objects or stratigraphic complex, in which the oil and gas source rocks are developed. Typically, the identification of petroleum systems begins with the defining of oil and gas source rocks and their correlation with hydrocarbon deposits or oil, gas and bitumen occurrences (Higley et al., 2006).

Results

Currently, the Vychegda trough, and most of the adjacent tectonic regions (Mezen syneclise, Syktyvkar arch, North-East of the Kazan-Kajim aulacogen, Kama arch and Western regions of the Timan ridge) industrial petroleum potential not established. The only exception is the Northwest area of the Solikamsk depression, where there are several oil fields (Lulinski, Verkhnekubansk, etc.). On the territory of the Vychegda trough marked oil-bitumen occurrences in the Proterozoic, and particularly in the Paleozoic section. A comparison of the materials previously completed geophysical surveys Vychegda trough the results of the last regional seismic profile 26-RS (2007) made adjustments to the study of the deep structure of the South-Eastern outskirts of the Mezen syneclise and Timan-Pechora province, including understudied areas Vychegda trough. For example, the capacity of the sedimentary cover in the central part and on the eastern side of the Vychegoda trough reaches 9-10 km, new large tectonic disturbances of the upthrow fault-thrust type have been confirmed and traced, new structural elements have been identified in the Paleozoic and Vend-Riphean complexes as possible traps (reef formations, non-structural traps, intrusions of various types, etc.) (Vakhnin, 2016). On the results of drilling and geophysical studies in the basin in addition to the powerful Riphean-Vendian deposits are widely spread Paleozoic formations, including the upper Devonian sediments are presented, which revealed domanik, the main source rocks of the Volga-Ural and Timan-Pechora oil and gas provinces (Fig.1).

A comprehensive analysis of the geological structure of the deflection, geophysical and geological-geochemical results, including those obtained by the

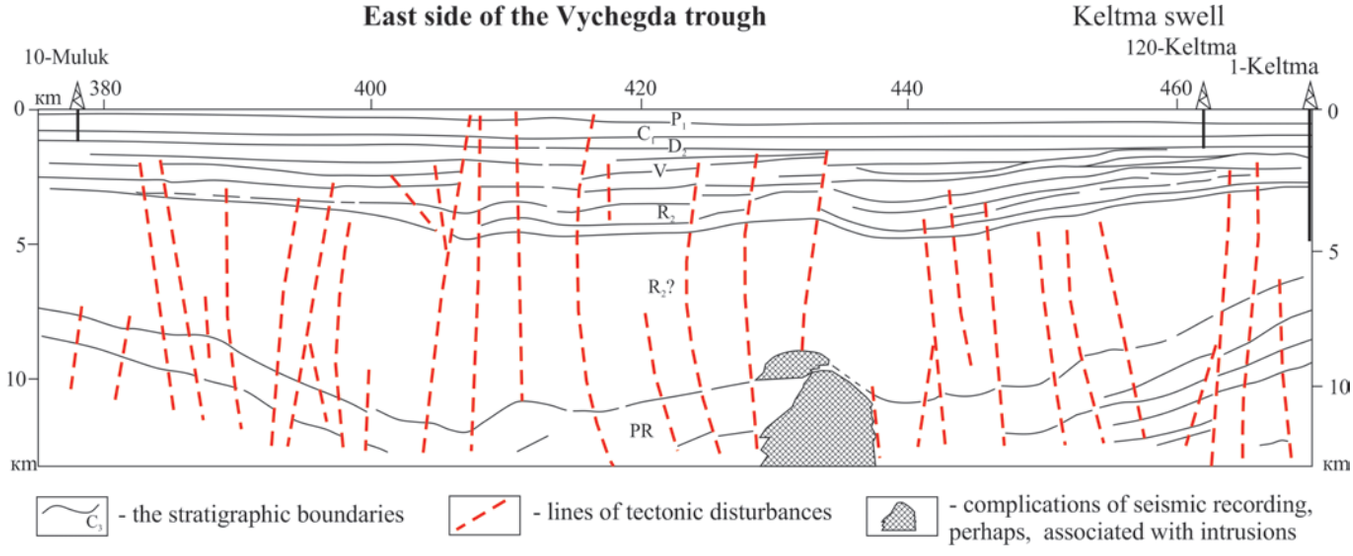

Fig. 1. Seismogeological section on profile 26A-RS (Vakhnin, 2016)

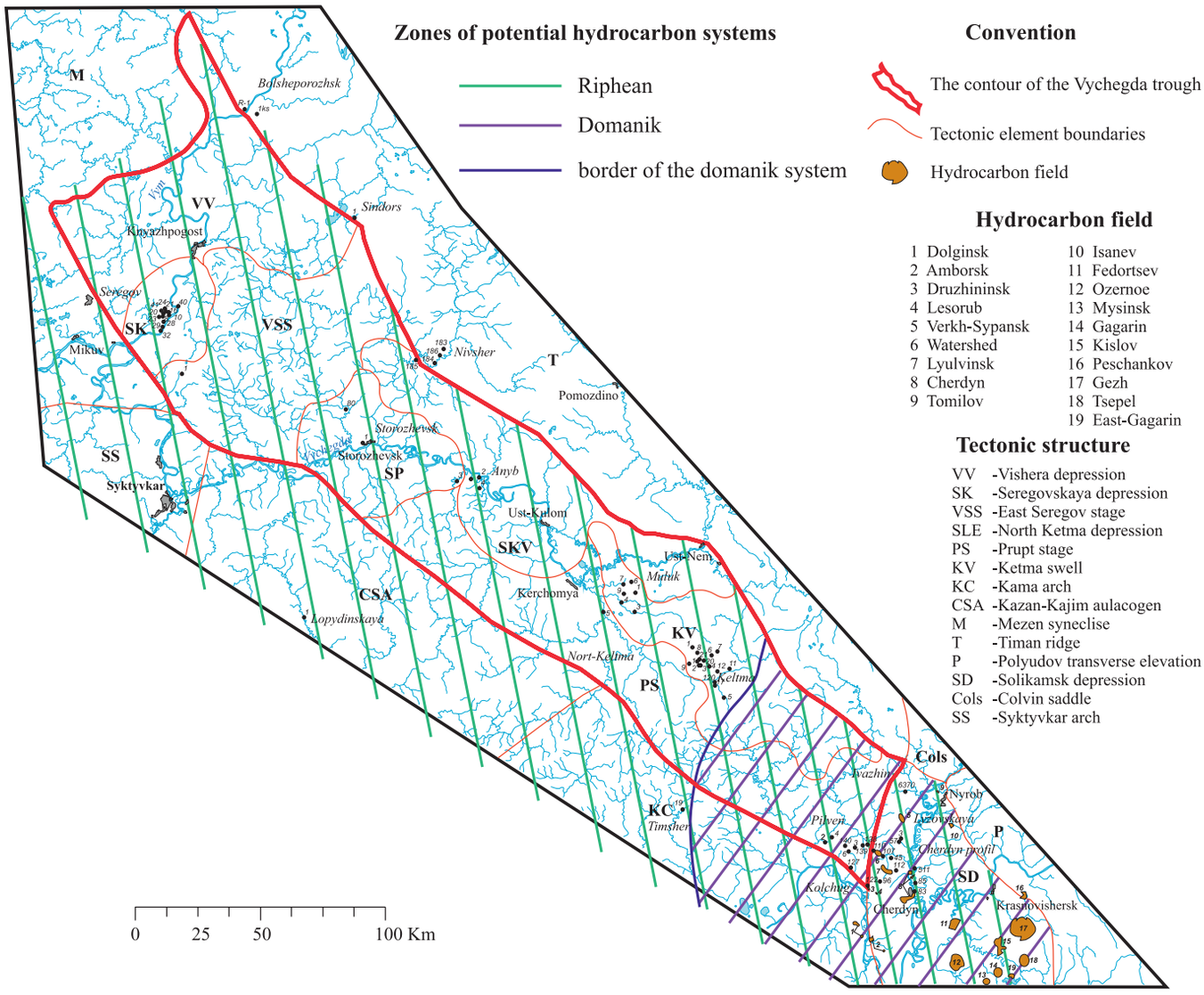

Fig. 2. Distribution of potential hydrocarbon systems in the Vychegda trough

authors, anable us to identify two potential petroleum systems – "domanik" and "riphean" (Fig. 2).

The potential domanik petroleum system of the Vychegda trough dominates in the Eastern regions and is a peripheral fragment of the regional petroleum system covering the territories of the Volga-Ural and Timan-Pechora oil and gas provinces (Lindquist, 1999; Klimenko, 2011; Timothy, Michael, Thomas, 2017). It is associated with the development in the South-Eastern part of the trough and the neighbouring Solikamsk depression of domanik biomarker and domanikoid (domanik-like) sediments as a source rocks. Genetic correlation of crude oils of Devonian-Carboniferous deposits of the northern districts of the Solikamsk depression with the domanik organic matter by biomarkers, such as metalloporphyrins (less than 10 mg/g rock in the oils and bitumens) and isoprenoids (the ratio of the pristan/phytane of less than or equal to 1) confirms this.

The stratigraphic range of the domanik system is upper Devonian-upper Permian; the formation time is late Devonian-Mesozoic.

According to the determination of the T_{max} parameter by the Rock eval method (Kolchugino Area) and the results of the basin modeling, the upper Devonian deposits here reached the sub-stage of the catagenesis MK_{1-2}, i.e. were in the interval of the "oil window" (Bashkova et al., 2018). The potential of the system in the studied area, rather remote from the powerful zones of oil formation in the domanik deposits, is estimated as relatively low in the regional plan, since the content of organic matter (OM) in rocks by C_{org} is only 0.5-0.7 % (Prishchepa et al., 2014). Petrographic studies of coal performed on Lisovsk and Kolchugino boreholes cores and other areas showed that vitrinite reflectance of the lower Carboniferous increases to the East from the Vychegda trough, as a result, the OM catagenesis increases up gradation to MK_2, i.e. emigration potential of the source rocks increases, but mainly outside the territory of the Vychegda trough.

In the Central and North-Western areas of the Vychegda trough k deposits have low yields or absent, catagenesis of OM rocks of the Paleozoic sediments does not exceed

protocatagenesis. The Vendian rocks were located in the oil window formation, and the OM of the Dorogorsk Formation of the Middle Riphean (depth 3653-3659 m) was transformed even till the gradation of MK_4, it entered the initial stage of the gas window. Thus, the domanik throughout its geological history was not included in oil window. According to the results of basin modeling 1D (Mubarak, Al-Hajer, Al Saeed, 2009; Hantschel, Kauerauf, 2009) of the Keltma 1 well section, only the Riphean and, partially, Vendian deposits entered the oil window (Fig. 3). At the same time, the Riphean rocks were in this zone for a very long time, which contributed to the significant development of hydrocarbon potential, and also partially entered the gas window.

Studies of rocks of Seregov well 1 by Rock Eval showed that Paleozoic deposits did not leave the zone of protocatagenesis, in the oil window there were Vend rocks, and the dorogor suite of the middle Riphean (depth 3653-3659 m) was transformed even to the gradation of MK_4, that is, entered the initial stage of gas window. A similar pattern is observed for the Storozhevskaya well 1 (the Central part of the studied region).

In the study of gases deeply absorbed on the Riphean limestone rocks, at the depth of 3006-3013 m 0.0388 cm^3/kg of gas enriched with heavy hydrocarbons was extracted: 44.3 % pentanes, 20.6 % butanes. Thus, in the studied part of the section of the well identified productive source rocks that were in oil

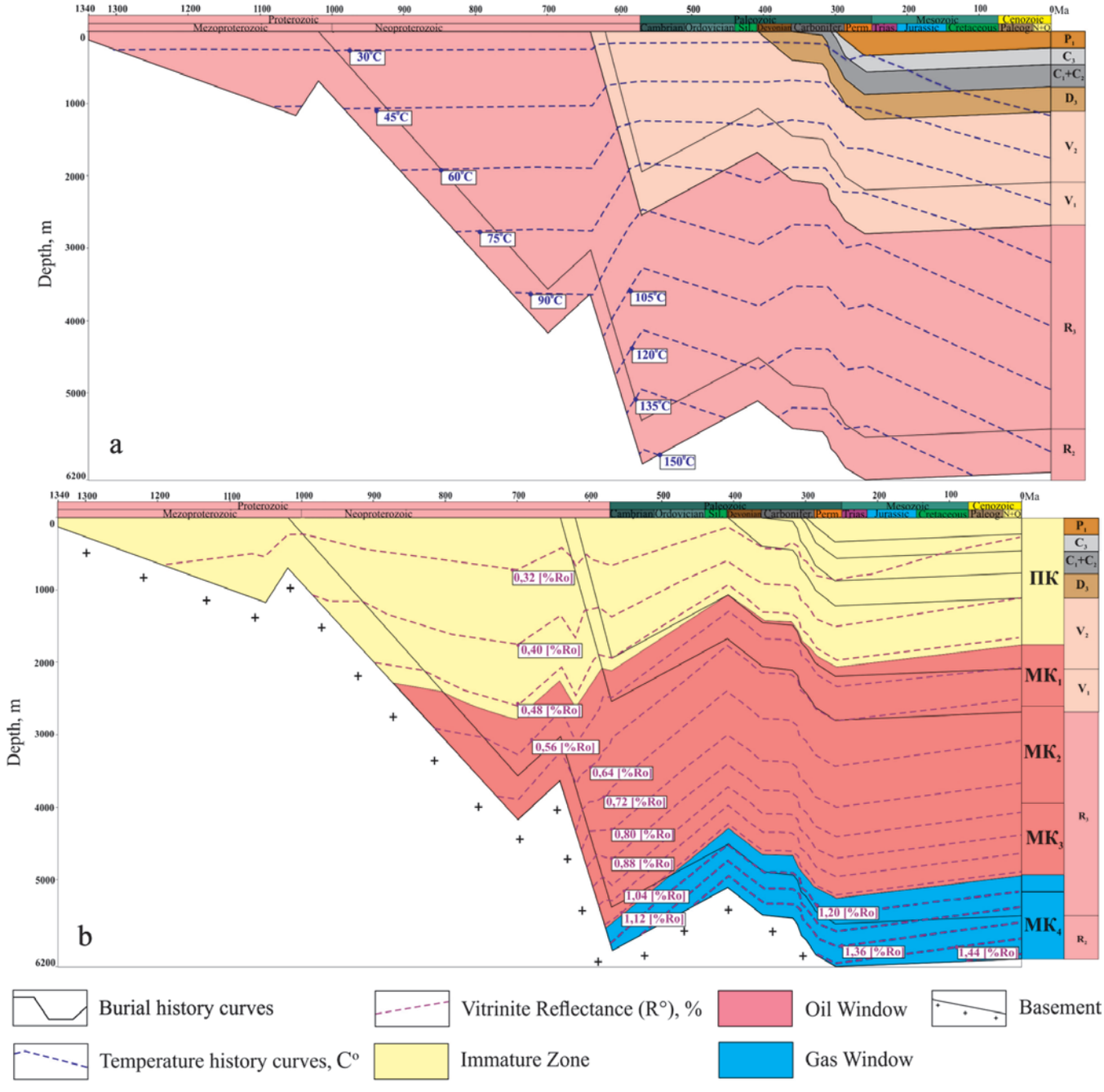

Fig. 3. The Model of the changes of paleotemperatures (a) and zoning of oil and gas windows (b), the well Keltma 1

window and genetically related zones of hydrocarbons micro-accumulation.

For the length of the Riphean system can cover the entire territory of the Vychegda trough, and for the depth – from the Riphean to upper Permian sediments. The time of formation of the system – Riphean-Mesozoic. In conditions of high tectonic activity of the region in the development of the Timan ridge in Caledonian (?) and the Hercynian stages of tectonogenesis repeatedly intensified the West Timan fault and its plumage. In this regard, favorable conditions may have formed for vertical migration of hydrocarbons, traces of which are observed in the form of micro-accumulation of liquid hydrocarbons and oil accumulations in the Paleozoic sediments on Seregowski, Storozhevsky, Nivshersky, Muluccas and Ketmensky areas, where Riphean-Vendian sediments reached the oil window. It is expected that the destruction of the Riphean system will decrease in the South-West as it moves away from the border with Timan. Given the large capacity of the Riphean sediments, it can be assumed that the residual potential of hydrocarbon resources of the Riphean petroleum system may be quite large despite the classification of source rocks as "poor" according to the Tissot and Velte classification (Tissot, Welte,1984; Tissot, Espitalie, 1980).

In the central part of the Vychegda trough in the area of the border with Kazan-Kajim aulacogen, where basement depth is 5 km and more, the Proterozoic magmatic rocks were identified, forming traps. The latter, playing the role of fluid seals, in combination with reservoirs in the Riphean, Vendian and Cambrian sandstones, can form hydrocarbon traps that determine high oil and gas potential (Shilovskaya, Shilovsky, 2011). In addition, areas of the trough of great interest from the point of view of the preservation of hydrocarbon deposits may be, where the catagenetic disagreement between Riphean and Vendian is slightly (Kuzmin, 2006), as well as areas of development of Riphean salts as zonal fluid seals. Particularly important is the presence of salts for the preservation of deposits of gas and gas condensates. Previously, the Seregov-Storozhev potential oil and gas region (Aplonov et al., 2004) stood out quite rightly as a promising one, where the possible oil and gas potential was associated exclusively with the sub-salt Riphean deposits, especially within the structural-tectonic projection of the Seregov structure.

It should be noted that outside the zone of development of the domanik system, there is a fairly frequent occurrence of oil show in the form of viscous oils and bitumen in the upper part of the section, that may be an indicator of the increased degree of destruction of the Riphean petroleum system. So, in shallow wells of the Keltma shaft there are selected layers, saturated with heavy viscous oil in the Permian and Carboniferous sediments. The presence of solid bitumen is recorded in the sandstones of the upper Riphean in the well Storozhevskaya 1 (Kuzmin, 2006). During the existence of the system at the stages of sedimentation breaks, when Proterozoic and Paleozoic sediments were repeatedly removed to the surface of the day, the existing hydrocarbon resource potential in them could be partially lost.

Probable signs of the Riphean system in the South-East is an oil discovery in the Devonian terrigenous deposits of the Cherdyn oil field, and a large oil show in the timan deposits of the Fedorov field by the wells Yasva-22, 27, 28 and Lisow-96. Minor oil shows along the core in the form of impregnation of sandstones with oil are noted in the well Lisow-101 (Lesorub oil field). Most of oil obtained from the devonian, famenian, turonian, visean and bashkirian deposits, are light-weight, low-viscosity and sulphur, resin, paraffin, light fractions with a high content. It is possible that they are generated by Riphean deposits, as indicated by their low density, but with vertical migration they were "diluted" by heavy sulfur oils of the later, domanik system.

It should be noted that the implementation of the own generation capacity of domanikits of the underlying Devonian clastic sediments in this area is unlikely. In the Vendian deposits of the Vychegda trough the content of OM is negligible (up to 0.10 %, in isolated cases increased to 0.14 %). According to pyrolysis data, the generation potential (S_2) of OM is also small – less than 0.05 mg HC/g of rock, and the concentration of free hydrocarbons (S_1) is less than 0.03 mg HC/g of rock, indicating the absence of source rocks.

Within the spatial development of the Riphean system in the middle Carboniferous on Elmach-Parmin, Nivsher and Muluk areas, and also in the Vendian sediments of the well Kolchugino-140 gas shows observed. The composition of gas was nitrogen with a very low content of hydrocarbon, but with a helium content of 0.6-1.89 % vol., which may be an indicator of the deep origin of the fluid. According to T.G. Karasik (1959), the formation of nitrogen gas associated with the destruction of oil deposits, and within the Keltma shaft has been offloading of hydrocarbons in deep faults. At the same time, it is known that nitrogen often dominates in the oil deposits of the Udmurt Republic.

The formation of two hydrocarbon systems within the Vychegda trough is largely predetermined by the active tectonic factor of the formation of the Timan ridge in the Mesozoic. An indicator of the stress impact of Timan on the section of Proterozoic and Paleozoic deposits is a high stratigraphic range of oil-bitumen occurrences (up to the upper Permian deposits) along the North-Eastern boundary of the trough, that may be associated with vertical migration channels along the West Timan fault and operating disjunctives. In this

regard, it can be assumed that in the South-Eastern parts of the Vychegda trough is probably a superposition of two potential hydrocarbon systems with more clearly defined "domanik" component.

Summary

Thus, according to the results of the research, the following is established.

1.The two potential petroleum systems – "riphean" and "domanik" – are identified on the territory of the Vychegda trough. The first developed throughout the trough, the second – in the South-Eastern regions adjacent to the Solikamsk depression.

2. The domanik system oil source rocks entered the oil window, while the emigration potential increased in the Eastern direction. The upper Devonian, lower Carboniferous and Bashkir deposits are promising to the discovery of oil deposits.

3. In relatively deep horizons, the increased generation potential may be associated with strong Riphean deposits located in the oil window and partially gas window.

4. Priority areas of exploration should be planned based on the territorial development of the domanik system, mainly in the South-Eastern part of the Vychegda trough, taking into account the analogs of oil deposits and deposits discovered in the North-Western regions of the Solikamsk depression. Search objects may be prepared depression structures with the opening of wells of terrigenous deposits of the Devonian and deeper horizons.

5. For objective evaluation of oil potential of the Riphean petroleum system, it is recommended to drill a parametric well with a depth of not less than 5000 m in the South-Western border of the Vychegda trough with the Kazan-Kajim aulacogen, where projected development of source rocks, reservoirs and seals.

References

Albrandt T.S., Charpentier R.R. et al. (2005). Global resource estimates from total petroleum systems. USGS Energy resource program, 325 p. https://doi.org/10.1306/M861061

Aplonov S.V., Lebedev B.A., Timoshenkova N.V. (2004). The oil and gas problem of the Mezen sedimentary basin. *Otechestvennaya geologiya*, 2, pp. 3-10. (In Russ.)

Barnaby R. (2006). Modeling the burial and thermal history, organic maturation, and oil expulsion of the North Louisiana petroleum system. *Gulf Coast Association of Geological Societies*, 56, pp. 23-25.

Bazhenova T.K., Shapiro A.I. (2014). Main features of organic geochemistry of the sedimentary section of the Vychegda trough (in connection with the assessment of its oil-producing properties). *Proc. XVI Geological Congress of the Komi Republic: Organic geochemistry.* Syktyvkar: IG Komi NTs UrO RAN, Vol. III, pp. 131-133. (In Russ.)

Bazhenova T.K, Bogoslovskiy S.A., Shapiro A.I., Vasil'eva, Rogozina V.V. (2013). Vychegda trough (Russian plate) - organic geochemistry and geothermal history of sedimentary fill. *Neftegazovaya geologiya. Teoriya i praktika,* 8(3), pp. 1-31. (In Russ.) https://doi.org/10.17353/2070-5379/37_2013

Bashkova S.E., Karaseva T.V., Kozlova I.A., Bashkov A.N. (2018). Modeling the structure and formation of the oil and gas potential of Riphean-Vendian deposits that belong to north-east regions of the Volga-Ural oil and gas province. *Perm Journal of Petroleum and Mining Engineering*, 18(2), pp. 104-117. (In Russ.) http://dx.doi.org/10.15593/2224-9923/2018.4.1

Hantschel T., Kauerauf A. (2009). Fundamentals of Basin and Petroleum Systems Modeling. Heidelberg: Springer, 27 p.

Higley D.K., Lewan M. Roberts L.N. (2006). Petroleum System Modeling. Capabilities for Use in Oil and Gas Resource Assessments. USGS Open-File Report, 1024 p. https://doi.org/10.3133/ofr20061024

Karasik T.G., Geyro S.S. (1959). Bitumens in dozhivetsky sediments. *Tr. VNIGRI*, 133, pp. 347-352. (In Russ.)

Klimenko S.S. (2011). The Timan-Pechora sedimentary basin: Palaeozoic reef formations and petroleum systems. *Geological Society, London Memoirs*, 35(1), August, pp. 223-236. https://doi.org/10.1144/M35.13·

Kuzmin D.A. (2006). Geological and geochemical preconditions of oil and gas potential of the Upper Proterozoic sediments of the Mezen basin. Abstract Cand. geol. and min. sci. diss. Moscow, 24 p. (In Russ.)

Lindquist S.J. (1999).The Timan-Pechora Basin Province of Northwest Arctic Russia: Domanik-Paleozoic Total Petroleum System. U.S. Department of the Interior. U.S. Geological Survey. Open-File Report 99-50-G, 24 p. https://doi.org/10.3133/ofr9950G

Magoon L.B., Schmoker J.W. (2000).The total petroleum system – the natural fluid network that constrains the assessment unite, Chapter PS in U.S. Geological Survey World Petroleum Assessment 2000 – Description and Results. U.S. Geological Survey Digital Data Series *DDS-60*, 4 CD-ROMS.

Mancini E.A., Puckett T.M., Parcell W.C., Llinas J.C. (2001). Smackover petroleum system (source, reservoir, seal and trap) and underdeveloped Smackover reservoirs in the Mississippi Salt Basin. U.S. Department of Energy, Topical Reports 5 and 8, Project DE-FG22-96BC14946, 442 p.

Mancini E.A., Goddard D.A., Barnaby R. and Aharon P. (2006). Basin analysis and petroleum system characterization and modeling, interior salt basins, central and eastern Gulf of Mexico. U.S. Department of Energy, Final Technical Report, Phase I, Project DEFC 26-03NT15395, 427 p.

Mubarak M., Al-Hajeri M., Al Saeed J. (2009). Basin and Petroleum System Modeling. *Schlumberger Oilfield Review*, pp. 14-29.

Payrazyan V.V. (2010). UHydrocarbon systems (basins of ancient platforms of Russia). Moscow: Sputnik+, 153 p. (In Russ.)

Prishchepa O.M., Aver'yanova O.Yu., Il'inskiy A.A. et al. (2014). Oil and gas of low-permeable shale strata is a reserve of the raw material base of hydrocarbons in Russia. St. Petersburg: VNIGRI. SPb.: VNIGRI, 323 p. (In Russ.)

Shilovskaya T.I., Shilovskiy A.P. (2011). Lithology and features of tectonic structure of the sedimentary sequence of the Upper Proterozoic and Paleozoic of the Mezen syneclise (in connection with the prospects of oil and gas potential). *Geology, geophysics and development of oil and gas fields*, 11, pp. 18-22. (In Russ.)

Timothy R.K., Michael E., Thomas M.F. (2017). Assessment of Undiscovered Continuous Oil and Gas. Resources in the Domanik-Type Formations of the Volga-Ural Region Province, Russia. U.S. Department of the Interior, U.S. Geological Survey, pp. 23-26.

Tissot B.P. Espitalie J. (1980). Principal factors controlling the timing of petroleum generation. *Geochimica et Cosmochimica Acta,* January, pp. 234-242.

Tissot B.P., Welte D.H. (1981). The formation and distribution of oil. Moscow: Mir, 502 p. (In Russ.)

Tissot B.P., Welte D.H. (1984). Petroleum formation and occurrence. Springer-Verlag, 699 p. https://doi.org/10.1007/978-3-642-87813-8

Vakhnin M.G. (2016). State of study and prospects of oil and gas potential of the Mezen syneclise. *Geology, Geophysics and development of oil and gas fields*, 2, pp. 8-14. (In Russ.)

About the Authors

Tatyana V. Karaseva – Dr. Sci. (Geology and Mineralogy), Honored Geologist of the Russian Federation, Head of the Department of Regional and Oil and Gas Geology, Perm State University

15, Bukireva st., Perm, 614016, Russian Federation

Yury A. Yakovlev – Cand. Sci. (Geology and Mineralogy), Associate Professor, Advisor to the Department of Geology and Oil and Gas Reservoirs, Kama Research Institute for Integrated Research of Deep and Superdeep Wells (KamNIIKIGS JSC)

15, Krasnoflotskaya st., Perm, 614016, Russian Federation

Galina L. Belyaeva – Cand. Sci. (Geology and Mineralogy), Head of the Department for Scientific Support of Parametric and Super-Deep Drilling, Kama Research Institute for Integrated Research of Deep and Superdeep Wells (KamNIIKIGS JSC)

15, Krasnoflotskaya st., Perm, 614016, Russian Federation

Svetlana E. Bashkova – Cand. Sci. (Geology and Mineralogy), Scientific Secretary, Deputy Head of the Department for Scientific Support of Parametric and Super-Deep Drilling, Kama Research Institute for Integrated Research of Deep and Superdeep Wells (KamNIIKIGS JSC)

15, Krasnoflotskaya st., Perm, 614016, Russian Federation. E-mail: sbashkova@mail.ru

Manuscript received 2 July 2019;
Accepted 21 November 2019; Published 30 March 2020

ORIGINAL ARTICLE
DOI: https://doi.org/10.18599/grs.2020.1.39-45

Hydrocarbon deposits in non-anticlinal traps of the Yamal Peninsula of Western Siberia

V.L. Shuster[1,2], A.D. Dziublo[1,2], O.A. Shnip[2]*
[1]*Institute of Oil and Gas Problems of the Russian Academy of Sciences, Moscow, Russia Federetion*
[2]*Gubkin Russian State University of Oil and Gas (National Research University), Moscow, Russia Federetion*

Abstract. The article considers various types of non-anticlinal traps of the Yamal Peninsula of Western Siberia. The task is to establish the features of their formation and structure. Gas and gas condensate deposits were allocated in the Akhskian stratum of the Neocomian section, associated with wedge-shaped traps (Bovanenkovsky, Kharasaveysky fields). This type of lithologically-shielded traps was formed due to clastic material entering the territory of the Yamal Peninsula from the East Siberian Platform, the Yenisei Ridge (from the east) and the Ural Mountains (from the west). Sand and clay material accumulated along the path of underwater hills, where wedging zones formed. Traps of various types are developed in the Jurassic deposits of the region. Traps of tectonically shielded type are formed in areas of the active influence of discontinuous disturbances on the structure of the section (for example, on the Nurminsky Swell). Lithologically-shielded traps are formed on the slopes of the erosive remnants of the paleorelief in zones of terrigenous horizons wedging. Such traps are also formed in zones of their screening by the surface of the pre-Cretaceous erosion. The considered examples made it possible to establish the confinement of various types of traps to the sediment section and their distribution over the area of the Yamal region.

Keywords: gas, oil, clinoforms, non-anticline trap, criterion, hydrocarbon deposit, Western Siberia, Yamal Peninsula

Recommended citation: Schuster V.L., Dziublo A.D., Shnip O.A. (2020). Hydrocarbon deposits in non-anticlinal traps of the Yamal Peninsula of Western Siberia. *Georesursy = Georesources*, 22(1), pp. 39-45. DOI: https://doi.org/10.18599/grs.2020.1.39-45

Introduction

In Western Siberia, in its northern part (including the Yamal Peninsula), most of the anticlinal traps have been identified. Large and medium fields of oil and gas have been discovered in the upper (up to 4-5 km) section. The stock of anticlinal structures is almost exhausted. There is a need to study and identify complex non-anticline, combined traps.

As the depth of the search objects increases, the geological structure of the deposits becomes more complicated, the lithological composition of the rocks changes significantly, the influence of the tectonic activity on the subsoil structure increases, the type of void space changes, the reservoir properties of the rocks decrease and, due to these factors, the depth the structure of traps becomes more complicated, which varies from anticlinal to non-anticlinal combined type (Aleksin et al., 1992; Brekhuntsov, Bochkarev et al., 2001; Shuster, Punanova, 2019).

*Corresponding author: Vladimir L. Shuster
E-mail: tshuster@mail.ru

In the world giants and large fields have been identified in non-anticlinal traps, along with a significant number of open hydrocarbon deposits with small reserves: Bolivar Coast (Venezuela) – 4.1 billion tons of oil, East Texas (USA) – 0.8 billion tons of oil, Hugoton (Mexico) – 1.1 trillion m^3 of gas and others (Aleksin et al., 1992).

According to the forecast estimate, the share of oil resources in non-anticlinal traps of Western Siberia is more than 50 % of their total volume. There is reason to believe that a significant amount of hydrocarbon resources and reserves are confined to non-anticlinal traps and on the Yamal Peninsula (Brekhuntsov, Kislukhin, 2001; Shuster, Dziublo, 2012; Shuster, Punanova, 2016).

Many classifications of non-anticlinal traps based on various principles (genetic, morphological, screen structure, etc.) have been developed (Brod, 1951; Aleksin et al., 1992). There are mainly three types of traps: lithologically-shielded, tectonically-shielded and stratigraphically-shielded. As well as traps of a combined type. A number of authors (Oknova, 2012; Polyakov et al., 2015; Zhemchugova, Berbenev, 2015) additionally distinguish subtypes and classes of traps.

It is necessary to determine the complex of geological and geophysical criteria for their prediction and searchin order to successfully identify and map non-anticlinal traps. The development of criteria requires the accumulation of significant factual material and special scientific research on various sedimentary basins of the world and Russia, which in recent years have been actively conducted in a number of countries (Russia, the USA, China, etc.).

In this article, we consider the features of formation, structure of traps, their areal distribution and confinement to the section in the Yamal oil and gas region in order to accumulate the necessary information on the genesis and structure of non-anticlinal traps to develop criteria for their prediction and searches.

Materials and methods

The northern part of Western Siberia, including the Yamal Peninsula, is one of the world centers of gas accumulation where large and giant gas, gas condensate and oil and gas condensate fields are discovered in the Jurassic-Cretaceous deposits. Formations of the pre-Jurassic complex of deposits and basements are also promising (Brekhuntsov, Bochkarev et al., 2001; Skorobogatov et al., 2003; Shuster, Dziublo, 2012; Shuster, Punanova, 2016). A number of open hydrocarbon deposits are confined to non-anticlinal traps of various types.

The authors of the article examined the structural features of the identified deposits and traps, to which these deposits are confined, for the fields of the Yamal Peninsula and the adjacent territory and water area (Fig. 1, 2) based on the accumulated geological and geophysical material and published works.

The authors had at their disposal factual materials of processing and interpretation of seismic materials of the CDP 3D with a volume of 400 km^2 in the Bovanenkovsky and Kharasaveysky areas, as well as the results of drilling deep wells. In 2005, with the participation of one of the authors (A.D. Dziublo), a structural-tectonic model of the Bovanenkovo-Kharasaveysky area was created, illuminating the structure of Jurassic, Cretaceous and younger deposits. A basin analysis has been carried out. The model was constantly updated. These materials form the basis of ongoing research.

Results and discussion

The geological structure and oil and gas potential of the Yamal Peninsula and the adjacent waters of the Kara Sea, especially in the upper (Cretaceous and, to a lesser extent, Jurassic) part of the section, have been studied quite fully and are reflected in a number of published works, including the authors of the article (Dziublo et al., 2019; Shuster, Dziublo, 2012; Shuster, Punanova, 2019). Therefore, we outline briefly the main features of the geological structure of the Yamal Peninsula and the adjacent waters of the Kara Sea.

In the section of the Yamal Peninsula, three structural-tectonic floors are distinguished:

- the lower floor (basement) is represented by rocks of the Paleozoic and Upper Precambrian – these are tuff-siltstones, porphyritic gabbro-diabases, schists (discovered at the Novoportovsky and Bovanenkovsky fields);
- the intermediate floor (Triassic-Upper Permian) is composed of clay, siliceous, carbonate and volcanic-sedimentary rocks. The thickness of the Triassic stands out in the hollows of the Paleozoic relief;
- the upper structural floor with stratigraphic disagreement lies on the deposits of the intermediate complex, represented by sandy clay rocks of marine and continental origin (Fig. 3).

The entire section of the Yamal oil and gas region, from the Paleozoic to the Cenomanian, has mostly gas saturated, gas condensate and oil and gas condensate fields (oil rims on Bovanenkovsky, Novoportovsky, etc.). HC deposits are discovered in the Lower Middle Jurassic, Upper Jurassic, Neocomian, Barrem-Aptian, Alb-Cenomanian oil and gas complexes. Hydrocarbon deposits are predicted and individual industrial tributaries in the Paleozoic, Triassic oil and gas condensate and in basement formations have already been obtained.

For exploration and development of already discovered hydrocarbon deposits, it is important to study the structural features and forecast capabilities of non-anticlinal, combined type traps.

Having analyzed the available data (including the published material (Brekhuntsov et al., 2001; Brekhuntsov, Kislukhin, 2001; Zhemchugova, Berbenev, 2015; Oknova, 2012; Skorobogatov et al., 2003)) on the structure of a number of Yamal hydrocarbon deposits, the authors studied these trap deposits.

In the northern part of Western Siberia and on the Yamal Peninsula, one of the most promising and, to a large extent, explored oil and gas objects in complex traps is the Lower Cretaceous wedge-shaped complex, confined to the Achimov stratum and its analogues, at the bottom of the Neocomian. These are wedge-shaped reservoirs of the Urengoy, Yambur, Novoportovsk and other giant fields.

The Achimov stratum is represented by interbedded sandstone, siltstone and mudstone strata with a thickness of 0.1-0.5 m, less often up to several meters, reaching 28 m in some cases. Sandstones are characterized by low reservoir properties, increased density, and fine-grained composition. The facies diversity of the stratum associated with the conditions of their formation is noted in different parts of the basin.

At the Novoportovsk oil and gas condensate field, the NovoportovskianLower Cretaceous is an analogue of the

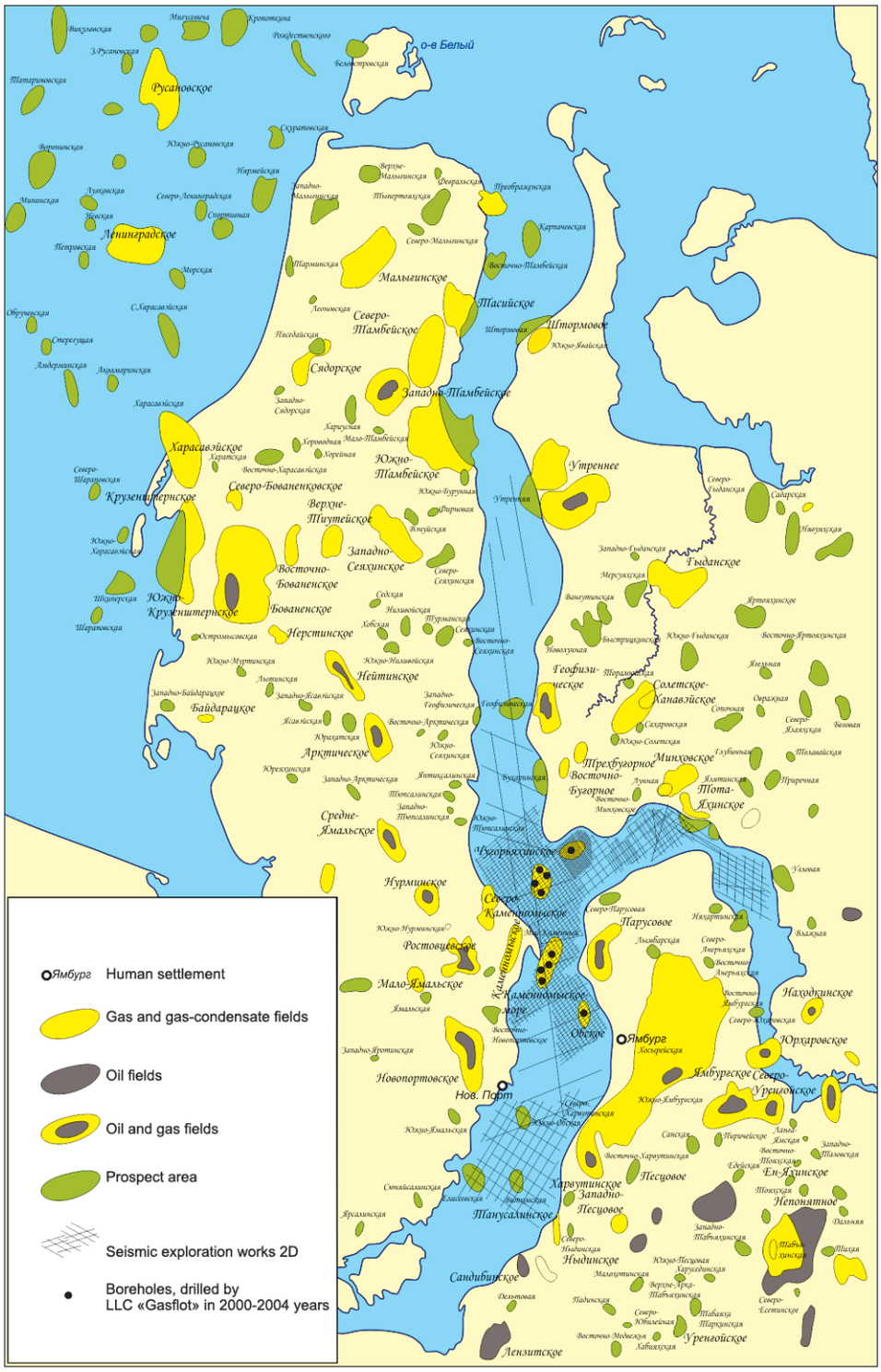

Fig. 1. Overview map of the Yamal Peninsula and the adjacent Kara Sea

Achimovstratum. The section of Cretaceous sediments begins with the Akhskian stratum, consisting of the Novoportovskian, Seyakhinskian, Znmuyakhinskian and Arctic strata (Skorobogatov et al., 2003).

The Novoportovskianstratum is represented by alternating wedge-shaped sand-aleurite and clay packs such as drift cones or underwater landslides. Horizontal sections of the section alternate with slanting. Facies of delta and drift cones are developed in the section of the sequence. From south to north, the thickness of the stratum decreases due to pinching of individual packs and lithological substitution of formations with good reservoir properties of clay horizons. In these areas, the formation of lithologically shielded traps is possible.

The Seyakhskian stratum is represented by dense clays.

The Nulmuyakhinskian stratum is composed of alternating sand-silt strata with clay strata.

The Arctic stratum is formed by clays.

To the north of the Novoportovsky field, the thickness

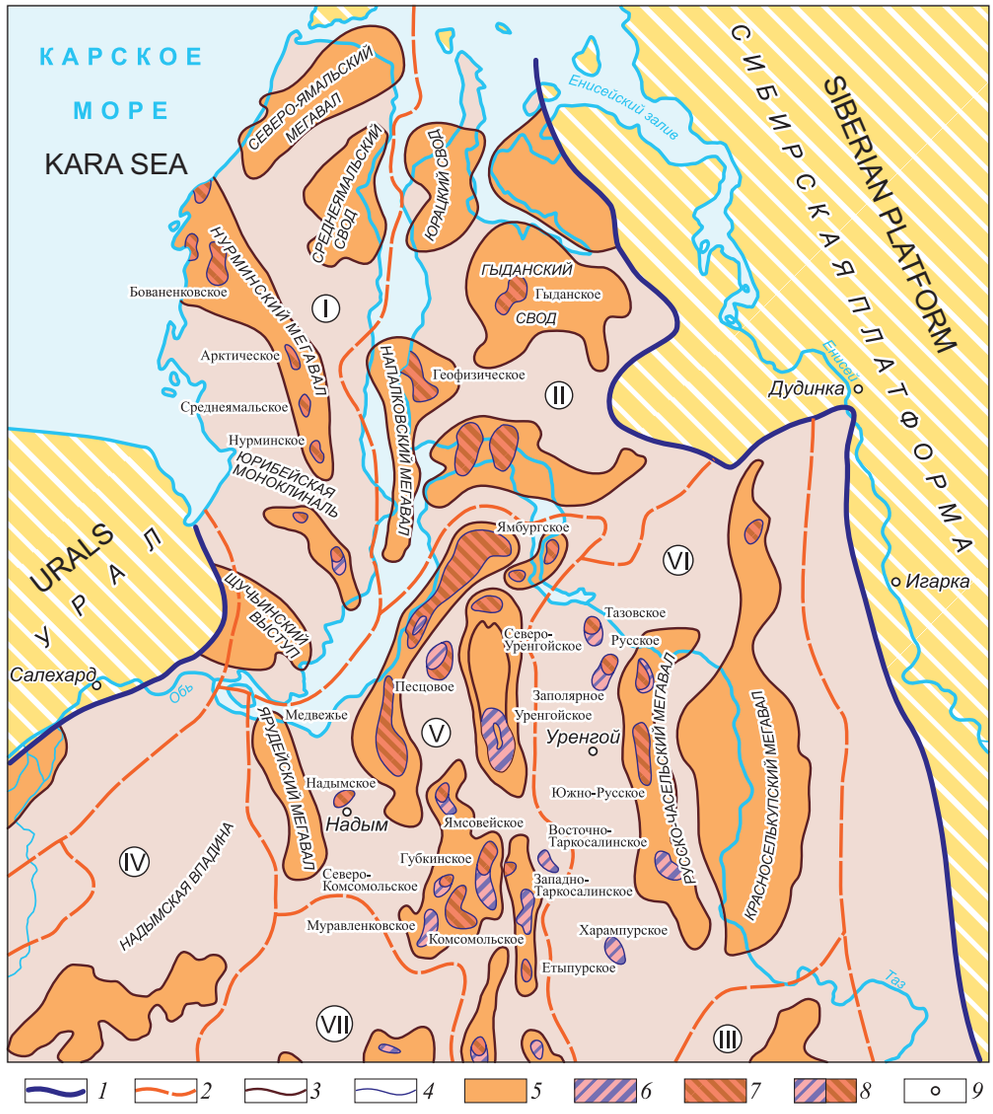

Fig. 2. Map of oil and gas geological zoning of the northern part of the West Siberian oil and gas basin (Oil and gas provinces ..., 1983, with additions and changes): 1-4 – borders: 1 – West Siberian oil and gas basin, 2 – oil and gas regions (I– Yamal, II – Gydansk, III – Payduginsky, IV – Frolovsky, V – Nadym-Pursky, VI – Pur-Tazovsky, VII – Sredneobsky), 3 – first-order structures (megaswells and vaults), 4 – field contours; 5 – megaswells and arches; 6-8 – fields: 6 – oil, 7 – gas and gas condensate, 8 – oil and gas condensate; 9 – settlements (Zhemchugova, Berbenev, 2015).

of the Akhskian stratum increases and the clay content of the section increases. The Novoportovskian sequence here is extremely complex, with frequent substitutions by other rocks with a lenticular structure. Sandstones are replaced laterally with mudstones and clays.

Within the Bovanenkovo-Kharasaveysky zone of the Yamal Peninsula, the sand-mudstone stratum in the Akhskian stratum of the Lower Cretaceous is an analogue of the Achimov sequence. Directly on the deposits of the Upper Jurassic, clinoforms are distinguished, plunging from west to east. Higher in the section, in the lower Tanopchinskian stratum, paleo-river basins are projected (based on seismic data). Deposits of gas and gas condensate were discovered in the Akhskian and Tanopchinskian stratums, in combined traps at the Kharasaveysky and Bovanenkovsky fields. Oil rims were encountered at the Bovanenkovsky field.

There is an idea (Brekhuntsov, Kislukhin, 2001) about the formation of clinoform strata due to clastic material coming from the east (East Siberian Platform, Yenisei Ridge) and to a lesser extent from the west (from the Urals), confirmed by seismic and drilling data. This explains the asymmetric structure of the neocomclinoforms.

The accumulation of sandy clay material occurred at the base of the underwater hills that impeded their advancement, which created wedging zones. Moreover, wedging zones are formed in the area of each new barrier. This is a favorable factor for the formation of lithologically-shielded type traps. This model is confirmed by modern well drilling materials.

There is also the point of view of TyumenNIIGiprogaz employees expressed at a scientific and practical conference in Tyumen (2010) about the deep-sea

Возраст		Литология	Мощн. м	Свита, описание		Газ на шельфе
ПАЛЕОГЕН-ЧЕТВ.			299-435	Глины и алевриты, пески, гравий		
ВЕРХНИЙ МЕЛ	Маастрихт		140	Ганькинская - глины, алевр.		
	Коньяк - сантон - кампан		470-567	Березовская. Верх - глины с просл. алевр. и песчаников. Низ - опоки, опоковидные глины, силициты		
	Турон		63-79	Кузнецовская - глины		
	Поздний альб - сеноман		490,8-700	Марресалинская - чередование песчаных, песчано-алевролитовых аркозовых и алевро-пелитовых пород. Углистые прослои		
НИЖНИЙ МЕЛ	Нижний - средний альб		115-186,8	Яронгская - аргиллиты с прослоями песчаников		
	Верхняя часть готерива - баррем - апт		500-950	Танопчинская - неравномерное преслаивание аркозовых песчаников, алевролитов и аргиллитов		
	Барриас - валанжин - начало готерива		460-1200	Ахская - клиноформные песчано-глинистые образования. Верх - аргиллиты часто битуминозные; низ - терригенные и глинистые породы с прослоями глинистых известняков		
ЮРА	Титон		8-10	Баженовская - аргиллиты		
	Кел. - оксф. - кимер.		65-82	Абалакская - аргиллиты		
	Бат		70-220	Большехетская серия	Малышевская - песчаники	
	Байосс		110		Леонтьевская - аргиллиты	
	Верхи аалена		90-120		Вымская - песч., алевр.	
	Верхи тоара - аален		20-120		Лайдинская - аргил., песч.	
	Плинсбах - тоар		278-350		Джангодская - песчаники и аргиллиты	
	Плинсбах - низы		100-150		Левинская - аргиллиты	
	Геттанг - синемюр		0-200		Зимняя - песчаники и аргиллиты	
ТРИАС			0-115	Мергели, карбонатно-глинистые,глинисто-кремнистые породы, долерито-базальты		
PCm - PZ3			>300	Слабо метаморфизированные сланцы, песчаники; мраморизован. известняки, габбро-диабазы		

Fig. 3. Summary lithological-stratigraphic section of the Yamal oil and gas region

underwater-landslide origin of these deposits, according to which the Novoportskian stratum has a macrolens structure and is represented by a series of sand-aleurite material cones.

Based on seismic data based on seismic facies analysis, wedge-shaped traps in the Novoportovsky sequence are predicted and discovered both at the Novoportovsky field and in adjacent territories in the Cretaceous and Jurassic deposits.

The conditions for the formation of terrigenous bodies of the Achimov stratum of the Neocomian and its analogues were fairly close in all parts of the territory, despite differences in the depth and distance from the drift sources. The best reservoirs were formed in front of the barriers to the "grain" material, i.e. on the slopes of the uplifts.

On the Yamal Peninsula, tectonically shielded traps are widespread, limited by discontinuous faults of the northwestern "Pai-Khoi" strike (Fig. 5).

Parusovsky field (east of the Novoportovsky field) is located in the zone of active fault tectonics. According to seismic data (Yamalgeofizika OJSC), about 30 tectonic faults have been identified here. Faults are usually represented by downthrows. The displacement of the layers along the faults reaches 100 m or more in some

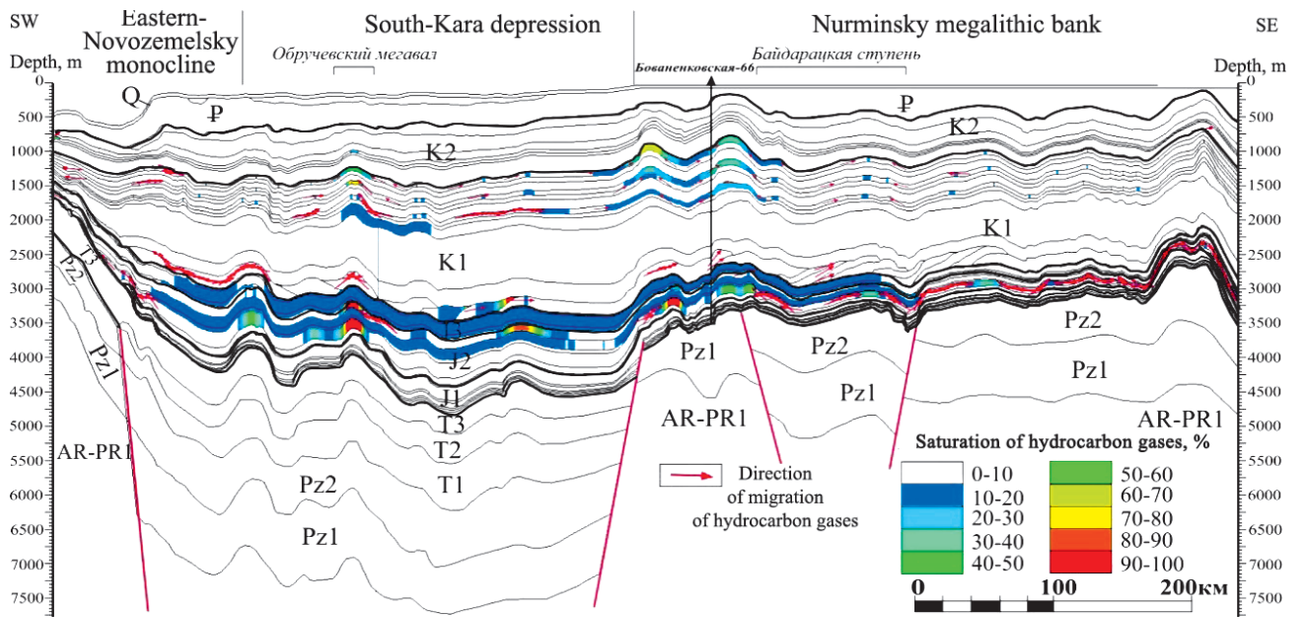

Fig. 4. Deep seismological section along the NW-SE profile

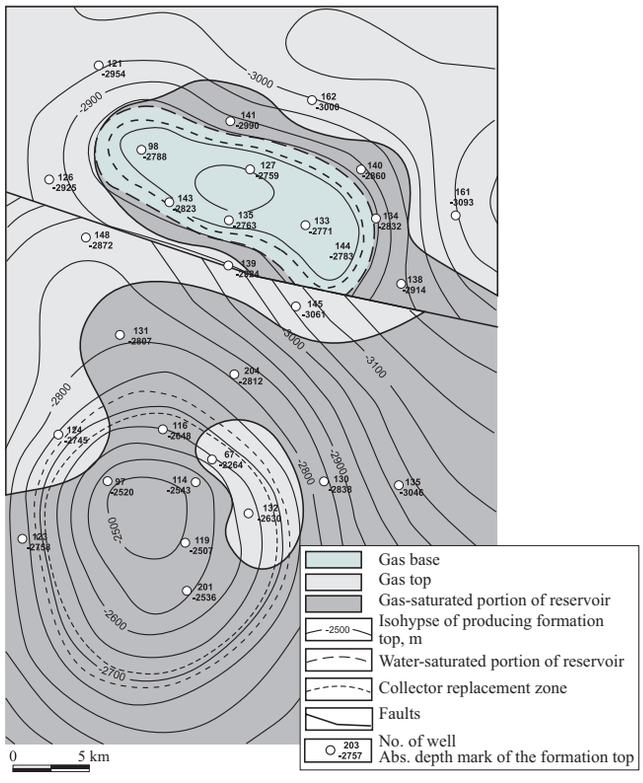

Fig. 5. Bovanenkovskyoil and gas condensate field. Structural map for the top of the Yu_3 formation (Skorobogatov et al., 2003).

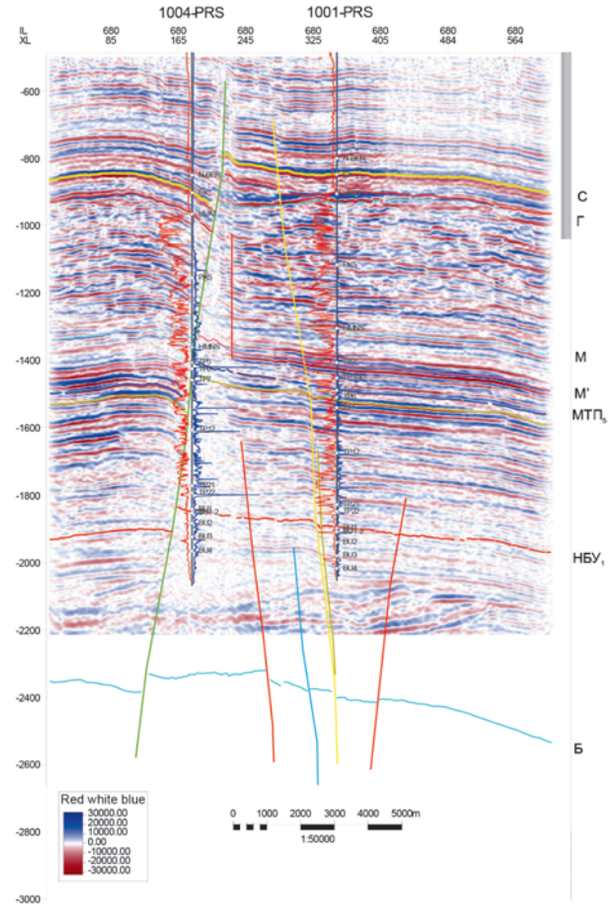

Fig. 6. Temporary seismic section along line 680 of the Parusovsky field (A.A. Doroshenko, Gazprom Geologorazvedka LLC, 2014)

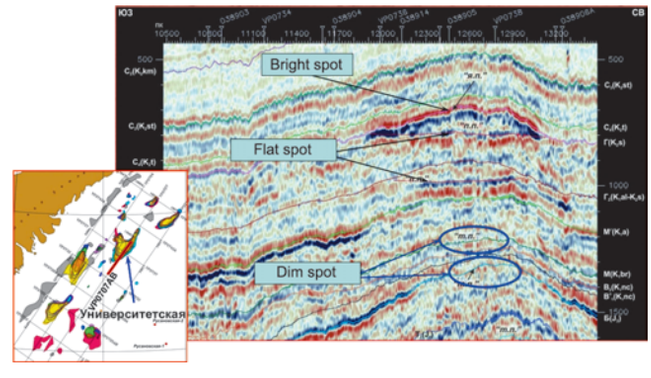

Fig. 7. Universitetsky structure. Anomalies of seismic recording in Cretaceous and Jurassic sediments (profile VP0707AB) (K.A. Dolgunov, Sevmorneftegeofizika OJSC, 2012)

intervals of the sedimentary cover. Violations are recorded not only on seismic data, but also in exploratory wells (Fig. 6). The system of explosive disturbances can be traced in the interval of the Jurassic and Cretaceous. Promising objects are associated with lithologically-shielded traps in the Achimov formations; tectonically-shielded traps in the Yu_2 – Tyumen Formation complex are predicted.

At the Bovanenkovsky field, a fault separating the north and south domes acts as a screen in a tectonically shielded trap in Jurassic deposits. Such traps are formed in the zones of tectonic disturbances of Jurassic and more ancient deposits, as well as in the basement formations.

Three fields have been discovered in the Kara Sea adjacent to the Yamal Peninsula: two gas condensate fields in the Cretaceous Alb-Cenomanian deposits and the Pobeda oil and gas field on Universitetsky area in the Jurassic deposits.

According to the Rosneft press center, recoverable gas reserves (499.2 billion m^3) in the Cretaceous deposits of the Cenomanian and Apt-Alb and oil (130 million tons) in Jurassic deposits have been registered. Judging by the seismic data presented (Fig. 7) there are traps in the Cretaceous and Jurassic sediments of the non-anticlinal combined type.

Conclusion

In the Yamal oil and gas region, the identified hydrocarbon deposits are confined to a wide range of non-anticlinal traps in the Jurassic-Cretaceous part of the section.

Clinoforms formed by clastic material coming from the East Siberian Platform, the Yenisei Ridge (from the east) and the Ural Mountains (from the west) are one of the widespread types of traps detected in the Achimov stratum at the bottom of the Neocomian sand-clay material accumulated along the path of movement underwater hills, where wedging zones formed.

The thickness has a macrolensed structure in the form of cones for the removal of sand-silt material. The formation of wedge-shaped bodies of the Achimov stratum and its analogues in the Yamal oil and gas region is fairly close throughout the territory. This provides a basis for predicting such traps in new areas of the region.

In the Jurassic deposits of the Yamal oil and gas region, traps of a tectonically shielded type are developed in areas of the active discontinuous faults of the northwestern strike influencing on the structure of local uplifts, as well as of a lithologically shielded type in the zones of wedging of terrigenous horizons on the slopes of erosive remnants of the paleorelief. Traps of a similar type are also formed in the zones of their screening by the surface of the pre-Cretaceous erosion.

The considered examples of the trap types common in the Yamal oil and gas regions, their genesis and structure, confinement to the sediment section and spread over the area allow expanding the capabilities of forecasting, searching and exploring non-anticlinal traps, as well as increasing the efficiency of oil and gas production at the field development stage.

Acknowledgments

The article was written as part of the state assignment on the topic "Development of the scientific and methodological foundations of the search for large hydrocarbon accumulations in non-structural traps of the combined type within platform oil and gas basins", No. AAAA-A19-119022890063-9).

References

Aleksin A.G., Gogonenkov G.N., Khromov V.T. et al. (1992). The methodology for the search for oil and gas deposits in traps of complex screened type. 2 parts. Moscow: VNIIOENG, 227 p., 220 p. (In Russ.)

Brekhuntsov A.M., Bochkarev V.S., Borodkin V.M., Deshchenya N.P. (2001). The allocation of the main oil and gas objects in the north of Western Siberia in connection with the development of oil and gas fields. *Geologiya, geofizika i razrabotka neftyanykh mestorozhdenii = Geology, geophysics and development of oil and gas fields*, 5, p. 4-15. (In Russ.)

Brekhuntsova E.A., Kislukhin V.I. (2001). Features of formation of oil and gas potential in the sedimentary cover of the Yamal Peninsula. *Geologiya, geofizika i razrabotka neftyanykh mestorozhdenii = Geology, geophysics and development of oil and gas fields*, 5, p. 36-41. (In Russ.)

Brod I.O. (1951). Oil and gas deposits. Moscow: Gostoptekhizdat, 340 p. (In Russ.)

Dziublo A.D., Maslov V.V., Evstafiev I.L. (2019). Geological structure and prospects for the discovery of oil deposits in the Lower Cretaceous and Jurassic sediments of the Ob and Taz Gulfs of the Kara Sea. *Neftyanoe khozyaystvo = Oil Industry*, 1, pp. 11-15. (In Russ.) https://doi.org/10.24887/0028-2448-2019-1-11-15

Oknova N.S. (2012). Nonanticlinal traps – examples from Volga-Ural and Western Siberia oil-and-gas provinces. *Neftegazovaya Geologiya. Teoriya I Praktika*, 7(1), pp. 1-14. http://www.ngtp.ru/rub/10/10_2011.pdf. (In Russ.)

Polyakov A.A., Koloskov V.N., Fonchikova M.N. (2015). On the classification of petroleum accumulations. *Neftegazovaya Geologiya. Teoriya I Praktika*, 10(1), pp. 1-15. (In Russ.) https://doi.org/10.17353/2070-5379/7_2015

Shuster V.L., Dzyublo A.D. (2012). Geological preconditions of oil and gas potential of deep-seated Jurassic and pre-Jurassic deposits in the north of Western Siberia. *Ekspozitsiya neft' gaz*, 2, pp. 26-29. (In Russ.)

Shuster V.L., Punanova S.A. (2016). Justification of Oil and Gas Potential of the Jurassic-Paleozoic Deposits and the Basement Formations of Western Siberia. *Georesursy = Georesources*, 18(4), pp. 337-345. http://dx.doi.org/10.18599/grs.18.4.13

Shuster V.L., Punanova S.A. (2019). Hydrocarbon accumulations in unconventional traps of deep-seated deposits in the north of Western Siberia are a reserve for the growth of oil and gas resources. *Int. Sci.-Pract. Conf.: New ideas in the geology of oil and gas. Coll. papers*. Moscow: Pero, pp. 544-548. (In Russ.)

Skorobogatov V.A, Stroganov L.V., Kopeev V.D. (2003). Geological structure and oil and gas potential of Yamal. Moscow: Nedra. 352 p. (In Russ.)

Zhemchugova V.A., Berbenev M.O. (2015). Basic principles for modeling reservoir structure (on the example of Cretaceous deposits of the Western Siberia. *Georesursy = Georesources*, 2(61), pp. 54-62. (In Russ.) http://dx.doi.org/10.18599/grs.61.2.5

About the Authors

Vladimir L. Shuster – Cand. Sci. (Geology and Mineralogy), professor, Chief Researcher, Institute of Oil and Gas Problems of the Russian Academy of Sciences

3, Gubkin st., Moscow, 119333, Russian Federation

E-mail: tshuster@mail.ru

Alexander D. Dziublo – Cand. Sci. (Geology and Mineralogy), Professor, Gubkin Russian State University of Oil and Gas (National Research University)

65, Leninsky ave., 119991, Russian Federation

Oleg A. Shnip – Cand. Sci. (Geology and Mineralogy), Professor, Gubkin Russian State University of Oil and Gas (National Research University)

65, Leninsky ave., 119991, Russian Federation

Manuscript received 15 August 2019;
Accepted 28 November 2019;
Published 30 March 2020

ORIGINAL ARTICLE
DOI: https://doi.org/10.18599/grs.2020.1.46-54

Biomarker hydrocarbons of oils from the Labagan field of the Timan-Pechora oil and gas province

O.V. Valyaeva[*], *N.N. Ryabinkina, D.A. Bushnev*
Institute of Geology of the Komi Science Centre of the Ural Branch of the Russian Academy of Sciences, Syktykvar, Russian Federation

Abstract. The results of geochemical studies of four oils samples from Paleozoic deposits of the Labagan field of the Timan-Pechora oil and gas province are presented. It is shown that the organic matter, which generated the oil of the Lower Devonian and Tournaisian deposits of the Labagan field, is sapropelic, its accumulation occurred in a marine sub-reducing environment. The oils of the Artinskian and Ufimian deposits are substantially biodegraded. Type of collectors is fissure-porous, secondary-porous. Carbonate reservoirs of the Devonian, Carboniferous and Permian (Artinian) age are characterized by good and medium reservoir properties. Terrigenous reservoirs of the Ufimian deposit have good reservoir properties.

Keywords: Timan-Pechora province, Paleozoic deposits, biomarker hydrocarbons, oil, genetic typification, correlation, reservoir

Recommended citation: Valyaeva O.V., Ryabinkina N.N., Bushnev D.A. (2020). Biomarker hydrocarbons of oils from the Labagan field of the Timan-Pechora oil and gas province. *Georesursy = Georesources*, 22(1), pp. 46-54. DOI: https://doi.org/10.18599/grs.2020.1.46-54

Introduction

The Labagan oil field is geographically confined to the Sorokin swell of the Varandey-Adz'va structural zone of the north of the Timan-Pechora oil and gas province (TPOGP) (Fig. 1). Currently, the field is developing 15 oil deposits located in reservoirs from the Lower Devonian to the Triassic (Kleshchev, Shein, 2010). The confinement of the deposit to the Varandey-Adz'va fault zone is of interest from the point of view of the genesis of petroleum hydrocarbons (HCs) and the formation of the field itself: what was exactly source of the hydrocarbons? What is their nature and trap filling time? The study of the properties and composition of oils from different oil and gas complexes and their genetic typification are an important stage in the comprehensive geological and geochemical study of the region's oil and gas potential in order to assess prospects and determine further directions for the search and exploration of deposits. The article is a continuation of the study we conducted earlier in this field (Ryabinkina, Valyaeva, 2018).

Short geological sketch

The Labagan structure is composed of Silurian to Quaternary sediments. Stage boundaries were drawn according to Stratigraphic Code (2006). The productive horizons of the Labagan deposit are confined to the Lower Devonian, Upper Devonian, Lower Carboniferous, Lower Permian and Lower Triassic deposits (Fig. 2). We studied only the rocks confined to the carbonate deposits of the Ovin-Parmian horizon of the Lower Devonian, the Tournaisian stage of the Lower Carboniferous and the Artinian stage of the Lower Permian, as well as to the terrigenous deposits of the Ufimian stage, which is currently attributed to the Lower Permian (Kotlyar, 2009; Kotlyar et al., 2013).

Lower Devonian sediments were intersected by well 76 in the central part of the Labagan structure at a depth of 3500-4130 m. The oil pool is confined to the anticline trap and is a reservoir, vault, with size of 5.0 km × 2.5 km, the height of the pool is 74 m. The enclosing deposits are represented by dark-gray strong dolomites, weakly cavernous and fractured with interlayers of greenish-gray, fractured mudstones. The rocks are oil-saturated with spots and vertical cracks. The average reservoir porosity is 8 %, and the extraction coefficient is up to 30 %. The reservoir is sealed by overlying Lower Devonian sulphate-dolomite deposits.

Carboniferous deposits conformably occur on Upper Devonian limestones and are overlain by Permian carbonate deposits with a stratigraphic gap. *Tournaisian sediments* are characterized by a core in all deep wells of the Labagan field. An industrial oil pool was identified and explored in the section. A mudstone member occurs at the base of the Tournaisian strata. The Tournaisian oil pool (C_1t) is confined to carbonate reservoirs of

[*]*Corresponding author: Olga V. Valyaeva*
E-mail: valyaeva@geo.komisc.ru

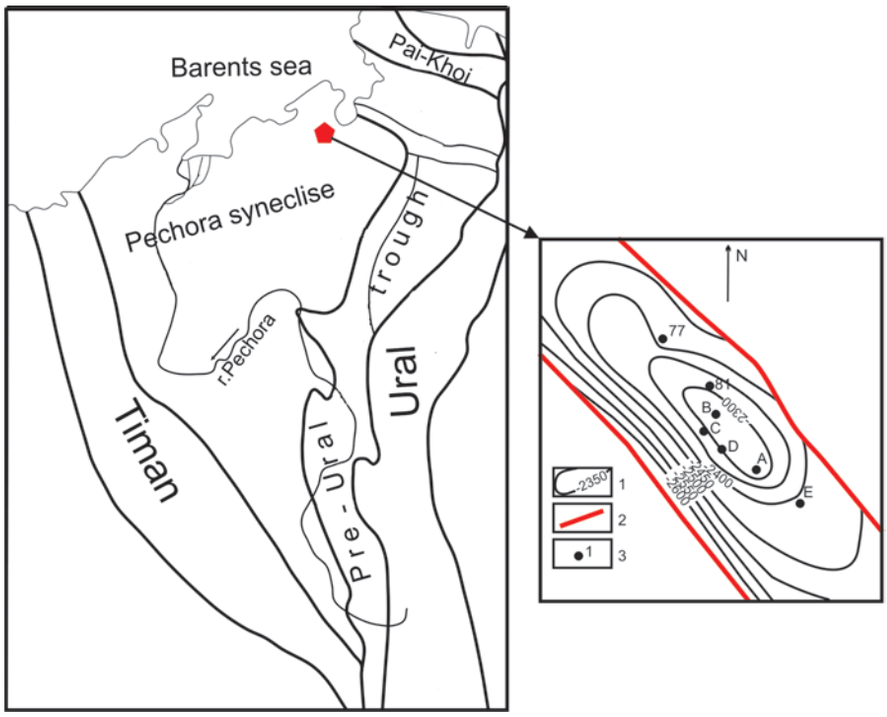

Fig. 1. General scheme of the TPOGP and structural map of the roof of the Tournaisian carbonate deposits. 1 – isogypses of the roof of carbonate deposits; 2 – tectonic disturbances; 3 – wells.

pore-fractured, rarely pore types, it has dimensions of 6.6 km × 3.2 km, the height of the pool is 82 m, the extraction coefficient is 34 %, the average porosity of the reservoirs is 12 %. All carbonate rocks are oil-saturated. In addition, minor layers of mudstone, anhydrite, siliceous rock, and clay siltstone are occasionally found in the section. The thickness of the Tournaisian stage ranges from 84 to 91 m.

The lower part of **Permian deposits** of the *Asselian, Sakmarian, and Artinskian stages* with stratigraphic unconformity occurs on carbonate rocks of the Middle and Upper Carboniferous divisions. The Lower Permian deposits are clearly divided into two strata according to their lithofacies features: the upper one is terrigenous and the lower one is carbonate.

At the base of the Permian productive layer in the sections of wells 73, 75 and 81, the development of a member of organogenic limestones of the *Asselian and Sakmarian age* is noted, which are replaced by fine-grained limestones with a more clay composition, often marl-like. The thickness of the strata is 60-120 m.

The main productive horizon of the *Artinskian age* is composed of permeable carbonate rocks and lies in the roof of the thickness. It is mainly represented by fine-grained limestones and organogenic detritus, porous and fractured, layered, clay-silty, to varying degrees, silicified, with numerous inclusions of fauna. Sometimes in the thickness of limestones there are single strata of marls. The thickness of the productive horizon varies from 26 to 57 m. The Artinskian oil pool (P_1ar) is

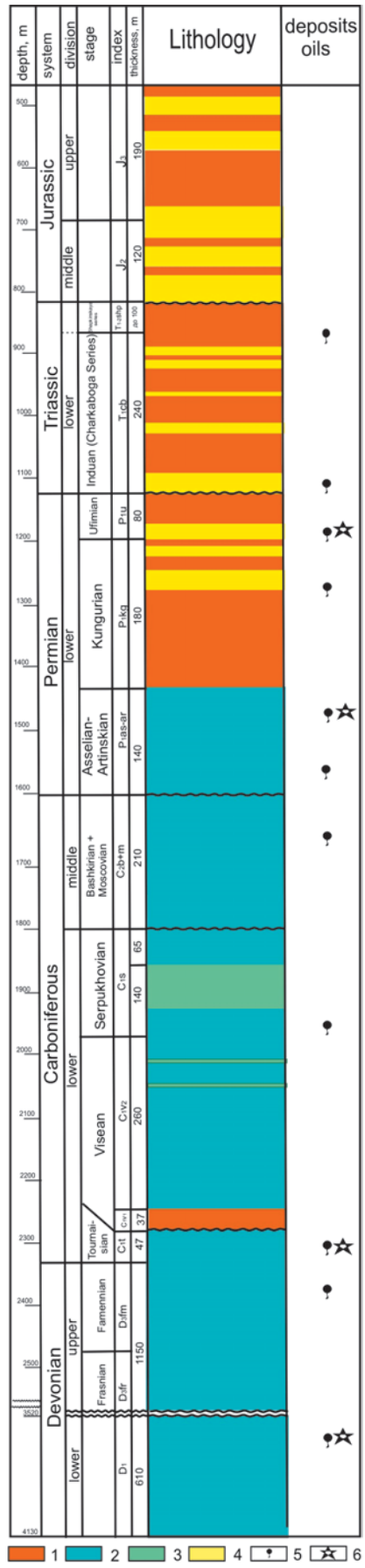

Fig. 2. Summary lithological column and location of oil deposits of the Labagan field. 1 – mudstones, 2 – limestones, dolomites, 3 – anhydrites, 4 – sandstones, 5 – oil deposits, 6 – analyzed oil samples.

confined to carbonate pore and pore-fracture reservoirs. It has a size of 12.0 km × 3.2 km, the height of the deposit is 97 m. The average porosity of the reservoirs is 22 %. Below the productive layer, small- and fine-grained clay and marl-like fractured limestones begin to play a dominant role in the section of the considered thickness, with prints and fragments of fauna, with inclusions of plant detritus and pyrite. Mudstones of the Kungurian age are a seal for the pool. The total thickness of undivided carbonate deposits (Asselian-Sakmarian-Artinskian) within the area varies from 167 to 202 m.

As part of the terrigenous strata of the Lower Permian, the *Kungurian age* is established, which is represented by sandstones, siltstones and mudstones that conformably occur on the Artinskian carbonate deposits. Argillites are clearly dominant in the section of the Kungurian stage. Thickness of the terrigenous strata is from 172 to 193 m.

The Ufimian stage is represented by an alternation of terrigenous rocks of continental, lagoon-marine and lagoon-freshwater facies with single layers of dense light-gray limestone based on the study of core from wells 74, 75, 82 and 141. Wells 75 and 73 received oil inflows from the Ufimian deposits (1235-1247 m in 73; 1112-1140 m in 75). The rocks are represented by fine-medium-grained light-gray polymictic sandstones with clay and carbonate cement. There are layers of coal and black mudstones. Coal and carbonaceous inclusions contain the imprints of plants. There are small layers of limestone light gray, massive, dense. The thickness of the Ufimian deposits is 80-236 m. The Ufimian oil pool (P_1u) is a reservoir, vault, and confined to terrigenous pore reservoirs. It has a size of 12.0 km × 3.2 km, the average porosity of the reservoirs is 28 %, and the extraction coefficient for development using steam-thermal (PTV) methods is 45 %.

Materials and methods

The collection of the studied oils includes samples from 5 wells located in the depth range of 1235-3980 m and in a wide stratigraphic range of deposits from the Lower Devonian Lohkovian to Permian Ufimian (Table 1). The studied oils differ in density, sulfur content, waxes and asphaltenes concentrations. So, in the Lower Devonian and Lower Carboniferous deposits, there are oils belonging to the class of heavy oils, and in the Permian deposits – to the class of bituminous oils. Oil in the P_1ar formation, as well as in the overlying P_1u formation, belongs to low-wax, sulfur, and high-tar. Classification of oil is given by (Guidelines for the application of the Classification of reserves..., 2016).

Fractionation of oil. Asphaltenes were separated from a weighted oil sample through precipitation by n-hexane (oil and n-hexane were used in the volume proportion of 1:40). The obtained maltene fraction was separated into apolar (50 ml of 20 % dichloromethane solution in n-hexane) and polar (resins, 50 ml of ethanol-benzene mixture (1:1)) on a column filled with aluminum. The apolar fraction was separated into fractions saturated HCs (eluent – n-hexane) and aromatic HCs (eluent – benzene) on a silica gel column.

The *gas chromatography (GC) analysis* was made by Kristall-2000M chromatograph (30 m × 0.25 mm column HP-5, 0.25 μm thick stationary phase). Temperature was programmed from 110 to 300 °C at a rate of 5 °C/min. The injector and detector temperatures were 300 °C.

Gas chromatography–mass spectrometry (GC-MS) analysis was carried out by Shimadzu QP 2010 Ultra (30 m × 0.25 mm column HP-5, 0.10 μm thick stationary phase). Temperature was programmed from 110 to 300 ºC at a rate of 5 °C/min. The injector temperature was 300 °C, detector temperature was 250 °C. Mass-chromatograms were reconstructed to m/z 217 for sterane hydrocarbons and m/z 191 for terpane hydrocarbons.

Results and Discussion

Geochemical characteristics of oils

Acyclic hydrocarbons

On chromatograms obtained by the GC method, the distribution of n-alkanes in the oil deposits, studied by us from the Lower Devonian and Lower Carboniferous deposits, is generally quite similar (Fig. 3a, b).

In the saturated fraction, n-alkanes of the C_{11}-C_{34} composition were identified, which were characterized by a single-mode distribution dominated by n-C_{11}–n-C_{18}

	Well	A	B	C	D	E
Parameters	Age	D_1l	C_1t	C_1t	P_1ar	P_1u
	Depth, m	3936-3980	2338-2369	2326-2350	1375-1390	1235-1247
	Density, g/cm^3	0.876	0.878	0.876	0.936	0.963
	Sulfur, %	0.42	0.66	0.63	2.25	2.7
	Waxes, %	1.09	4.80	5.01	1.26	0.6
	Resins, %	8.82	9.53	13.63	15.21	19.14
	Asphaltenes, %	1.45	2.77	6.77	6.01	3.83

Table 1. Physico-chemical properties of the Labagan field oils

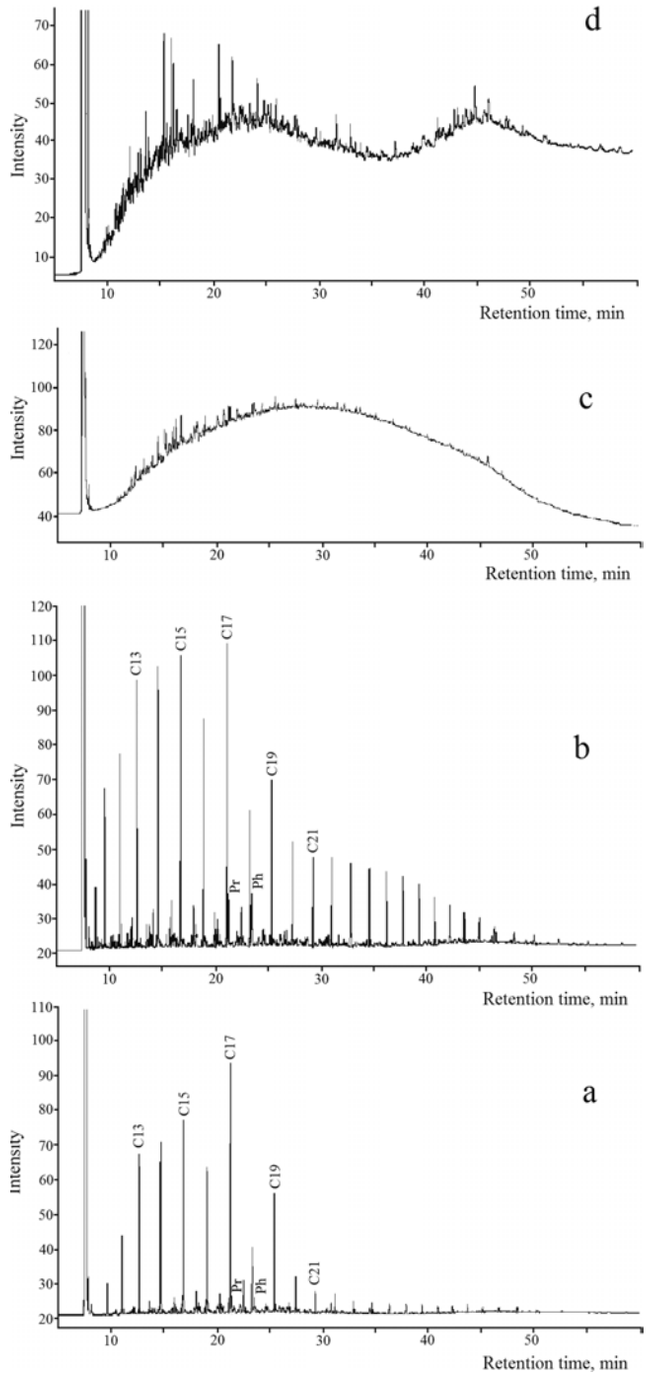

Fig. 3. Chromatogram of the distribution of normal and isoprenoid alkanes in the oils of the Labagan field: a) well A, b) well B, c) well D, d) well E. C (number) – n-alkanes, Pr – pristane, Ph – phytane

(Table 2). Thus, the relative concentration of low molecular weight alkanes of the composition n-C_{11}-n-C_{18} varies from 54.36 to 71.38 %. Then there is a marked decrease in the content of high-molecular n-alkanes: n-C_{25}-C_{34} accounts for 5.39 to 15.45 %. This distribution of alkane HCs indicates that the accumulation of the initial organic matter (OM) of the studied samples occurred under marine conditions (Tissot, Welte, 1981; Ilyinskaya, 1985). Oils are characterized by the prevalence of n-C_{17} over neighboring homologs; the odd ratio of $2\times C_{17}/(C_{16}+C_{18})$ varies from 1.71 to 2.51, which may indicate the contribution of algal OM to the initial biomass (Tissot, Welte, 1981; Hunt, 1982). The value of the odd ratio of high-molecular n-alkanes $2\times C_{29}/C_{28}+C_{30}$ for sapropelic OM, the formation of which took place under reducing conditions, rarely exceeds 1 (Peters, Walters, Moldowan, 2005). The CPI (Carbon Preference Index) is in the range of 1.13-1.30, characterizing oil as mature (Peters, Walters, Moldowan, 2005).

The content of iso-alkanes is very low (iso/n-alkanes – 0.08-0.11). The Pr/Ph ratio is close to 1, which may indicate that accumulation of the initial OM occurred most likely in a reducing environment (Peters et al., 2005). The indicators Pr/n-C_{17} and Ph/C_{18} are characterized by small values: 0.07-0.21 and 0.3-0.5, respectively. The ratio $(Pr + Ph)/(C_{17} + C_{18})$ is low (0.120-0.30).

According to the authors (Reed et al., 1986; Jacobson et al., 1988), the prevalence among the alkanes of the normal structure of the odd homologues of the composition C_{15}-C_{19} (sometimes C_{21}) in combination with low concentrations of higher molecular n-alkanes and low concentrations of isoprenoids is widespread in OM of the Ordovician source rocks and the oils produced by them.

The dominance of n-alkanes of C_{17} and C_{19} together with low concentrations of isoprenoid HCs, recorded in the Lower Paleozoic TPOGP oils, allowed us (Bushnev et al., 2018) to suggest the possibility of generating these oils by deposits containing *G. Prisca* microalgae typical of Ordovician deposits.

For the oils of the Timan-Pechora basin T.A. Kiryukhina (Kiryukhina, 1995) gives a classification based on the distribution of n-alkanes and isoprenoids; according to this classification the oils we studied are of type I, that can be confirmation of generative accessory oils of the Labagan field to Ordovician-lower Devonian oil and gas complex (Fig. 4).

According to the formation-genetic typification proposed for the Timan-Pechora sedimentary basin oils by the authors (Prischepa et al., 2011), the oil from the wells A-C can be attributed to the family B (oil and gas source rock horizon S_2-D_1), a detailed description of which is given by O.M. Prischepa and co-authors.

There are no n-alkanes and isoprenoids on the oil chromatograms from Permian deposits (Fig. 3c, d), indicating biological oxidation of oils involving microorganisms (Bailey et al., 1973; Reed, 1977; Jobson et al., 1979; Connan, 1984; Petrov, 1984; Kashirtsev et al., 2001; etc.). Intensive biodegradation of oils has changed their hydrocarbon composition and makes it difficult to carry out their genetic typing. It is not possible to determine the type of initial OM as well as the conditions of its precipitation by GC analysis results for these oils.

Well	A	B	C	D	E
Age / Geochemical parameters	D_1l	C_1t	C_1t	P_1ar	P_1u
$\sum C_{11}$-C_{18}	71.38	61.32	54.56	-	-
$\sum C_{19}$-C_{24}	15.97	19.24	21.45	-	-
$\sum C_{25}$-C_{34}	5.39	9.82	15.45	-	-
iso-/n-alkanes	0.08	0.11	0.09	-	-
Pr/Ph	1.01	0.98	0.94	-	-
$(Pr+Ph)/(C_{17}+C_{18})$	0.12	0.29	0.30	-	-
Pr/C_{17}	0.07	0.21	0.21	-	-
Ph/C_{18}	0.30	0.49	0.50	-	-
$2*C_{17}/(C_{16}+C_{18})$	2.51	1.73	1.71	-	-
$2*C_{29}/(C_{28}+C_{30})$	0.88	0.86	0.89	-	-
CPI	1.13	1.30	1.26	-	-
$C_{27} : C_{28} : C_{29}$	35:26:39	31:28:41	31:29:40	31:21:48	32:22:46
Dia/reg	1.23	0.59	0.61	0.39	0.42
Steranes/hopanes	0.10	0.15	0.15	0.18	0.26
Tri/penta	0.07	0.07	0.07	0.26	0.39
$C_{35}/(\sum C_{31\text{-}35})$	0.15	0.14	0.12	0.15	0.17
H_{29}/H_{30}	0.52	0.59	0.71	1.30	1.31
$*K_1$	0.41	0.50	0.49	0.46	0.50
$**K_2$	0.48	0.50	0.51	0.56	0.55
βα, % C_{30}	8.50	8.40	9.41	6.65	8.08
22S/22S+22R	0.60	0.60	0.61	0.54	0.53
Ts/Tm	1.15	1.37	1.42	0.48	0.47

Table 2. Geochemical characteristics of the saturated fraction of the Labagan field oils. $*K_1$ = 20S/20S+20R (C29 5α(H),14α(H),17α(H) steranes); $**K_2$ =abb/abb+aaa (C29 5α(H),14β(H),17β(H)- and 5α(H),14α(H),17α(H)-steranes).

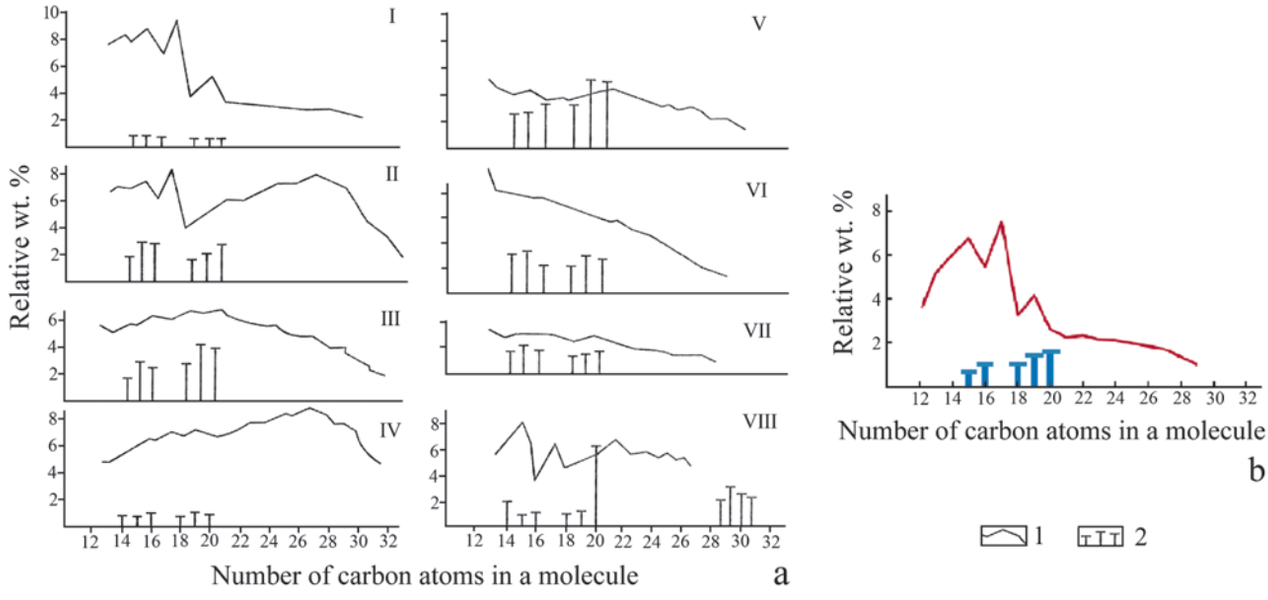

Fig. 4. Molecular weight distribution of n-alkanes (1) and isoprenanes (2) in high boiling fractions of oils: a) of different geochemical types (I-VIII), by (Kiryuchina, 1995); b) in the oil of Labagan field (average values for wells A-C)

Polycyclic hydrocarbons

In oils, the composition of polycyclic HCs-biomarkers has been studied, which contains important information on the composition of the initial organic matter of oils, conditions of its accumulation and thermal transformation (Peters et al., 2005). Their distribution and the resulting coefficients are shown in Table 2.

The distribution of steranes is shown in m/z 217 mass chromatograms (Fig. 5). Cholestane (C_{27}) varies from 31 to 35%. There is a slight prevalence of ethylcholestane (C_{29}) over neighboring homologs, its oil content varies from 39 to 48 %. Triangular diagram shows αββ steranes of the C_{27}-C_{29} distribution (Fig. 6). Figure 6 clearly shows that the oils from Lower Devonian Lokhkovian deposits and Lower Carboniferous Tournaisian deposits have a slightly different composition of the initial OM than Permian oils, but are characterized by similar sedimentation conditions of the initial OM, which occurred in coastal-marine environments.

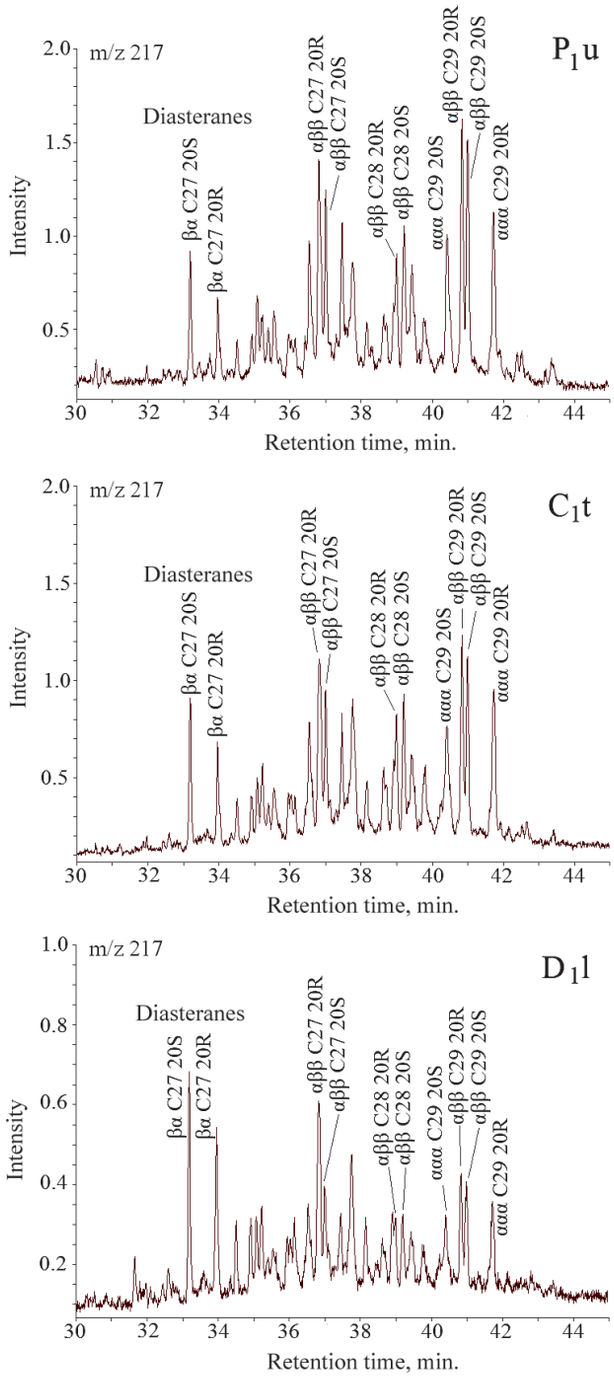

Fig. 5. Mass chromatograms of steranes (m/z 217) of methane-naphthene fractions of oils from deposits of different ages

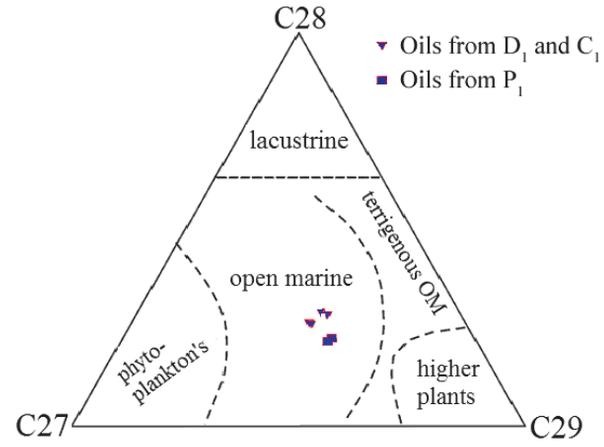

Fig. 6. Diagram of the relative distribution of C_{27}-C_{29} isosterans in oils

One indicator of the facial conditions of sediment accumulation (Brassell et al., 1984; Petrov, 1991) is the ratio of diasteranes to regular steranes (dia/reg). The increased values of this coefficient (0.59-1.23) indicate the prevalence of the clay component in source rocks (which is consistent with the data on the lithological composition of the rocks).

To assess the contribution of algal and bacterial organics, the authors (Peters et al., 2005) suggested using the ratio of steranes/hopanes. The ratio steranes/hopanes varies from 0.10 to 0.26, which indicates an insignificant or moderate bacterial processing of the initial organic matter in an early diagenesis.

The distribution of terpanes is shown in m/z 191 mass chromatograms (Fig. 7). Tricyclic HCs, hopanes, moretane are clearly identified on mass chromatograms. The D_1l and C_1t oils are low in tricyclic hydrocarbons (tri/penta ratio is 0.07), and in biodegradated oils this value rises to 0.39.

Hopanes are represented by compounds from H_{27} to H_{35}. The distribution of αβ hopanes of C_{31}-C_{35} composition – the homohopane index ($C_{35}/C_{31}+C_{35}$) – is characterized by low values, which indicates the existence of sub-reducing conditions in sedimentation of the initial OM in early diagenesis.

The ratio of adiantane (C_{29}) to hopane C_{30} for oils, the genotype of which we have defined as the Ordovician-Lower Devonian, varies from 0.52 to 0.71, and for oils from Permian deposits – more than 1. In 1994, Al.A. Petrov (Petrov, 1994) found that for TPOGP oils the prevalence of adiantane over hopane is most often characteristic only of the Upper Permian. The C_{29}/C_{30} ratio <1 is characteristic of the OM of the Cambrian and Phanerozoic of Siberia and other regions of the world, as well as of oils (Parfenova, 2018). In the same work, as well as in a number of others (Höld et al., 1999; Filndani et al., 2005; Yandarbiev et al., 2017), data are presented for oils and OM when the hopane ratio C_{29}/C_{30} exceeds unity.

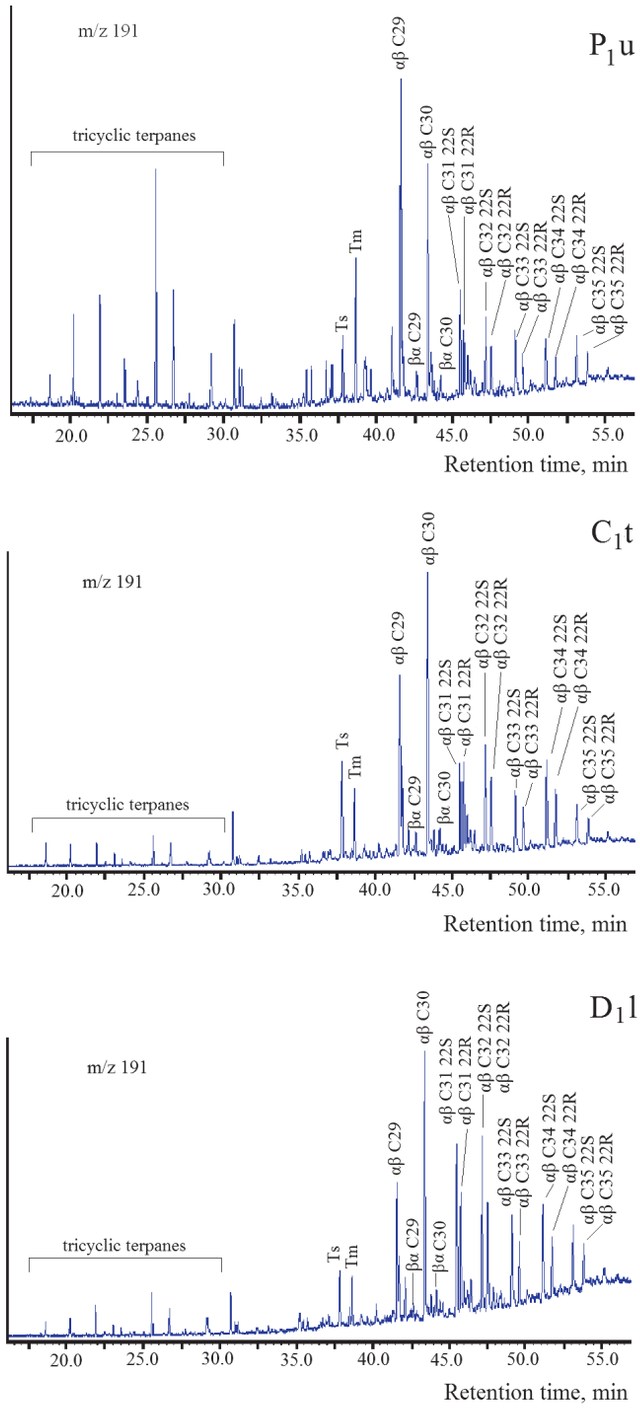

Fig. 7. Mass chromatograms of terpanes (m/z 191) of methane-naphthene fractions of oils from deposits of different ages

T.M. Parfenova believes that "biochemistry of microorganisms that occupied some ecological niche in Cambrian seas was presumably inherited from organisms of Precambrian biospheres. ... The biochemical composition of prokaryotes of some Proterozoic, Phanerozoic, and Quaternary communities was characterized by the elevated adiantane-hopane coefficient" (Parfenova, 2018). According to the authors (Clark, Philp, 1989), the ratio $C_{29}/C_{30} > 1$ indicates the presence of a significant fraction of the carbonate component in the initial source rocks.

The degree of biodegradation (Vinogradova, Punanova, 2012) of Permian oils is defined as medium (moderate). Formation of a series of demethylated 25-norhopanes (reliably identified by the fragment ion m/z 177) characteristic of high-stage biodegradation oils (Volkman et al., 1983) is not observed here.

To determine the degree of the maturity of the OM, the relationship between the initial biological steranes (configuration ααα20R) of C_{29} composition and isosteranes that have been newly formed as a result of catagenetic processes (αββ 20R + 20S) (coefficient K_1) is often used; as is the ratio of geosteranes – 5α(H)14β(H)17β(H) – to biosteranes – 5α(H)14α(H)17α(H) (coefficient K_2); as well as the relative content of moretane (βα C_{30}); the ratio of neohopane C_{27} (Ts) to the regular hopane C_{27} (Tm) (0.47-0.48); and the coefficient 22S/22S+22R for homohopane C_{31}.

Ts/Tm ratio differs slightly in the studied oil groups. Thus, Ts/Tm for oils from D_1l and C_1t deposits correspond to values of 1.15-1.42, while for oils from P_1ar and P_1u deposits they do not exceed unity (Table 2). However, based on other coefficients, we can say that the studied oils are equally catagenetically transformed. The maturity of all the studied oils is low, probably corresponding to the beginning of the main phase of oil formation. These differences may well correspond to the formation of A-C and D-E oils in various source rocks. The effect of biodegradation on the composition of biomarkers is not excluded.

Oil-oil correlation

For the oil-oil correlation, we built so-called star diagrams. For correlation of oil M.V. Dakhnova and co-authors propose to use ratios between concentrations of hydrocarbon pairs close in chemical structure (Dakhnova et al., 2007). As such parameters we used the ratios: n-C_{11}/n-C_{12}, n-C_{13}/n-C_{14}, i-C_{15}/i-C_{16}, n-C_{16}/n-C_{17}, Pr/n-C_{17}, Ph/n-C_{18} (Fig. 8). The results obtained by the distribution of normal and iso-alkanes show the identity of diagrams, which indicates a common genotype of the Lower Devonian and Lower Carboniferous oils and good vertical fluid communication of reservoir rocks. These conclusions are confirmed by the tectonic structure of the investigated territory.

A comparative analysis of diagrams of oils based on sterane and hopane coefficients (Fig. 9) revealed insignificant differences between the Lower Devonian and Carboniferous oils from Permian oils, which are most likely associated with hypergene changes in the latter.

Conclusions

According to the set of data, obtained by hydrocarbon composition, two oil genotypes are determined at

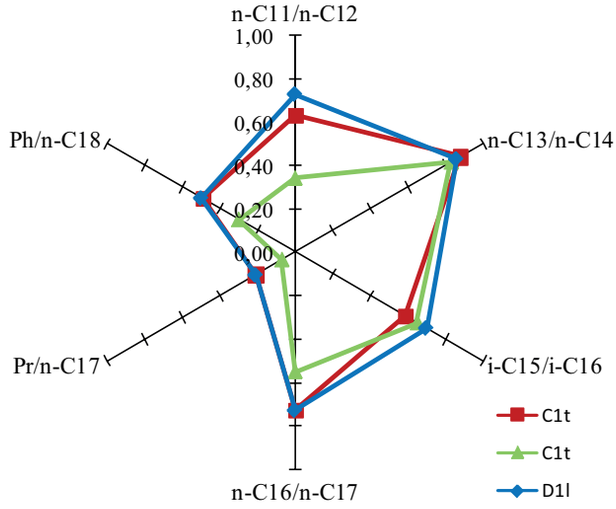

Fig. 8. Correlation of oils by the ratio of the concentrations of pairs of close acyclic hydrocarbons

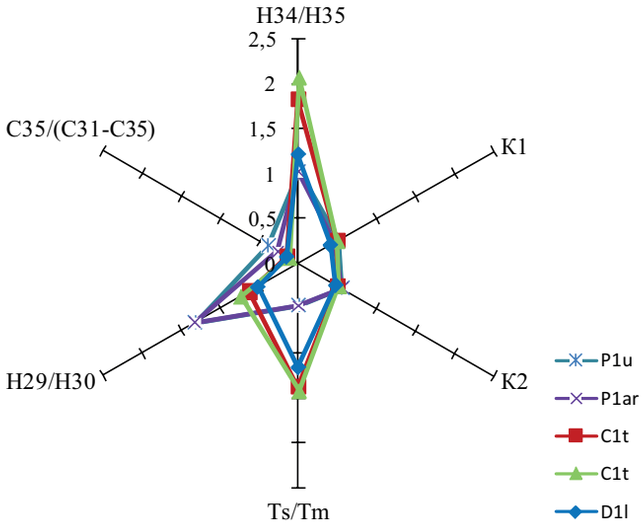

Fig. 9. Star diagram by sterane and hopane coefficients

Labagan field. Oils from the deposits of the Lokhkovian stage of the Lower Devonian and Lower Carboniferous belong to the same genotype – the Ordovician-Lower Devonian. The initial organic matter of oils is sapropelic, the accumulation of which took place in a sub-reducing environment. It is assumed that oil migrated from the Silurian-Lower Devonian sediments to overlying sediments in the decompression zones.

Due to biodegradation, it is not possible to reliably determine the genotype of oils from Permian deposits. This requires additional geochemical studies, such as thermolysis of oil asphaltenes. However, by the distribution of polycyclic hydrocarbon biomarkers we determined that the oil had a slightly different composition of the initial OM.

The maturity of oils of all the oil and gas complexes, studied by us, established by the sterane and hopane coefficients, corresponded to the beginning of the "oil window".

Acknowledgments

The authors would like to thank the reviewer for valuable criticisms and recommendations, which contributed to improving the content of the article.

Geochemical study was performed in the "Geonauka" Center for Common Use.

References

Bailey N. J. L., Jobson A. M., Rogers M. A. (1973). Bacterial degradation of crude oil: comparison of field and experimental data. *Chemical Geology*, 11(3), pp. 203-221. https://doi.org/10.1016/0009-2541(73)90017-X

Brassell S.C., Fu Jiamo, Eglinton G. (1984). Isomerisation, rearrangement and aromatisation of steroids in distinguishing early stages of diagenesis. *Organic Geochemistry*, 6, pp. 11-23. https://doi.org/10.1016/0146-6380(84)90022-6

Bushnev D.A., Valyaeva O.V., Burdelnaya N.S. (2018). Biomarkers of lower paleozoic oils in the northern part of the Timan-Pechora basin. *Vestnik IG Komi SC UB RAS,* 4, pp. 45-48. DOI: 10.19110/2221-1381-2018-4-45-48. (In Russ.)

Clark, J. P., Philp, R. P. (1989). Geochemical Characterization of Evaporite and Carbonate Depositional Environments and Correlation of Associated Crude Oils in the Black Creek Basin, Alberta. *Bulletin of Canadian Petroleum Geology*, 37(4), pp. 401-416.

Connan J. (1984). Biodegradation of crude oil in reservoirs. In: Advances in petroleum geochemistry I. Brooks J, Welte D (eds.). London: Academic Press, pp 299-335. https://doi.org/10.1016/B978-0-12-032001-1.50011-0

Dachnova M.V. (2007). The use of geochemical methods of research in the search, exploration and development of hydrocarbon deposits. *Russian oil and gas geology*, 2, pp. 81-89.

Fildani A., Hanson A. D., Chen Z., Moldowan J., Graham S., Arriola P.R. (2005). Geochemical characteristics of oil and source rocks and implications for petroleum systems, Talara basin, northwest Peru. *AAPG Bulletin*, 89(11), pp. 1519-1545. https://doi.org/10.1306/06300504094

Höld I.M, Schouten S, Jellema J, Sininghe Damsté J.S (1999). Origin of free and bound mid-chain methyl alkanes in oils, bitumens and kerogens of the marine, Infracambrian Huqf Formation (Oman). *Organic Geochemistry*, 30(11), pp. 1411-1428. https://doi.org/10.1016/S0146-6380(99)00115-1

Hunt J. (1982). Geokhimiya i geologiya nefti i gaza. [Geochemistry and geology of oil and gas]. Moscow: Mir, 704 p. (In Russ.)

Ilyinskaya V.V. (1985). Genetic connection of hydrocarbons of organic matter of rocks and oils. Moscow: Nedra, 160 p. (In Russ.)

Jacobson S.P., Hatch J.R., Teerman S.C., Askin R.A. (1988). Middle ordovician organic matter assamblages and their effect on ordovician-derived oils. *The AAPG Bulletin*, 72(9), pp. 1090-1100. https://doi.org/10.1306/703C97C6-1707-11D7-8645000102C1865D

Jobson A.M., Cook F.D., Westlake D.W.S. (1979). Interaction of aerobic and anaerobic bacteria in petroleum biodegradation. *Chemical Geology*, 24, pp. 355-365. https://doi.org/10.1016/0009-2541(79)90133-5

Kashirtsev V.A., Kontorovich A.E., Philp R.P. Chalaya O.N., Zueva I.N. Zueva, Ivanova I.K., Memetova N.P. (2001). Biodegradation of saturated cyclic chemofossils. *Geologiya i geofizika = Russian Geology and Geophisics*, 42(11-12), pp. 1792-1800. (In Russ.)

Kiruchina T.A. (1995). Types of oils of the Timan-Pechora basin. *Vestnik Moskovskogo Universiteta, Seriy 4; Geologiya = Moscow university geology bulletin,* 2, pp. 39-49. (In Russ.)

Kleshchev K.A., Shein V.S. (2010). Oil and gas fields of Russia. Reference guide in two books. The first book – European part of Russia. Moscow: VNIGNI, 832 p. (In Russ.)

Kotlyar G.V. (2009). Perm Stratigraphy. Status and development prospects. *Proc. II AllRuss. Conf.: The Upper Paleozoic of Russia. Stratigraphy and facies analysis*. Kazan: KSU, pp. 26-29. (In Russ.)

Kotlyar G.V., Golubev V.K., Silantyev V.V. (2013). General stratigraphic scale of the Perm system: current status. *Proc. AllRuss. Conf.: The general stratigraphic scale of Russia: state and prospects of arrangement.* Moscow: GIN RAS, pp. 187-195. (In Russ.)

Guidelines for the application of the Classification of reserves and resources of oil and combustible gases (approved by the Order of the Ministry of Natural Resources of Russia, 01.02.2016 No. sp). (2016). 32 p. (In Russ.)

Parfenova T.M. (2018). New Geochemical Data on the Organic Matter in Rocks of the Lower and Middle Cambrian Kuonamka Complex, the Lena-Amga Interfluve Area, Southeastern Siberian Platform. *Geochimiya =*

Geochemistry International, 5, pp. 448-460. (In Russ.) https://doi.org/10.7868/S0016752518050035

Peters K.E., Walters C.C., Moldowan J.M. (2005). The Biomarker Guide II. Biomarkers and Isotopes in Petroleum Systems and Earth History. 2nd ed. V. 2. Cambridge: Cambridge University Press, 1156 p.

Petrov Al.A. (1984). Oil Hydrocarbons. Moscow: Nauka, 264 p. (In Russ.)

Petrov Al.A. (1991). Geochemical value of steranes. Scientific and applied aspects of oil and gas geochemistry. Moscow: IGIRGI, pp. 21-30. (In Russ.)

Petrov Al.A. (1994). Bio-marks and geochemical conditions of oils formation in Russia. *Geologiya i geofizika = Russian Geology and Geophisics*, 6. pp. 13-19. (In Russ.)

Prischepa O.M., Bazhenova T.K., Bogatskii V.I. (2011). Petroleum systems of the Timan-Pechora sedimentary basin (including the offshore Pechora Sea). *Geologiya i geofizika = Russian Geology and Geophisics*, 52(8), pp. 1129-1150. (In Russ.) https://doi.org/10.1016/j.rgg.2011.07.011

Reed W.E. (1977). Molecular compositions of weathered petroleum and comparison with its possible source. *Geochimica et Cosmochimica Acta*, 41, pp. 237-247. https://doi.org/10.1016/0016-7037(77)90231-9

Reed J.D., Illich H.A., Horsfield B. (1986). Biochemical evolutionary significance of Ordovician oils and their sources. *Organic Geochemistry,* 10(1-3), pp. 347-358. https://doi.org/10.1016/0146-6380(86)90035-5

Ryabinkina N.N., Valyaeva O.V. (2018). Petroleum geology and geochemistry of Labagan oil field (Timan-Pechora petroleum province). *Neftegazovaya geologiya. Teoriya i praktika*, 13(4). (In Russ.) https://doi.org/10.17353/2070-5379/36_2018

Tissot W., Welte D. (1981). Formation and distribution of oil. Moscow: Mir, 502 p. (In Russ.)

Vinogradova T.L., Punanova S.A. (2012). Geochemical regularities of changing patterns of changes oil composition under hypergenesis. *Geologiya nefti i gaza = Geology of oil and gas*, 3, pp. 45-54. (In Russ.)

Volkman J.K., Alexander R., Kagi R.J., Woodhouse G.W. (1983). Demethylated hopanes in crude oils and their applications in petroleum geochemistry. *Geochimica et Cosmochimica Acta*, 47, pp. 785-794. https://doi.org/10.1016/0016-7037(83)90112-6

Yandarbiev N.Sh., Kozlova E.V., Fadeeva N.P., Krylov O.V., Naumchev Yu.V. (2017). Geochemistry of hydrocarbons of the Terek-Caspian trough. *Georesursy = Georesources*, Special issue, pp. 227-239. (In Russ.). http://doi.org/10.18599/grs.19.22.

About the Authors

Olga V. Valyaeva – Cand. Sci. (Geology and Mineralogy), Senior Researcher, Laboratory of Organic Geochemistry

Institute of Geology of Komi Science Centre of the Ural Branch of the Russian Academy of Sciences

54, Pervomayskaya st., Syktyvkar, Komi Republic, 167982, Russian Federation

E-mail: valyaeva@geo.komisc.ru

Nadezhda N. Ryabinkina – Cand. Sci. (Geology and Mineralogy), Senior Researcher, Laboratory of Geology of Oil and Gas Bearing Basins

Institute of Geology of Komi Science Centre of the Ural Branch of the Russian Academy of Sciences

54, Pervomayskaya st., Syktyvkar, Komi Republic, 167982, Russian Federation

Dmitriy A. Boushnev – Dr. Sci. (Geology and Mineralogy), Chief Researcher, Laboratory of Organic Geochemistry

Institute of Geology of Komi Science Centre of the Ural Branch of the Russian Academy of Sciences

54, Pervomayskaya st., Syktyvkar, Komi Republic, 167982, Russian Federation

Manuscript received 26 August 2019;
Accepted 10 February 2020;
Published 30 March 2020

ORIGINAL ARTICLE
DOI: https://doi.org/10.18599/grs.2020.1.55-62

Methods of suppressing free thermal convection in water-filled wells during temperature research

D.Yu. Demezhko[*], *B.D. Khatskevich, M.G. Mindubaev*
Institute of Geophysics of the Ural Branch of the Russian Academy of Sciences, Yekaterinburg, Russian Federation

Abstract. Temperature measurements in boreholes are widely used in oil and gas geophysics, hydrogeology, geoecology, geocryology, and in the operation of hydrothermal resources. The number of applications of borehole temperature data is continuously growing. Requirement for temperature measurement accuracy is also growing. However, increasing the accuracy is limited by free thermal convection phenomenon (FTC). It occurs under a positive temperature gradient and causes temperature noise, the level of which may exceed the useful signal.

It was believed for a long time that the FTC currents are organized as a vertical sequence of convective cells having a certain vertical dimension. Existing methods of FTC suppressing by horizontal discs are based on these ideas. Theoretical and experimental studies conducted by the authors showed that these ideas are incorrect. FTC currents are organized as a rotating helical system of ascending and descending jets, not limited vertically. Under these conditions, the most efficient and technological way is dividing the borehole by vertical stripes of polymer film into separate segments. Another method of FTC suppressing uses spherical hydrogel granules. The test results of the developed devices in a real borehole are described. Using of these devices allows to reduce the temperature noise by 16-20 times (from 0.025-0.044 K to 0.002-0.003 K).

Keywords: geothermy, borehole temperature measurements, free thermal convection, temperature monitoring

Recommended citation: Demezhko D.Yu., Khatskevich B.D., Mindubaev M.G. (2020). Methods of suppressing free thermal convection in water-filled wells during temperature research. *Georesursy = Georesources*, 22(1), pp. 55-62. DOI: https://doi.org/10.18599/grs.2020.1.55-62

Introduction

Temperature studies in wells are used to solve a wide range of problems. In scientific research, thermometry is used to estimate the density of deep heat flow in solving global tectonics problems (Polyak, Khutorskoy, 2018). Temperature monitoring is used to assess geodynamic processes (Shimamura et al., 1985; Demezhko et al., 2012a,b). Thermometry is part of exploration and production-geophysical studies of oil wells to assess the technical condition of wells, to identify intervals of annular cross-flows, flood zones, intervals and profiles of inflow, etc. (Dakhnov, 1982). Temperature measurements are indispensable in hydrogeological (Anderson, 2005; Pehme et al., 2014), geoecological, geocryological studies, and in the exploitation of geothermal water deposits.

In recent years, in connection with the advent of new temperature sensors, distributed measurement systems (including fiber optic), means of recording and transmitting data, the range of thermometry tasks has expanded significantly. There has been a tendency to move from single or occasional temperature measurements to permanent temperature monitoring (Ipatov et al., 2018), methods of active thermometry using a heating cable are being developed (Valiullin et al., 2016; Vélez Márquez et al., 2018; Klepikova et al., 2018). At the same time, the accuracy requirements for temperature measurements are significantly increased. However, hardware accuracy often cannot be implemented in real well conditions due to the influence of free thermal convection (FTC) of liquid or air. The temperature noise caused by unsteady convective flows, in amplitude, can significantly exceed the level of the useful signal.

Obviously, technical devices for suppressing temperature noise, in order to be effective, must take into account the structure of convective flows. The article shows how the ideas about the structure of FTC flows have changed recently and describes the technical devices developed by the authors that can effectively reduce the temperature noise level.

[*]*Corresponding author: Dmitry Yu. Demezhko*
E-mail: ddem54@inbox.ru

Conditions under which free thermal convection occurs

In water-filled boreholes FTC occurs with a positive temperature gradient. Its occurrence and character are determined by the value of the dimensionless Rayleigh number. For downhole conditions (vertical cylinder):

$$Ra = \frac{g\beta r^4}{\nu a} G, \quad (1)$$

where g is the gravitational acceleration, β is the coefficient of volumetric thermal expansion, v is the kinematic viscosity, a is the thermal diffusivity, r is the radius of the well, G is the temperature gradient. The parameters β, v, a included in this ratio, in turn, depend on temperature. The critical Rayleigh number Ra_{crit}, which determines the occurrence of convection in the well, lies in the range 68-216, depending on the ratio of the thermal conductivities of the fluid filling the well and the surrounding λ_f/λ_m array (Gershuni, Zhukhovitsy, 1972):

$$Ra_{crit} = \frac{96}{5(1+7\lambda_f/\lambda_m)}\left[3(33+103\lambda_f/\lambda_m) - \sqrt{3(2567+14794\lambda_f/\lambda_m+26927(\lambda_f/\lambda_m)^2}\right]. \quad (2)$$

For an uncased well (fluid – water, $\lambda_f = 0.6$ W·m^{-1}·K^{-1} at 20 °C, external array – rocks, $\lambda_m = 2.5$ W·m^{-1}·K^{-1}), $Ra_{crit} = 154$, for cased (steel casing, $\lambda_m = 74$ W·m^{-1}·K^{-1}), $Ra_{crit} = 212$.

It can be seen from (1) that in order to reduce the Rayleigh number below a critical level, it is necessary to reduce the characteristic size, in this case, the internal radius of the well.

Conventional views about the structure of FTC flows and methods for its suppression

Conventional methods of controlling FTC are based on ideas about the structure of convective currents that developed in the middle of the last century. According to these ideas (Van der Merwe, 1951; Diment, Urban, 1983; Cermak et al., 2008; Berthold, Börner, 2008), FTC flows are organized in the form of a vertical sequence of convective cells (similar to Rayleigh-Benard cells in a flat layer), having a certain vertical size (Fig. 1a-c), which, in turn, determines the amplitude of the temperature noise.

Based on these ideas, all well-known technical means of suppressing convection in a well have been created. They divide the well vertically into separate intervals using packers (Beck et al., 1971; Colombani et al., 2016) (Fig. 1e-f) or horizontal disks (Harries, Ritchie, 1981; Vroblesky et al., 2006; Vélez Márquez et al., 2018) (Fig. 1d-e). It was assumed that for effective suppression of convection this interval should be less than the vertical size of the convective cell. However, the size is not known: until now no convincing estimates have been submitted. The use of packers is very time-consuming, and the effectiveness of dividing disks is recognized as low (Pavlov, 2006).

More radical methods for solving the problem are also known. I.L. Dvorkin et al. (1981) propose lowering the tubing string into the interval under study, which effectively reduces the effective radius and, consequently, the Rayleigh number. The disadvantage of this method is the high cost of research and high complexity. In (GOST 25358-82. Soils. Field Temperature Method, 1982), for suppressing free thermal convection of air in shallow (up to 5 m) wells with a diameter of more than 100 mm, it is prescribed, after installing sensors, to fill the entire well with sand or fine gravel, and in (Klepikova et al., 2018) water-filled wells with dry hydrogel. The disadvantages of these methods are obvious, and in deeper wells they are simply not applicable.

Modern concepts and methods of suppressing FTC

Theoretical and experimental studies of free thermal convection in a well (Mindubaev, Demezhko, 2012; Khoroshev, 2012; Demezhko et al., 2017, 2019) showed that FTC flows form a rotating spiral system of ascending and descending jets and are not limited vertically (Fig. 2).

Taking into account the revealed structural features of the FTC, we developed an effective method of suppressing the FTC, based on dividing the well by vertical stripes from a polymer film into separate segments. Such a separation, on the one hand, reduces the effective section of the well and the Rayleigh number, on the other hand, prevents the possibility of the system rotation (Khatskevich et al., 2019). Possible implementations of this method are shown in Fig. 3a-b.

Methods based on filling a well with bulk material (GOST 25358-82. Soils. Field Temperature Method, 1982; Klepikova et al., 2018) are quite effective in conducting long-term temperature monitoring, but are not technologically advanced. They are suitable only for shallow wells and make it difficult, if not completely excluded, to re-monitor, for example, after calibration. We have developed a method based on filling only a limited portion of the well (monitoring interval) with spherical hydrogel granules (Khatskevich, Demezhko, 2019)(Fig. 3c-d). Before installing temperature sensors in the well, a cylindrical sleeve of a stretching polymer mesh is attached to the cablewith spherical hydrogel granules placed in it. Within several hours after the sensors are installed in the well, spherical granules swell and increase in size by 30-100 times, stretching the grid, until they fill the entire space of the well within the studied interval. Since the dimensions of the free space are smaller than the radius of spherical granules, thermal convection is completely suppressed even in the

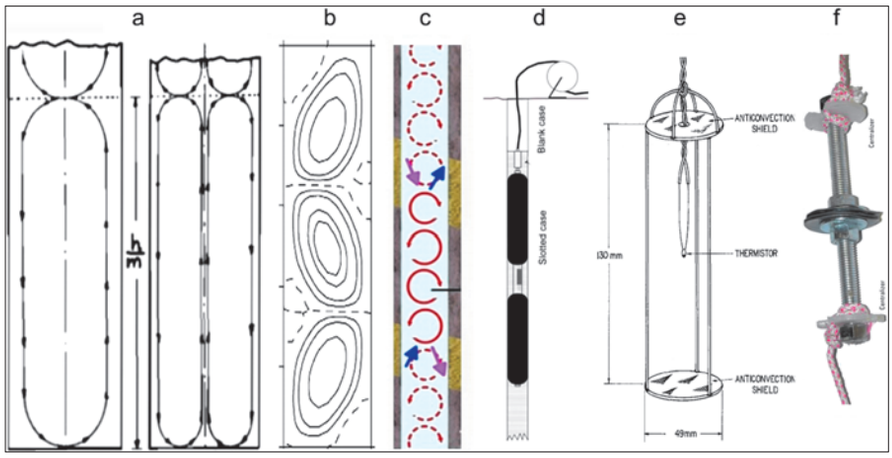

Fig. 1: Conventional views on the structure of FTC flows (a-c) and methods for suppressing it (d-f): a – Van der Merwe, 1951; b – Cermak et al., 2008; c – Berthold, Borner, 2008; d – a device for suppressing FTC using packers – Colombani et al., 2016; e-f – using horizontal disks: (e) – Harries, Ritchie, 1981; (f) – Vroblesky et al., 2006.

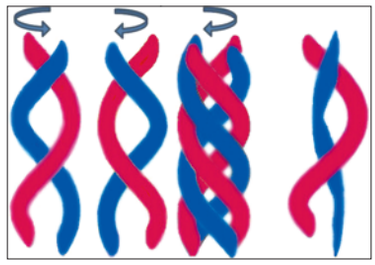

Fig. 2. Spiral systems of ascending (highlighted in red) and descending (blue) flows of free thermal convection. Black arrows indicate the direction of the system rotation (Demezhko et al., 2019)

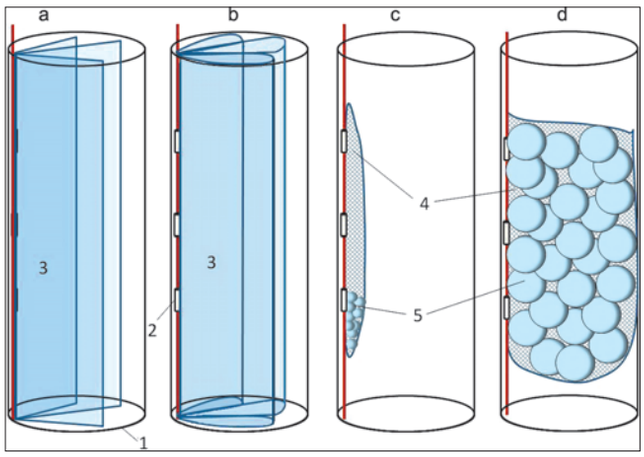

Fig. 3. Methods of suppressing FTC in a well: a, b – two options for implementing the method using polymer film strips (Khatskevich et al., 2019); c, d – using a hydrogel (Khatskevich, Demezhko, 2019). The location of the hydrogel granules immediately after installing the cable with the sensors in the monitoring interval (c) and a few hours after swelling of the granules (d). 1 – well, 2 – cable with sensors, 3 – polymer film, 4 – sleeve of polymer mesh, 5 – spherical hydrogel granules.

case of large Rayleigh numbers (10^5-10^8). At the same time, the densest packing of spheres (face-centered cubic and hexagonal) preserves the porosity e = 0.26, and with arbitrary packing it increases to e = 0.48. This allows vertical movements of the liquid column in the well. When removing the cable after monitoring, the sleeve from the polymer network breaks and the granules are lowered into the well sump.

Test results

Tests for FTC suppression devices were tested in an IGF-60 well 60 m deep drilled in 2007 at the Institute of Geophysics of the Ural Branch of the Russian Academy of Sciences (Yekaterinburg). To a depth of 43 m, the well is cased with steel pipes: in the range of 0.3-27.0 m – Ø 114 mm (internal Ø 105 mm), in the range of 27-43 m – Ø 108 mm. Below, to a depth of 60 m, there is an open trunk Ø 93 mm. The well revealed a soil layer (0-0.3 m), loam (0.03-10.0 m), fractured (10.0-43.0 m) and durable (43.0-60.0) gabbro. The groundwater level in the well was established at a depth of 5.9-6.5 m.

Temperature monitoring was carried out during the period from November 6, 2008, to October 10, 2009 using an autonomous digital 16-channel temperature meter (AIT) developed at the Trofimuk Institute of Petroleum Geology and Geophysics of the Siberian Branch of the Russian Academy of Sciences (Kazantsev, Duchkov, 1992). MMT-4 thermistors were used as temperature sensors. 6 temperature sensors were installed in the IGF-60 well at depths of 10, 20, 30, 40, 50, 60 m (below groundwater level), 4 sensors – in a 4.5-meter hole located a meter from it, into which a closed hole was inserted from the lower end and water-filled steel pipe Ø 32 mm (internal Ø 29 mm) at depths of 1, 2, 3, 4.38 m, 3 sensors were located in the soil at depths of 0.2; 0.3; 0.5 m. The monitoring results to a depth of 10 m are presented in Fig. 4. Below this mark, the temperature field practically did not change during the year, and the temperature gradient was close to zero.

In the annual cycle, a positive temperature gradient (0.08-0.22 K/m) is observed in the flooded part of the well at a depth of 6-10 m at the end of May, in June. At $T = 5$°C, the constants included in (1) are equal for water: $\beta = 1.54 \cdot 10^{-5}$ K^{-1}, $\nu = 1.54 \cdot 10^{-6}$ m^2/s, $a = 1.32 \cdot 10^{-7}$ m^2/s and the Rayleigh numbers corresponding to temperature gradients are Ra = 450-1200. The critical value for cased steel pipe well, according to (2) Ra_{cr}, is 212. Therefore, during this period, developed free thermal convection can be expected in this interval.

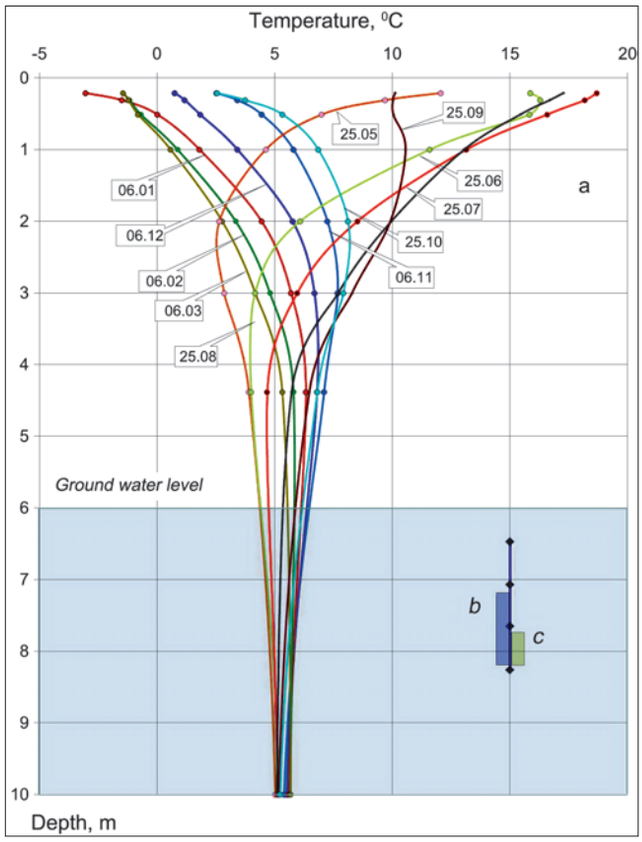

Fig. 4. Results of temperature monitoring in the IGF-60 well in November 2008 – October 2009 (a) and intervals for installing temperature sensors and FTC suppressors: b – vertical plates, c – grids with hydrogel

Tests of the FTC suppressor device using vertical plates were tested in late May – early June 2019. At the first stage, temperature was monitored for a week at depths of 6.47, 7.07, 7.65, and 8.26 m with a sampling frequency 30 sec. Then the sensor string was removed and equipped with an FTC suppression device consisting of folded strips of a polyethylene film 1 m long (Fig. 3b, Fig. 5 – photo). The middle of the device was located at the sensor 7.65 m, so the neighboring sensors were not blocked by it (Fig. 4b). After this, monitoring continued for another 5 days. Thermograms of the results of monitoring and evaluation of temperature noise are shown in Fig. 5 and Tab. 1.

Under conditions of free thermal convection, the amplitude of temperature noise is σ = 26-44 mK. After installing the device after about 1.5 days, it decreases by 6-22 times – to σ_p = 2-4 mK. The maximum suppression coefficient $k = \sigma/\sigma_p$, naturally, appears at a depth of

Depth, m	6.47	7.07	7.65	8.26
Before suppression, σ, K	0.0271	0.0409	0.0440	0.0262
After suppression, σ_p, K	0.0044	0.0021	0.0020	0.0019
Suppression coefficient, $k=\sigma/\sigma_p$	6.1	19.2	21.8	13.5

Table 1. Amplitudes of temperature noise (standard deviations of residuals from smoothing thermograms with a 6-hour filter) in the IGF-60 well before and after FTC suppression using vertical plates

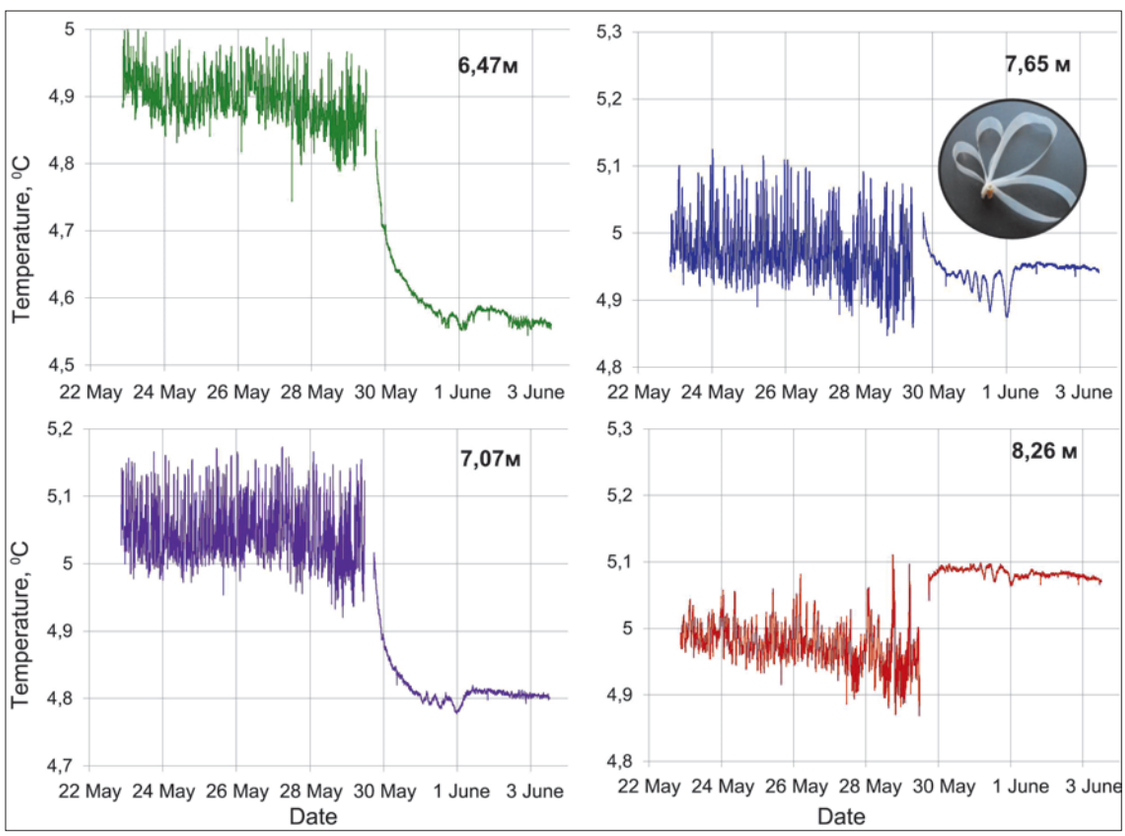

Fig. 5. The results of temperature monitoring in the IGF-60 well during testing of an FTC suppression device based on vertical plates. A sectional photo of the deviceis in the upper right corner.

7.65 m – in the area covered by the FTC suppression device. However, beyond the boundaries of the overlapped interval, the temperature noise decreases to 2 mK, and at a depth of 6.47 m (0.68 m from the upper edge of the device) to 4 mK.

Interestingly, after the installing the device in its middle part (7.65 m), temperature fluctuations occurred for about 1.5 days, the range of which reached 70 mK, and the period increased from 5 to 10 hours. These fluctuations, but with a smaller scale, were recorded by neighboring sensors. Their nature is not clear to us. We can only assume the appearance of a self-oscillating system in the process of heat exchange between the device and the surrounding fluid. Similar temperature self-oscillations were observed by us earlier (Demezhko, Yurkov, 2017) – they appeared and continued (with a period of 14-26 hours and a span of up to 300 mK) for several months, and then suddenly disappeared. At the same time, no additional devices were introduced into the well.

Figure 6 shows the amplitude spectra of temperature fluctuations at a depth of 7.65 m before and after installing the FTC suppression device. Free thermal convection is most pronounced in the range of periods 5-140 min. It is in this range that its most effective suppression occurs. Non-convective factors make a significant contribution to fluctuations with periods of more than 12 hours, for example, those associated with fluctuations in temperature and atmospheric pressure, and precipitation.

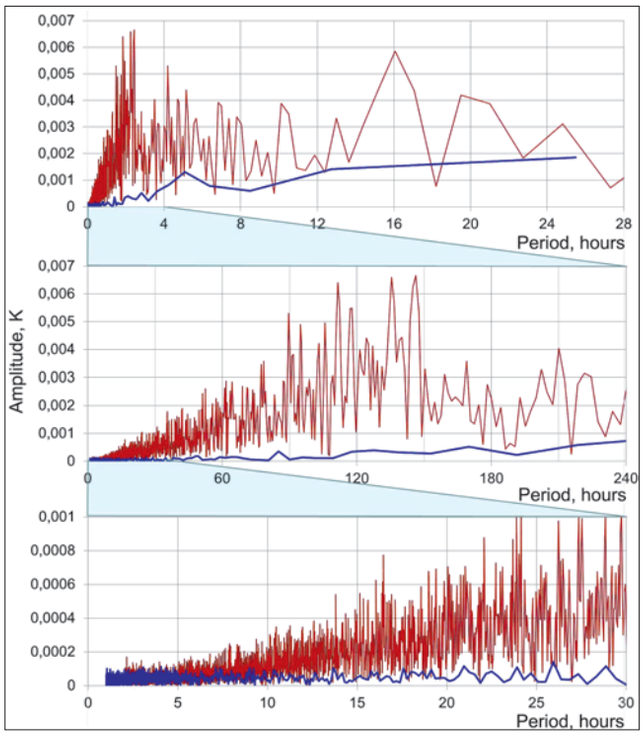

Fig. 6. Spectral composition of temperature noise without convection suppression (red) and after suppression (blue)

Here the amplitudes before and after the installation of the device are comparable. They are also comparable for periods of less than 5 minutes – in this range temperature fluctuations are already associated with instrument noise.

In addition to temperature noise – fluctuations relative to the average value for a given depth – free thermal convection causes a long-term, or quasi-stationary, effect (Demezhko et al., 2017). It is expressed in a regular decrease in the temperature gradient at the convection development site and is similar to the effect of forced convection, for example, during circulation of well fluid during drilling or flushing a well (Astrakhan, Maron, 1969; Cheremensky, 1977; Sass et al., 1992). Mathematical modeling (Demezhko et al., 2017) showed that the maximum decrease in the gradient in the well compared with the gradient in the surrounding rocks is observed at the upper and lower boundaries of the well, while in the middle part it remains close to the rock. Significant distortions of the average rock temperatures were noted just during measurements in shallow wells (Pavlov, 2006, and references in this work).

In our case, the measurements were carried out in the upper part of the well, near the water/air interface, and here we should also expect the manifestation of the quasistationary thermal effect of convection. Figure 5 shows that after installing the FTC suppression device, the temperature profiles diverge: the sensors installed above the device detect a decrease in temperature, lower – an increase, and the sensor located in the middle of the device at a depth of 7.65 m does not change the temperature trend. In Fig. 7a shows

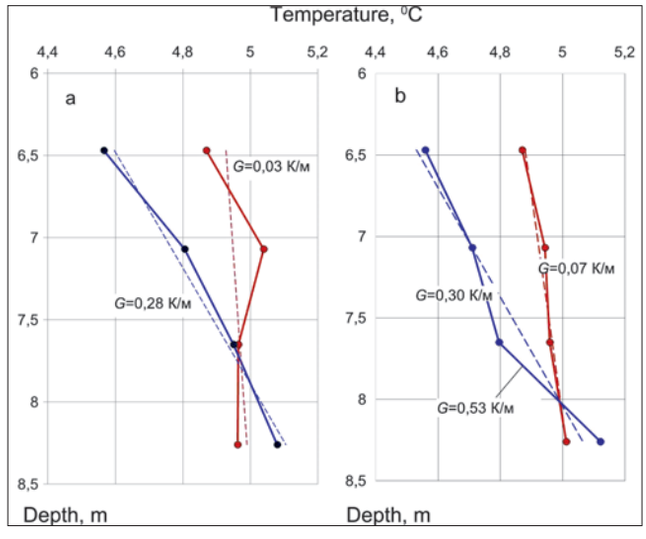

Fig. 7. Temperature profiles recorded in the IGF-60 well before (red lines) and after (blue lines) the installation of FTC suppression devices: a – graphs for the device in the form of vertical plates, b – for the hydrogel-based device. Dotted line indicates linear approximations of profiles.

averaged vertical temperature profiles recorded in the IGF-60 well before and after installation of the FTC suppression device. Under the conditions of developed convection, the average measured temperature gradient was 0.03 K/m, and after suppressing convection, it increased to 0.28 K/m – i.e. to its real value in the rocks. At $T = 4.9$ °C, this gradient corresponds to $Ra = 1400$. Let us note that with an average gradient of 0.03 K/m ($Ra = 150$), convection should not have occurred.

To prove that the suppression of the FTC using the device in question made it possible to evaluate the real geothermal gradient, we consider the relationship between the amplitude of the temperature noise and the gradient. We proposed this $\sigma/r \approx 3G$ dependence based on the results of mathematical modeling of the FTC (Demezhko et al., 2017) and confirmed by laboratory experiments (Demezhko et al., 2019). It follows from it that $G \approx \sigma/3r$. In this example (for a depth of 7.65 m) σ = 0,044 K, r = 0,0525 m, which corresponds to a value of G = 0.28 K/m, exactly equal to the gradient measured after suppression of the FTC. True, estimates from neighboring sensors will no longer be as accurate: 0.26 K/m (7.07 m) and 0.17 K/m (8.26 m). Thus, even without convection suppression, by measuring only the temperature noise induced by it, we can try to estimate the temperature gradient not disturbed by convection, or at least to assume that it is significantly distorted.

The test procedure for the device for suppressing FTC using a hydrogel is similar to that described above. The tests were carried out in mid-June 2019. After two-day temperature monitoring at depths of 6.47, 7.07, 7.65 and 8.26 m (sampling frequency – 1 min.) in the interval 7.75-8.15 m on a separate suspension, a device was installed – a 0.4-meter sleeve made of polyethylene mesh, filled with spherical hydrogel granules. Since the initial granule size (approx. 2 mm) was smaller than the cell size (5 mm), the granules were placed inside a sleeve in a small cylinder of permeable fabric. As the granules swell and increase in size (up to 10-12 mm), they fall into the sleeve, gradually filling the entire space of the well in the range of 7.75-8.15 m. After this, monitoring continued for about 6 days. Note that in this experiment, none of the sensors was blocked by the device (Fig. 4c). Thermograms of the results of monitoring and evaluation of temperature noise are shown in Fig. 8 and Table 2.

Under conditions of free thermal convection, the amplitude of temperature noise was σ = 25-38 mK. The device allowed to reduce noise 10-17 times near its installation (sensors "7.65 m" and "8.26 m") and up to 3-6 times – at a distance (sensors "6.47 m" and "7.07 m"). It is noteworthy that the greatest residual noise was registered not by the sensor farthest from the installation, but by the intermediate one – "7.07 m". When convection was suppressed by hydrogel, a transient self-oscillation process was not observed.

As in previous tests, after installing the device, the average temperature gradient over the entire interval increased significantly (Fig. 7b): from 0.07 to 0.30 K/m ($Ra = 1500$ at $T = 4.9$ °C), and directly in the installation interval of the device – up to 0.53 K/m (Ra = 2700 at $T = 4.9$ °C).

Depth, m	6.47	7.07	7.65	8.26
Before suppression, σ, K	0.0253	0.0315	0.0362	0.0375
After suppression, σ_p, K	0.0044	0.0119	0.0034	0.0023
Suppression coefficient, $k=\sigma/\sigma_p$	5.8	2.6	10.8	16.3

Table 2. Amplitudes of temperature noise (standard deviations of residuals from smoothing thermograms with a 6-hour filter) in the IGF-60 well before and after FTC suppression using a hydrogel.

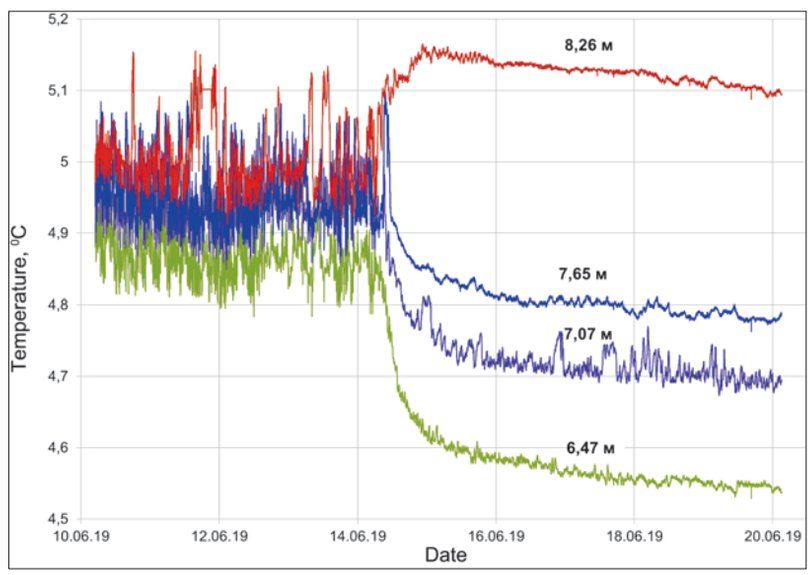

Fig. 8. The results of temperature monitoring in the IGF-60 well during testing of a hydrogel-based FTC suppression device

Conclusion

The latest ideas about the structure of flows of free thermal convection, obtained on the basis of theoretical and experimental studies, have allowed the development of effective and technological methods and devices for its suppression and increase the accuracy of temperature studies in wells. Tests have shown that they can reduce temperature noise by 16-20 times (to 0.002-0.003 K) – to the hardware level. Installed in the well, these devices do not limit the vertical movements of the liquid column associated with changes in atmospheric pressure, tidal deformations, and activation of hydrogeological processes – movements that can be considered as a useful signal. The designs of the developed devices are cheap, easy to implement, exclude the seizure of downhole tools, and allow repeated studies in shallow wells.

Acknowledgements

The studies were carried out with financial support from the state budget research theme No. 0394-2019-0002 (theoretical and laboratory studies of the structure of the FTC) and the Russian Foundation for Basic Research, project No. 19-05-00050 (justification, development and full-scale testing of devices for suppressing the FTC).

References

Anderson M. P. (2005). Heat as a ground water tracer. *Ground water*, 43(6), pp. 951-968. https://doi.org/10.1111/j.1745-6584.2005.00052.x

Astrakhan I.M., Maron V.I. (1969). Non-stationary heat transfer in the well washing. *Journal of Applied Mechanics and Technical Physics*, 1, pp. 148-152. (In Russ.)

Beck, A.E., Anglin, F.M. and Sass, J.H. (1971). Analysis of heat flow data – in situ thermal conductivity measurements. *Can. J. Earth Sci*., 8, pp. 1-19. https://doi.org/10.1139/e71-001

Berthold S., Börner F. (2008). Detection of free vertical convection and double-diffusion in groundwater monitoring wells with geophysical borehole measurements. *Environmental geology*, 54(7), pp. 1547-1566. https://doi.org/10.1007/s00254-007-0936-y

Cermak V., Bodri L., Safanda J. (2008). Precise temperature monitoring in boreholes: evidence for oscillatory convection? Part II: theory and interpretation. *Int J Earth Sci*, 97(2), pp. 375-384. https://doi.org/10.1007/s00531-007-0250-7

Cheremenskiy G.A. (1977). Applied Geothermy. Leningrad: Nedra, 224 p. (In Russ.).

Colombani N., Giambastiani B. M. S., Mastrocicco M. (2016). Use of shallow groundwater temperature profiles to infer climate and land use change: interpretation and measurement challenges. *Hydrological Processes*, 30(14), pp. 1-20. https://doi.org/10.1002/hyp.10805

Dakhnov V.N. (1982). Interpretation of the results of geophysical surveys of well sections. Leningrad: Nedra, 310 p. (In Russ.).

Demezhko, D.Yu.; Yurkov A.K.; Utkin V.I., Klimshin A.V. (2012a) On the nature of temperature variations in borehole KUN-1 (Kunashir Island). *Russian Geology and Geophysics*, 53(3), pp. 313-319. https://doi.org/10.1016/j.rgg.2012.02.008

Demezhko D.Yu., Yurkov A.K., Outkin V.I., Shchapov V.A. (2012b). Temperature changes in the KUN-1 borehole, Kunashir Island, induced by the Tohoku Earthquake (March 11, 2011, M = 9.0). *Doklady Earth Sciences*, 445(1), pp. 883-887. https://doi.org/10.1134/S1028334X12070124

Demezhko D.Yu., Mindubaev M.G., Khatskevich B.D.(2017). Thermal effects of natural convection in boreholes. *Russian Geology and Geophysics*, 58(10), pp. 1270-1276. https://doi.org/10.1016/j.rgg.2016.10.016

Demezhko D.Y., Yurkov A.K. (2017). On the Origin of Quasi-Periodic Temperature Variations in Kun-1 Well (Kunashir Island).*Izvestiya, Atmospheric and Oceanic Physics*, 53(8), pp. 804-812. https://doi.org/10.1134/S0001433817080023

Demezhko D.Yu., Khatskevich B.D., Mindubaev M.G. (2019). Natural Thermal Convection in a Vertical Water-Filled Cylinder: Infrared Thermography Investigation. *Russian Geology and Geophysics,* 60(7), pp. 813-818.

Diment W. H., Urban Th. C. (1983). A simple method for detecting anomalous fluid motions in boreholes from continuous temperature logs. *GRC Trans.*, 7, pp. 485-490.

Dvorkin I.L., Filippov A.I., Buevich A.S., RamazanovA.Sh., Patskov L.L. (1981). A method of evaluating the nature of the formation saturation. Inventor's certificate No. 796399 SSSR. (In Russ.)

Gershuni G., Zhukhovitskii E. (1976). Convective stability of incompressible fluids. Jerusalem: Keter Publishing House, 330 p.

GOST 25358-82. Soils. Field Temperature Method. (1982). State standart. Moscow: Izd-vo Goskomiteta SSSR podelamstroitel'stva, 14 p. (In Russ.).

Harries J. R., Ritchie A. I. M. (1981). The use of temperature profiles to estimate the pyritic oxidation rate in a waste rock dump from an opencut mine. *Water, Air, and Soil Pollution*, 15(4), pp. 405-423. https://doi.org/10.1007/BF00279423

Ipatov A.I., Kremenetskiy M.I., Kaeshkov I.S., Buyanov A.V. (2018). Statsionarnyy monitoring geofizicheskikh parametrov pri kontrole razrabotki mestorozhdeniy. Vozmozhnosti, problem i perspektivy ispol'zovaniya. *Aktual'nye problem nefti i gaza*, 2(21), pp. 1-13. (In Russ.)

Kazantsev S.A., Duchkov A.D. (2008). Equipment for monitoring temperature and measuring the thermophysical properties of frozen and thawed rocks. *Proc. Int. Conf.: Cryogenic resources of the polar and mountainous regions. Status and prospects of permafrost engineering.* Tyumen: IKZ SO RAN, pp. 236-239. (In Russ.)

Khatskevich B.D., Demezhko D.Yu., Mindubaev M.G. (2019). The method of temperature monitoring in waterfilled boreholes. Patent RF, no. 2678174.

Khatskevich B.D., Demezhko D.Yu. (2019). The method of temperature monitoring in waterfilled boreholes. Patent RF, no. 2701261.

Khoroshev A.S. (2012). Numerical study of free convective flows in extended vertical cylindrical areas under a constant vertical temperature gradient on the side surface. *Vestnik of Samara University. Aerospace and Mechanical Engineering*, 5-1(36), pp. 46-48. (In Russ.).

Klepikova, M. V., Roques, C., Loew, S., & Selker, J. (2018). Improved characterization of groundwater flow in heterogeneous aquifers using granular polyacrylamide (PAM) gel as temporary grout. *Water Resources Research*, 54(2), pp. 1410-1419. https://doi.org/10.1002/2017WR022259

Mindubaev M.G., Demezhko D.Yu. (2012). Free thermal convection in boreholes: numerical modeling and experimental data. *Monitoring. Science and Technologies*, 4(13), pp. 12-18. (In Russ.).

Pavlov AV. (2006). Evaluation of temperature measurements errors of grounds in shallow boreholes in permafrost. *Kriosfera Zemli*, 10(4), pp. 9-13. (In Russ.)

Pehme P., Parker B.L., Cherry J.A., Blohm D. (2014). Detailed measurement of the magnitude and orientation of thermal gradients in lined boreholes for characterizing groundwater flow in fractured rock. *Journal of hydrology*, 513, pp. 101-114. https://doi.org/10.1016/j.jhydrol.2014.03.015

Polyak B.G., Khutorskoy M.D. (2018). Heat flow from the Earth interior as indicator of deep processes. *Georesursy = Georesources*, 20(4), pp. 366-376. https://doi.org/10.18599/grs.2018.4.366-376

Sass J. H., Lachenbruch A. H., Moses T. H., & Morgan P. (1992). Heat flow from a scientific research well at Cajon Pass, California. *Journal of Geophysical Research: Solid Earth*, 97(B4), pp. 5017-5030. https://doi.org/10.1029/91JB01504

Shimamura H., Ino M., Hikawa H., Iwasaki T. (1985) Groundwater microtemperature in earthquake regions. *Pure and applied geophysics*, 122(6), pp. 933-946. https://doi.org/10.1007/BF00876394

Valiullin R.A., Sharafutdinov R.F., Fedotov V.Y., Kanafin I.V. (2016). Experimental device for studying free heat convection during induction heating of the casing. *Vestnik Bashkirskogo Universiteta*, 21(2), pp. 264-268. (In Russ.)

Van Der Merwe, J.H. (1951). The influence of convection on measured borehole temperatures. *South African Journal of Science*, 47(8), pp. 235-238.

Vélez Márquez, M., Raymond, J., Blessent, D., Philippe, M., Simon, N., Bour, O., & Lamarche, L. (2018). Distributed thermal response tests using a heating cable and fiber optic temperature sensing. *Energies*, 11(11), 3059. https://doi.org/10.3390/en11113059

Vroblesky, D.A., Casey, C.C., and Lowery, M.A. (2006). Influence of in-well convection on well sampling. *U.S. Geological Survey Scientific Investigations Report* 5247, 13 p.

About the Authors

Dmitry Yu. Demezhko – Dr. Sci. (Geology and Mineralogy), Chief Researcher, Laboratory of Geodynamics, Institute of Geophysics of the Ural Branch of the Russian Academy of Sciences

100, Amundsen st., Yekaterinburg, 620016, Russian Federation. E-mail: ddem54@inbox.ru

Bogdan D. Khatskevich – Junior Researcher, Laboratory of Geodynamics, Institute of Geophysics of the Ural Branch of the Russian Academy of Sciences

100, Amundsen st., Yekaterinburg, 620016, Russian Federation

Mansur G. Mindubaev – Cand. Sci. (Physics and Mathematics), Senior Researcher, Laboratory of Geodynamics, Institute of Geophysics of the Ural Branch of the Russian Academy of Sciences

100, Amundsen st., Yekaterinburg, 620016, Russian Federation

Manuscript received 20 November 2019;
Accepted 26 February 2020;
Published 30 March 2020

ORIGINAL ARTICLE
DOI: https://doi.org/10.18599/grs.2020.1.63-72

A model of the deep structure of the Earth's crust and upper mantle in the area of the Karymshinsky gold-ore cluster according to geophysical data (South Kamchatka)

A.G. Nurmukhamedov[1], M.D. Sidorov[1], Yu.F. Moroz[2]*
[1]*Scientific Research Geotechnological Centre of the Far Eastern Branch of the Russian Academy of Sciences, Petropavlovsk-Kamchatsky, Russian Federation*
[2]*Institute of Volcanology and Seismology of the Far Eastern Branch of the Russian Academy of Sciences, Petropavlovsk-Kamchatsky, Russian Federation*

Abstract. In the South of Kamchatka, modern geodynamic processes are actively taking place. A deep geological and geophysical model of the structure of the Earth's crust and upper mantle along the regional profile of the Apacha Village-Mutnaya Bay in the zone of Tolmachevsky active magmatic center is presented. The profile passes near the South-Western border of the Karymshinskaya volcano-tectonic structure (VTS) and crosses the Ahomtenskaya VTS. The model created on the basis of integrated interpretation of materials of the earthquake converted-wave method (ECWM), gravity and magnetotelluric sounding (MTS). The thickness of the Earth's crust along the profile varies from 30-33 km at the edges reaching 44-46 km, in its central part. The dominant feature of the model is a high-density formation – a block of the Earth's crust, saturated with intrusions of the main and ultrabasic composition. The formation of the block is associated with a permeable zone between the crust and the upper mantle. In the block correlation of seismic boundaries is disturbed and in a density model the area with massive heterogeneity is allocated. A significant increase in depth to the M-Boundary in the center of the model is explained by the presence of a "bloated" transition layer between bark and mantle in this place. The thickness of the layer is about 10 km, and the density of the mantle reaches 3.4 g/cm^3. It is assumed that this is a site of eklogization of breeds in a zone of paleosubduction of oceanic lithosphere under a continental. The area is favorable for the accumulation of meteor waters, which are in contact with high-temperature environment and postmagmatic solutions of intrusions, which leads to the formation of hydrothermal systems. The genetic connection of Karymshinsky gold-ore cluster with the intrusive array of medium-sour composition, allocated in the zone of the Tolmachevsky active Magmatic Center is shown.

Keywords: crust, upper mantle, transition layer, deep model, heat flow, ECWM, MTS, South Kamchatka

Recommended citation: Nurmukhamedov A.G., Sidorov M.D., Moroz Yu.F (2020). A model of the deep structure of the Earth's crust and upper mantle in the area of the Karymshinsky gold-ore cluster according to geophysical data (South Kamchatka). *Georesursy = Georesources*, 22(1), pp. 63-72. DOI: https://doi.org/10.18599/grs.2020.1.63-72

Introduction

Currently, it is of great interest to solve the problems of the distribution and localization of volcanogenic gold fields in the area of the Nachikinsky (Krutogorovsk-Petropavlovsk) zone of transverse dislocations and on its flanks (Fig. 1). The zone crosses the area of modern volcanism in the south of Kamchatka, where several gold deposits and ore occurrences have been identified. The area of the Porozhisty field and ore occurrences to the east of it is distinguished under the general name "Karymshinsky ore cluster". The site is located in the area of the Tolmachev Active Magmatic Center (TAMC) (Nurmukhamedov, 2017; Nurmukhamedov, Sidorov, 2019), the contours of which are shown in Fig. 1. Two regional geophysical profiles pass through the central part of TAMC: in the northeast direction, the profile of the Opala Mountain-Vakhil River and in the north-west direction, Apacha Village-Mutnaya Bay.

Along the profiles from 1987 to 1993 the Elizovsky geophysical expedition of Production Geological Association Kamchatgeologiya conducted in-depth studies using the earthquake converted-wave method and magnetotelluric sounding. The results are presented in scientific publications (Moroz et al., 1995; Mishin, 1996, 1997). However, much later analysis of the earthquake converted-wave method showed that on the western fragments of regional profiles a systematic overestimation of the depths to the Moho boundary and other boundaries in the Earth's crust was allowed. Therefore, reinterpretation of the earthquake converted-

*Corresponding author: Alexander G. Nurmukhamedov
E-mail: nurmuxamedov1949@mail.ru

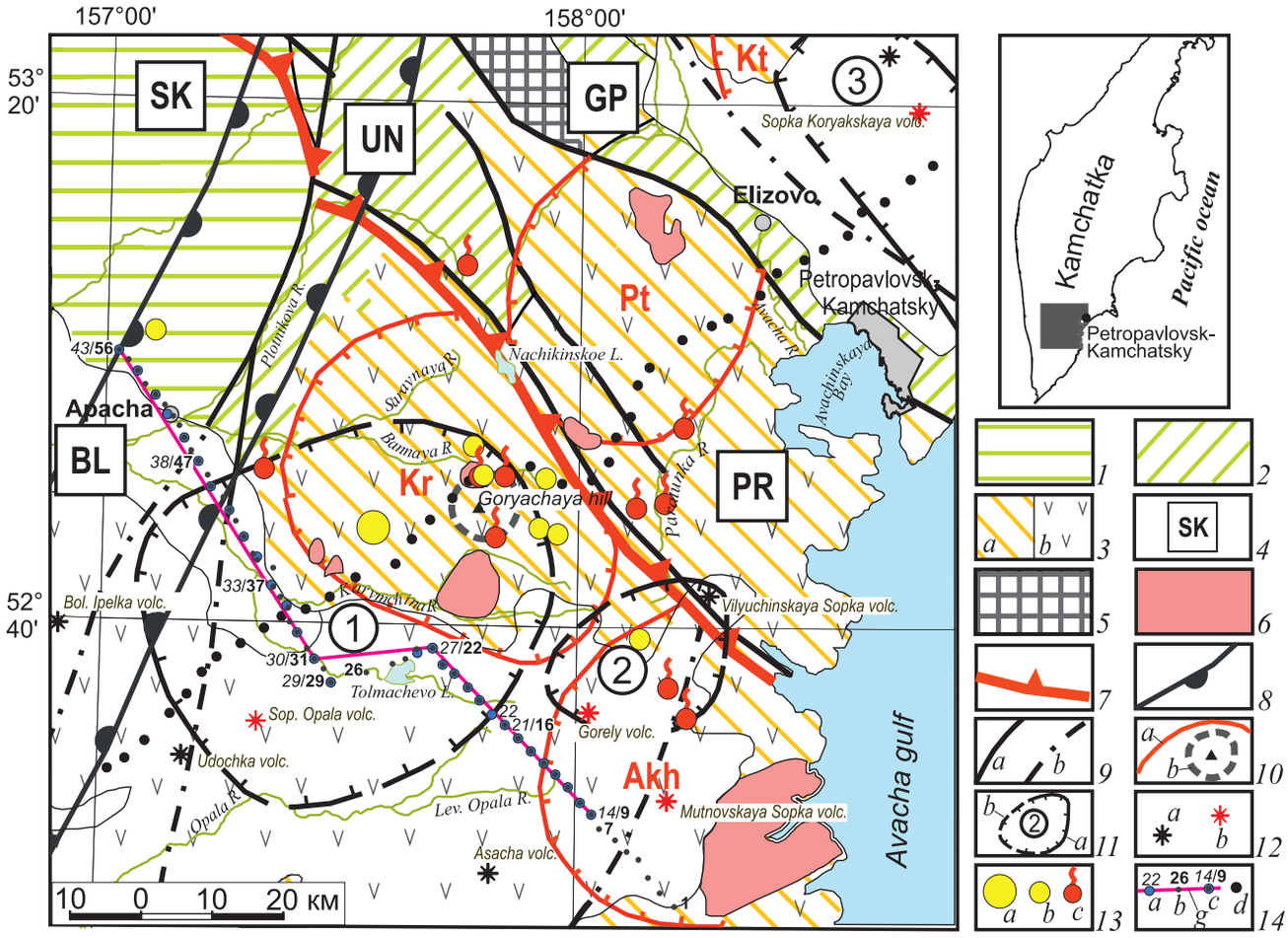

Fig. 1. A fragment of the tectonic diagram of the Koryak-Kamchatka folded region (based on materials (Nurmukhamedov, Sidorov, 2019) with additions). 1 – Koryak-West-Kamchatka folded zone; 2 – East Kamchatka subzone of the Olyutor-East Kamchatka folded zone; 3 – Kuril-South Kamchatka island arc volcanic zone (a), South Kamchatka volcanic belt (b); 4 – structures of folded zones and their designations: BL – Bolsheretsky Uplift, SK – Srednino-Kamchatsky horst-anticlinorium, horsts: UN – Unkanovichy, GP – Ganalsko-Petropavlovsky, PR – Pribrezhny; 5 – late Cretaceous metamorphic complexes; 6 – intrusive formations of predominantly medium and acidic composition; 7 – boundaries of the Nachikinsky zone of transverse dislocations; 8 – borders of the Central Kamchatka deep seam zone; 9 – the main faults extending to the day surface (a) and overlapped by overlying formations (b); 10 – volcanic-tectonic structures: Kr – Karymshinsky, Pt – Plotnikovsky, Kt – Kitkhoysky, Akh – Akhomtensky (a), the contours of the paleovolcano of the Goryachaya hill (b); 11 – boundaries (a – confident, b – assumed) of crustal and coromantium anomalously low-resistance zones, identified according to magnetotelluric sounding and their numbers: 1 – zone of melting and circulation of hydrothermal solutions – Tolmachevsky active magmatic center, 2 – zone of melting in the area of volcanoes Gorely, Mutnovskaya Sopka, Vilyuchinskaya Sopka; 3 – a zone of high fluid saturation in the region of the Avachinsky-Koryak group of volcanoes; 12 – extinct volcanoes (a), active (b); 13 – Porozhisty field (a) and ore occurrences (b) of gold, sources and deposits of thermal mineral waters (c); 14 – points of observations and their numbers on the profile of Apacha Village-Mutnaya Bay: earthquake converted-wave method (ECWM) (a), magnetotelluric sounding (MTS) (b), combined points of ECWM-MTS (c); line of density modeling (g); ECWM points on the profile of Opal M.-Vakhil R. (d).

wave method was carried out (Nurmukhamedov et al., 2016). Subsequently, for the profile of the Opala Mountain-Vakhil River performed geo-density modeling, using a modern software package and based on a set of updated data, a geological and geophysical model of the structure of the Earth's crust and upper mantle was developed (Nurmukhamedov, Sidorov, 2019).

This article presents the results of the interpretation of earthquake converted-wave method, gravimetry, and magnetotelluric sounding obtained along the profile of Apacha Village-Mutnaya Bay in conjunction with geological and geophysical data on the TAMC area. The profile length is about 120 km (Fig. 1).

Brief description of the research area

A review of regional geological and geophysical studies is described in detail in publications (Nurmukhamedov, 2017; Nurmukhamedov, Sidorov, 2019). Profile of Apacha Village-Mutnaya Bay crosses the territory studied by geological, gravimetric and aeromagnetic surveys of the 1: 200,000 scale and its

significant part by the geological and aeromagnetic scale of 1:50,000. Based on these data, structural-formation map of the South Kamchatka (Aprelkov, Olshanskaya, 1986) was constructed and a tectonic diagram of the scale 1: 1,000 000 with elements of the deep structure of the Earth's crust was prepared (Nurmukhamedov, 2013), a fragment of which is shown in Fig. 1.

The profile from north-west to southeast intersects two folded zones: the Koryak-West-Kamchatka zone and the East-Kamchatka subzone of the Olyutor-East-Kamchatka zone. In the west of the area, there is a fragment of the Central Kamchatka deep seam zone – the zone of the joining of island arc blocks (Paleoarc) in the Eocene (Seliverstov, 2009; Shapiro et al., 2009) to the Paleokamchatka. The north-eastern part of the area is occupied by the Nachikinsky zone of transverse dislocations, which is characterized by discontinuous violations of the north-western strike. A significant part of the territory is covered by areal volcanism, spread south of the latitude of the Paratunka and Karymchina rivers (Geological structure..., 1980).

The profile runs near the southwestern border of the Karymshinsky volcanic-tectonic structure and crosses the Akhomten volcanic-tectonic structure. In the central part of the Karymshinsk volcanic-tectonic structure there is a Pliocene paleovolcano with the center of the Goryachy hill. Thermal mineral springs and the Bolshe-Banny steam-water mixture deposit are located along the perimeter of the paleovolcano. Active hydrothermal activity is observed in a significant part of the territory near the Karymshinsky ore cluster. The described region is characterized by an increase in the thickness of the Earth's crust up to 40-45 km against a background of 32-35 km. The thickening of the crust is explained by an increase in the transition layer thickness between the crust and the upper mantle in the region of active volcanoes and areas of areal volcanism (Balesta, Gontovaya, 1985). Such places (Nurmukhamedov, 2017; Nurmukhamedov, Sidorov, 2019) have high permeability and the presence of a powerful heat flow. The flow is localized closer to the upper layers of the crust, its density increases, which leads to the formation of a focal region of melting (Nurmukhamedov, Smirnov, 1985).

In the south of Kamchatka, modern geodynamic processes are actively proceeding. In 1987-1988 in the TAMC region, a swarm of weak ($M \leq 5$) earthquakes was recorded (Fig. 2), named the Tolmachev Epicentral Zone (TEZ) (Nurmukhamedov, 2017).

In terms of TEZ, it coincides with the site of the maximum density of slag cones and the zone of high permeability. The depth of the earthquake hypocenters is about 8 km. Probably, earthquakes are associated with the advancement of magma (Nurmukhamedov, Sidorov, 2019). Indirectly, this is indicated by the confinement of the TEZ to the proposed melting zone. Miocene

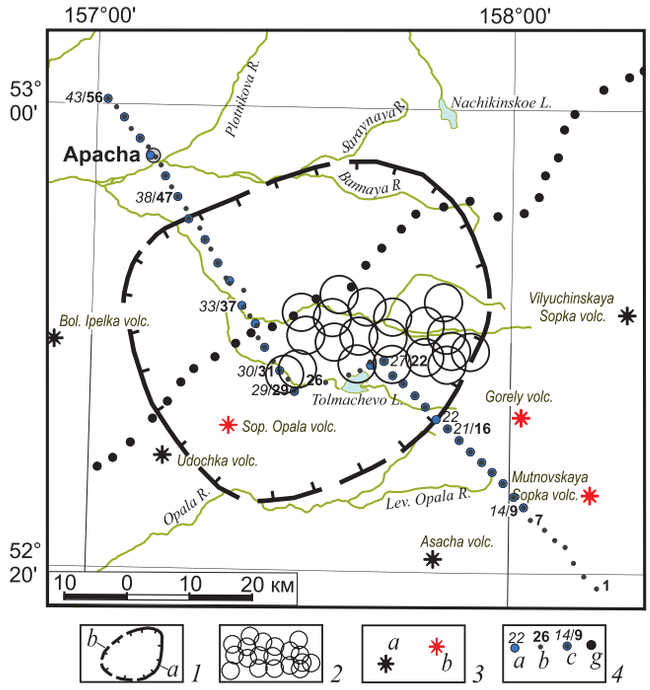

Fig. 2. A swarm of earthquakes in the Tolmachevsky epicenter zone – based on materials (Nurmukhamedov, 2017; Nurmukhamedov, Sidorov, 2019). 1 – TAMC borders: confident (a), alleged (b); 2 – epicenters of local earthquakes (data for 1987-1988); 3 – extinct volcanoes (a), active (b); 4 – observation points and their numbers on the profile of Apacha Village-Mutnaya Bay: ECWM (a), MTS (b), combined points ECWM-MTS (c), points ECWM on the profile of the Opal M.-Vakhil R.(g).

intrusions of medium and acidic compositions (Fig. 1) are associated with a large intrusive array formed in the weakened zone (Nurmukhamedov, 2017).

In the area of TAMC, the magnetotelluric sounding along the profile of the Opala Mountain-Vakhil River, in the depth interval 10-35 km was performed. A contrast anomaly of electrical conductivity (5 Ohm·m against a background of 500-1000 Ohm·m) was revealed. According to the authors (Mishin, 1996; Moroz et al., 1995; Nurmukhamedov, Smirnov, 1985), the anomaly is due to the circulation of hydrothermal solutions in the Earth's crust and the presence of melting zones. In the geological and geophysical model along the profile of the Opala Mountain-Vakhil River (Nurmukhamedov, Sidorov, 2019), a block of the Earth's crust is allocated in the central part of TAMC, saturated with intrusions of the basic and ultrabasic composition. From the east, at a depth of 8-27 km, an intrusive mass of predominantly medium-medium acid composition adjoins it, from which apophyses are introduced into the upper layers along weakened zones (Fig. 1).

Research methodology

Earthquake converted-wave method field observations on the profile of Apacha Village-Mutnaya Bay performed

according to standard methods (Pomerantseva, Mozhenko, 1977). Three-component registration of seismic waves was carried outat 43 points. The distance between points is 2.5-5.0 km. Registration of seismic events is implemented in the "detection" mode. The duration of one parking ranged from 20 to 30 days, which provided the necessary set of information to highlight the boundaries of the exchange. The "Tcherepakha" hardware complex was used in the process of work. The methodology of field work, interpretation and reinterpretation of earthquake converted-wave method data is covered in the article (Nurmukhamedov, Nedyad'ko et al., 2016). The modern version of the earthquake converted-wave method section along the profile of Apacha Village-Mutnaya Bay, combined with the density model, is shown in Fig. 3.

Field observations using the magnetotelluric sounding method were carried out according to the standard method (Moroz et al., 1995; Nurmukhamedov, Moroz, 2008, 2009) using the DEpS-2 digital electric prospecting station. A total of 56 sounding points were completed, of which 4 components (Ex, Ey, Hx, Hy) of the magnetotelluric field (MT field) were recorded in half the points in a period range of 0.1-100 s. At every second magnetotelluric sounding point combined

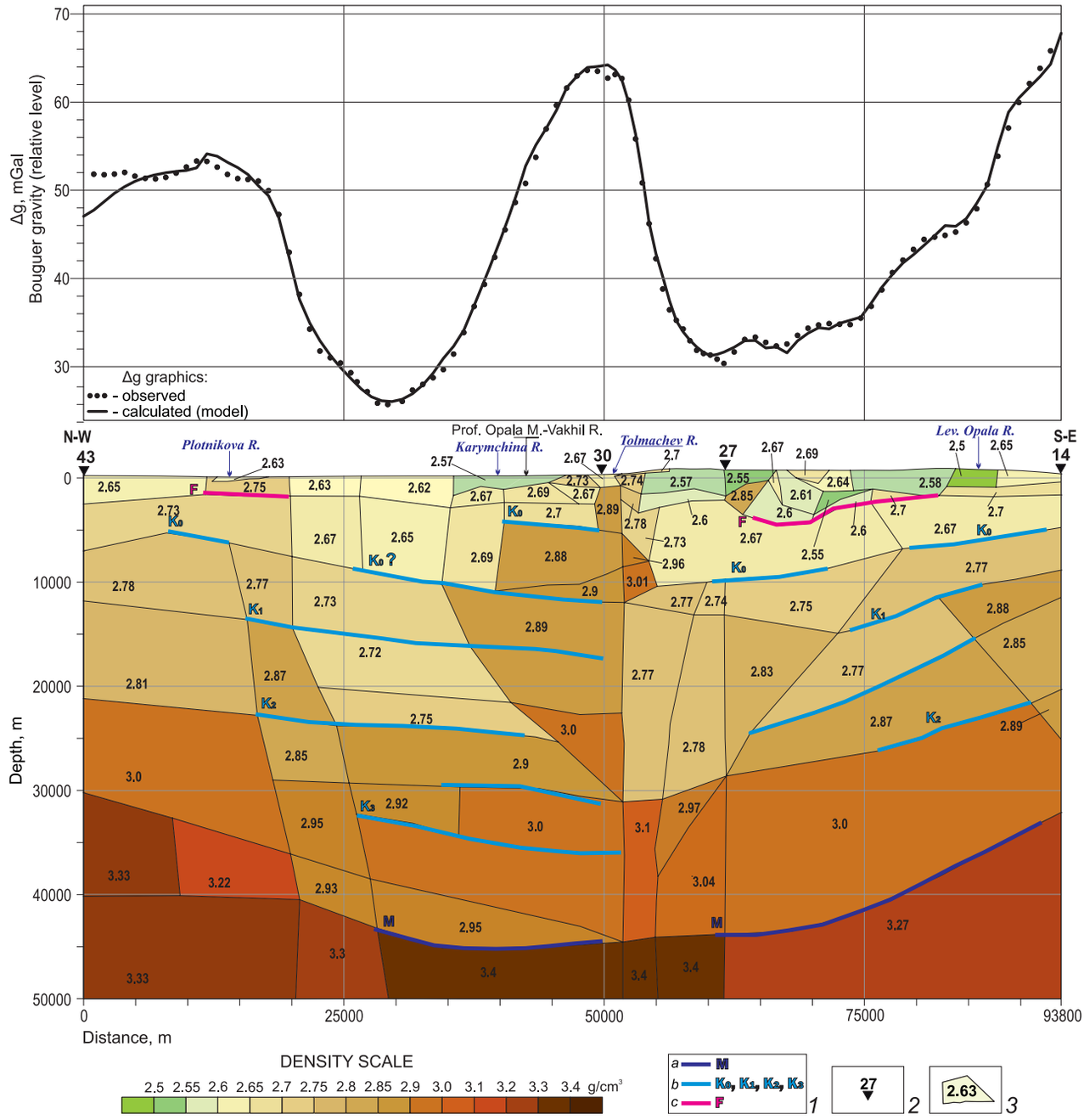

Fig. 3. A deep density model along the profile of Apacha Village-Mutnaya Bay. 1 – seismic boundaries according to the earthquake converted-wave method (a – the boundary of Mokhorovicic; b, c – other seismic boundaries identified in the Earth's crust); 2 – earthquake converted-wave method points and their numbers; 3 – the boundaries of the blocks and the average density value (g/cm³) for them.

with the earthquake converted-wave method point, registration of the fifth component (Hz) was added. At combined points, the range of variations of the MT field is expanded to 1000 s. Primary processing of magnetotelluric sounding data was carried out in the Computing Center of the Production Geological Association Kamchatgeology. The inverse problem was solved using two-dimensional numerical simulation of the MT field (Yudin, Kazantsev, 1977) at the Laboratory of Geophysical Fields of the Institute of Volcanological Geology and Geochemistry FEB RAS.

In the modeling process, we used regional-longitudinal curves, since they are practically free of the induction effect formed in the Sea of Okhotsk and the Pacific Ocean (Moroz, Moroz, 2011). Before the modeling procedure according to the profile of Apacha Village-Mutnaya Bay identified 6 zones, characterized by conformal, but different in terms of resistance, magnetotelluric sounding curves. A different level indicates lateral heterogeneity of the upper part of the section, which leads to the emergence of strong galvanic near-surface effects. The average curves for each zone were calculatedin order to suppress them. For the formation of a starting model according to the profile of Apacha Village-Mutnaya Bay we used the previously developed normal deep model of South Kamchatka (Moroz et al., 1995).

During iterative selection of model elements, a satisfactory convergence was achieved between the average experimental and calculated magnetotelluric sounding curves (Fig. 4) for each zone of the geoelectric model (Fig. 5). The model shows the distribution of electrical conductivity in the Earth's crust and upper mantle and is consistent with the geoelectric model along the profile of the Opala Mountain-Vakhil River (Moroz et al., 1995; Mishin, 1996) in the zone of their intersection.

To study the density distribution of rocks in the Earth's crust and upper mantle, two-dimensional density modeling was performed (Fig. 3) using materials from the gravimetric survey with a scale of 1: 200,000. Previously, modeling was performed according to the profile of the Opala Mountain-Vakhil River. The results are published in an article (Nurmukhamedov, Sidorov, 2019). The initial frame of the model was the boundaries and faults identified by the reinterpretation of the earthquake converted-wave method data. A priori density values of the upper layers of the section are determined by geological formations overlooking the day surface. For deep layers, density values are taken from published sources. For the Upper Cretaceous deposits, the density value is taken to be 2.67 g/cm^3, for the granite-metamorphic ("granite") layer – 2.64-2.8 g/cm^3, for the lower crust ("basalt" layer) – 2.80-3.07 g/cm^3 and for the upper mantle – 3.30 g/cm^3. The indicated densities are taken as initial data for iterative selection of the model. In the process of modeling, we used the Geosoft software package (GMSYS, Oasis Montaj, Grav/Mag Interpretation, 3D Euler, MAGMAP filtering), where it is possible to take into account the terrain and approximate body sections with contours of complex configuration. The modeling technique is described in the articles (Sidorov, 2014, 2015).

As a result of a comprehensive interpretation, a deep geological and geophysical model is constructed (Fig. 6), in which the following are distinguished: the Mokhorovicic boundary (M), which separates the Earth's crust from the upper mantle; border K_2, separating the upper cortex from the lower; the roof of the consolidated crust (K_0) – the crystalline basement; the roof of the Upper Cretaceous rock complex (F). In addition, other boundaries in the Earth's crust (K_1, K_3) have been identified. Layers corresponding to (from top to bottom) the Cenozoic volcanic-sedimentary cover, the Mesozoic complex of rocks, the granite-metamorphic ("granite") and granulite-basite ("basalt") layers are located between the boundaries. At the very bottom of the model, the upper mantle layer is highlighted. Crustal and crustal-mantle faults penetrate the entire thickness, dividing the Earth's crust and upper mantle into separate blocks. The fundamental similarity of geological and geophysical models is noted in the zone of intersection of the profiles of the Opala Mountain-Vakhil River (Nurmukhamedov, Sidorov, 2019) and Apacha Village-Mutnaya Bay.

Analysis of the geological and geophysical model, discussion of the results

When starting the model analysis, we emphasize that the authors call the K_2 wave exchange boundary – the boundary dividing the Earth's crust into upper and lower parts (Nurmukhamedov et al., 2016). Given information on the Kola superdeep well (Kola superdeep..., 1998; Sharov, 2017) and other scientific publications, the names of the granite and basalt layers are enclosed in quotation marks, implying a certain convention.

Compared with other regional profiles on the territory of Kamchatka, the profile of Apacha Village-Mutnaya Bay has a small extent. It is difficult to isolate systemic changes in the structure of the Earth's crust and upper mantle in such a short segment. According to the earthquake converted-wave method data, the picture of the deep structure is substantially supplemented by the results of density modeling. So, for example, the boundaries marked along but not tracked over long distances along the earthquake converted-wave method are further extended in the form of contacts between layers and blocks with different densities. An analysis of the obtained data indicates that the results of density modeling do not contradict the prevailing ideas about the density characteristics of the lithosphere layers.

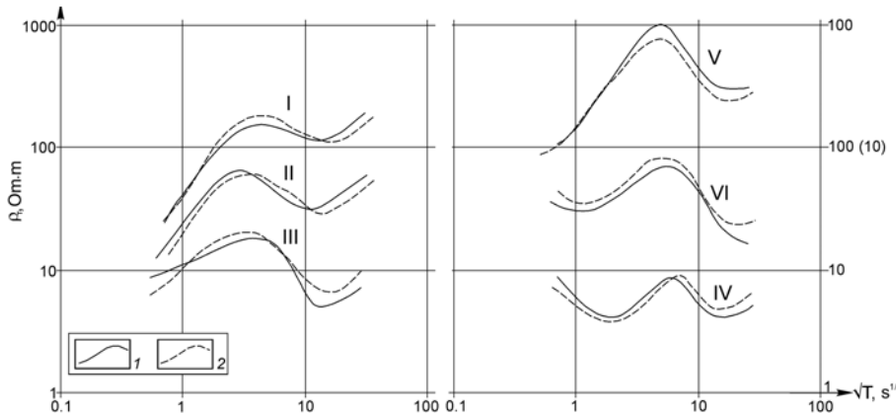

Fig. 4. Comparison of the experimental (1) and calculated (2) curves of magnetotelluric sounding for the geoelectric model shown in Fig. 5

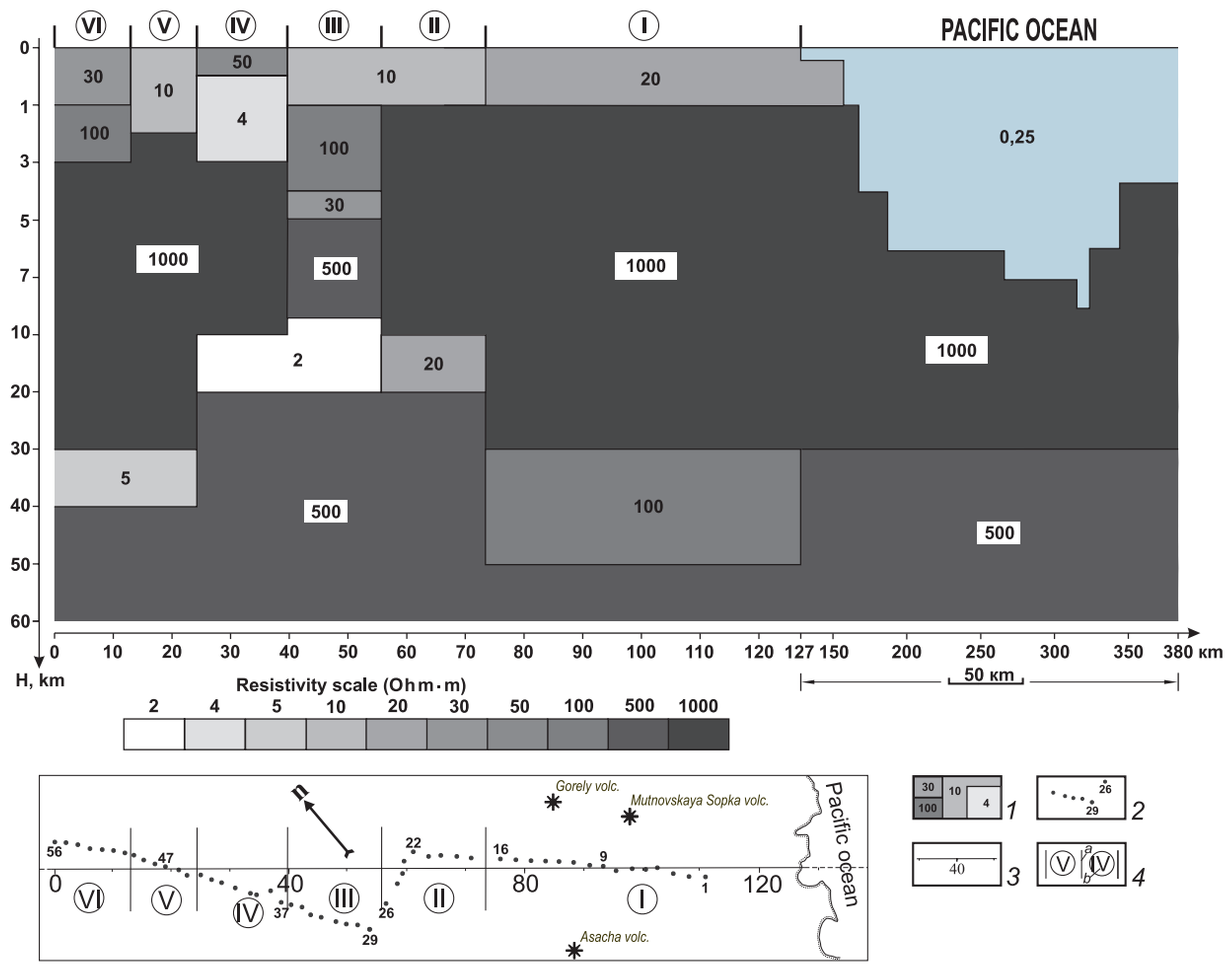

Fig. 5. Two-dimensional geoelectric model of the Earth's crust and upper mantle along the profile of Apacha Village-Mutnaya Bay. 1 – blocks characterized by different levels of resistivity in Ohm·m; 2 – magnetotelluric sounding observation points and their numbers; 3 – modeling line and its marking in kilometers; 4 – boundaries of the modeling zones (a) and their numbers (b).

In the model (Fig. 6), the thickness of the crust along the profile varies from 30-33 km at the edges to 44-46 km, in its central part. The morphology of the K_2 boundary basically repeats the morphology of the M section. Moreover, the thickness of the "granite" layer is stably greater than the "basalt" one. Such a crust belongs to the continental type crust (Kosminskaya, 1958). A significant increase in the depth to the boundary M in the center of the model can be explained by the presence of a "swollen" transitional layer between the crust and the upper mantle at this location. If we take section K_3 as the top of the layer, then its estimated capacity will be about 10 km. As can be seen from the model, in the southeastern direction the layer gradually wedges out, and in the northwest direction its distribution is limited by the Central Kamchatka deep seam zone.

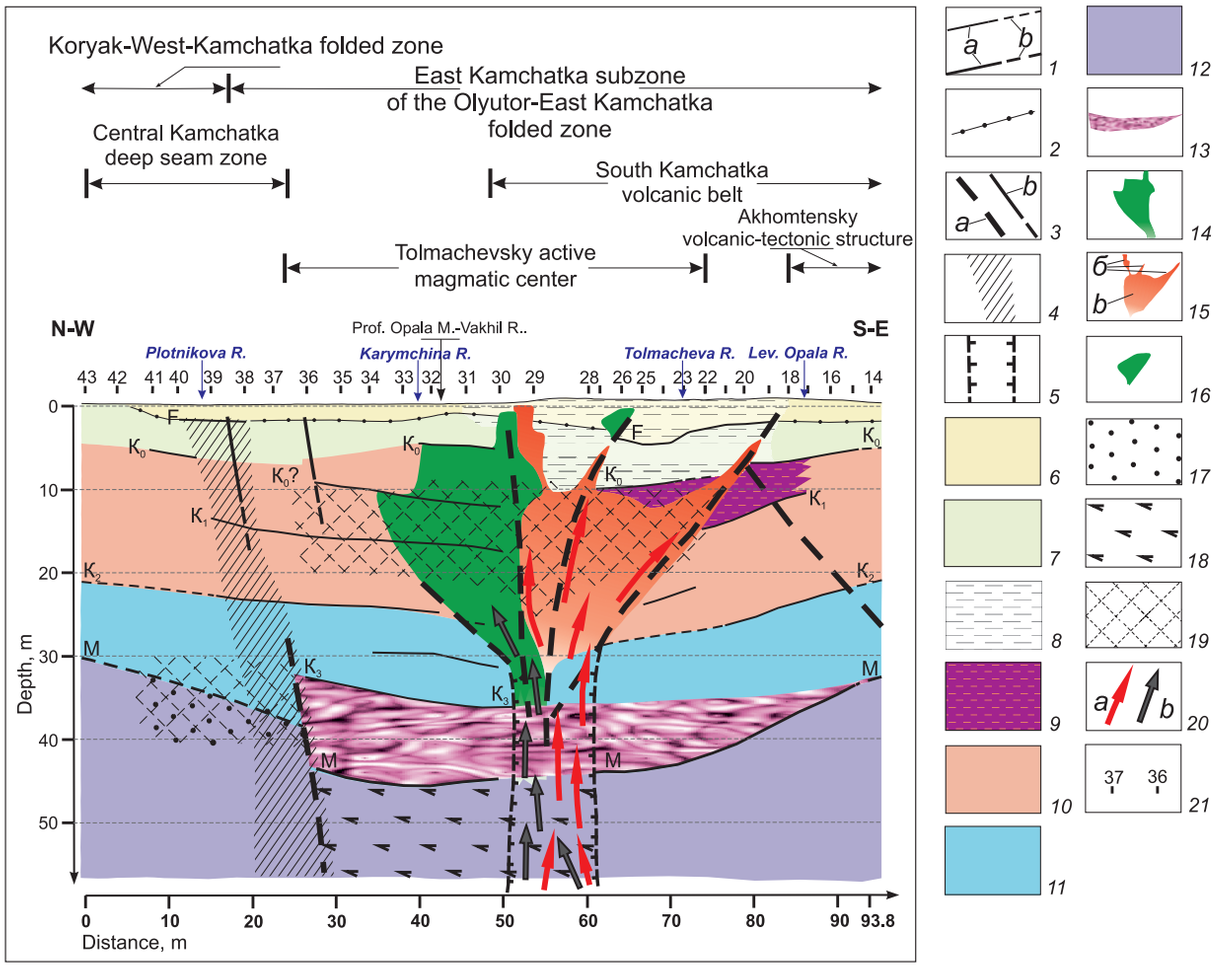

Fig. 6. Geological and geophysical model along the profile of Apacha Village-Mutnaya Bay. 1 – boundaries according to the earthquake converted-wave method data: confident (a), alleged (b), identified with the roof of the Upper Cretaceous rock complex (F), the roof of the consolidated crust (K_0), the boundary between the upper and lower crust (K_2), the Mohorovicic border (M), other boundaries in the Earth's crust (K_1, K_3); 2 – the roof of the Upper Cretaceous complex of rocks, according to magnetotelluric sounding; 3 – discontinuous violations according to the earthquake converted-wave method(a) and geological data (b); 4 – subvertical zone, selected according to the results of density modeling, identified with the axial part of the Central Kamchatka deep seam zone; 5 – zone of absence of exchange boundaries correlation; 6 – Cenozoic volcanic-sedimentary rock complex; 7 – Mesozoic rock complex; 8 – hydrothermally altered Meso-Cenozoic rock complex; 9 – the upper layer of metamorphic complexes mainly in the green shale and epidote-amphibolite facies; 10 – granite-metamorphic ("granite") layer of the upper crust; 11 – granulite-mafic ("basalt") layer of the lower crust; 12 – upper mantle; 13 – the estimated position of the transition layer between the Earth's crust and the upper mantle; 14 – block of the earth's crust, saturated with intrusions of the basic and ultrabasic composition; 15 – intrusive array (a) and its apophyses (b) mainly of medium-medium acid composition; 16 – intrusion of the main structure; 17 – decompression site (3.22 g/cm³ against the background of 3.33 g/cm³) in the upper mantle, coinciding with the anomalously low resistance zone (5 Ohm·m against the background of 500-1000 Ohm·m); 18 – plot of increased density (3.4 g/cm³) in the upper mantle, presumably of peridotite-eclogite composition; 19 – crust and crust-mantle anomalies of electrical conductivity (2-20 and 5 Ohm·m, respectively, against a background of 500-1000 Ohm·m); 20 – direction of the estimated heat flows (a) and magmatic melts (b); 21 – earthquake converted-wave methodobservation points and their numbers.

The density characteristics of the rocks in the transitional zone practically do not differ from the density of the lower part of the "basalt" layer, but a block of low density – 2.95 g/cm³ against a background of 3.0 g/cm³ – is distinguished northwest of its middle. Further, to the northwest at a depth of 30-40 km, a zone with an abnormally low level of resistivity (5 Ohm·m against a background of 500-1000 Ohm·m), which coincides with the local area of decompression in the upper mantle (3.22 g/cm³ against the background of 3.33 g/cm³). It is possible that the anomalous site was formed as a result of the interaction of lithospheric blocks during the joining of island-arc blocks to the Paleokamchatka (Seliverstov, 2009; Shapiro, Soloviev, 2009).

In the lower part of the model, the density of individual fragments (Fig. 3) varies from 3.27 g/cm³ to 3.33 g/cm³, which corresponds to the density of rocks of the upper mantle – peridotites. Where the boundary M

drops to the maximum depth (ECWM 27-36), a block with a high density value of 3.4 g/cm^3 is distinguished, which according to A.E. Ringwood (Ringwood, 1972) corresponds to peridotites and "unchanged eclogites" (3.4-3.65 g/cm^3). It is assumed that the selected site belongs to the site of eclogitization of the upper mantle rocks formed in the paleosubduction zone of the oceanic lithosphere beneath the mainland (Nurmukhamedov, Smirnov, 1985; Nurmukhamedov, Sidorov, 2019). Subduction processes preceded the incorporation in the Eocene of relatively light island-arc blocks to the folded region of Paleokamchatka.

In the upper part of the section, the roof of the consolidated crust (K_0) confidently stands out, which experiences immersion from 4-5 km at the edges of the model to 10 km or more in its central part. Structurally, this site coincides with the Tolmachevsky active magmatic center. In general, the K_0 border repeats the morphology of the K_2 and M sections. Above the section, at a depth of about 4 km (ECWM 30-33), a border is distinguished that is close in its characteristics to the K_0 border. The question remains open of which section these boundaries belong to. At this stage of the research, the authors are inclined to believe that, with the general tendency of the boundary K_0 to sink to the central part of the model, in the TAMC region, a protrusion of the Earth's crust block is saturated with intrusions of the basic and ultrabasic composition (Fig. 6). The roof of this block coincides with the boundary K_0. Above the section, a smooth rise in the boundary of F is noted, which is obviously inherited from the indicated protrusion. It should be noted that in the same place, above the boundary K_0, in the depth interval 4-5 km (Fig. 5), a low-resistance, space-limited object (30 Ohm·m against a background of 100-1000 Ohm·m) was identified, which can be explained the presence of a "heated" intrusion and/or thermal water circulation zone here. Below is the border marked with the index "K_0?". It reflects the waves exchange boundary inside the crystalline basement. The aforesaid is consistent with the geological and geophysical model according to the profile of the Opala Mountain-Vakhil River (Nurmukhamedov, Sidorov, 2019).

The dominant model is the block of the Earth's crust, saturated with intrusions of the basic and ultrabasic composition. In the field of gravity, it is expressed by a contrast increase in Δg values (Fig. 3). It seems to the authors that the penetration of the melts occurred along the weakened zone formed in the crust, at its border with the upper mantle. In the earthquake converted-wave section (Nurmukhamedov, Nedyad'ko et al., 2016), a zone of seismic boundaries correlation absence is fixed in this place, and a region with heterogeneities is identified in the density model. The subvertical zone permeates the horizontally layered crustal medium, and from a depth of 30 km from it faults are spread, which are migration routes to the upper crust of mantle material (magma, high-temperature fluids) and powerful heat flows (Nurmukhamedov, Sidorov, 2019).

To the south-east of the described block (ECWM 20-29) the density of the medium corresponds to rocks of medium and medium acid composition. In the Δg graph, a minimum of the gravity field is observed (Fig. 3), complicated by local low-amplitude maxima. We can assume here a large intrusive mass of diorite-granodiorite composition. Apophyses depart from the array, some of which are exposed on the day surface (Fig. 1). In the section, the array region is characterized by the absence of seismic boundaries correlation with an abnormally low level of electrical resistivity (2-20 Ohm·m against a background of 500-1000 Ohm·m). It is assumed that the formation of the array is associated with a powerful heat flow and the formation of focal melting zones (Nurmukhamedov, Smirnov, 1985; Nurmukhamedov, 2017; Nurmukhamedov, Sidorov, 2019).

The movement of magma into the upper layers of the Earth's crust is accompanied by a swarm of weak earthquakes (Fig. 2), which are probably caused by the local system of stresses characteristic of volcanic earthquakes (Zobin, 1979). However, there are no active volcanoes near the indicated swarm. We can talk about the formation of an eruptive crack, or about the "revival" of an existing one (Zobin, 1979) in the zone of areal volcanism. The swarm is elongated in the latitudinal direction and is located near the Opalinsko-Gorelovsky fault, identified by gravimetric data (Aprelkov et al, 1989).

In the study area, favorable conditions exist for accumulations of underground meteoric waters (Kononov et al., 1964; Kraevoy et al., 1976). These waters through the infiltration zone interact with the high-temperature environment of the melting centers and cooling intrusions, as evidenced by active geothermal activity in the zone of the intrusive array.

Conclusions

1. Density modeling was performed along the profile of Apacha Village-Mutnaya Bay. As the initial data, the results of the reinterpretation of the earthquake converted-wave method materials were used. An analysis of the data shows that the simulation results do not contradict the prevailing ideas about the density characteristics of the lithosphere layers. Based on the earthquake converted-wave method, gravity exploration, magnetotelluric sounding and other data, a geological and geophysical model of the Earth's crust and upper mantle is built along the profile. The model presents the specified position of the main sections of the lithosphere – the bottom of the crust, the border between the granulite-mafic and granite-metamorphic parts of

the consolidated crust, its roof. The Earth's crust along the profile of Apacha Village-Mutnaya Bay corresponds to a continental-type crust. Good convergence of the models at the intersection of the profiles of Apacha Village-Mutnaya Bay and the Opala Mountain-Vakhil River is noted.

2. The dominant model is a high-density formation – a block of the Earth's crust saturated with intrusions of the basic and ultrabasic composition. The formation of the block is associated with the presence of an active permeable zone between the Earth's crust and the upper mantle. From the southeast, an intrusive array of medium-sour composition adjoins the block. The formation of the array is explained by the formation of focal melting sites.

3. A swarm of weak earthquakes from 1987-1988 coincides with the maximum density of slag cones on the surface and the deep zone of high permeability between the Earth's crust and the upper mantle. Perhaps these earthquakes are associated with the advancement of magma in the existing eruptive crack or with the formation of a new one.

4. The area is favorable for the accumulation of meteoric waters that come in contact with a high-temperature environment and post-magmatic solutions of intrusions. Probably, these circumstances contributed to the formation of closed hydrothermal systems and, as a consequence, the formation of ore occurrences of the Karymshinsky ore cluster.

5. Active modern magmatic processes in the south of Kamchatka indicate the relative youth of this part of the peninsula in the system of mountain-folding structures of the entire Kamchatka region. This is clearly observed in geological and geophysical sections along the profiles of the Opala Mountain-Vakhil River and Apacha Village-Mutnaya Bay.

References

Aprelkov S.E., Olshanskaya O.N. (1986). Report on the generalization of gravimetric survey materials on a scale of 1: 200 000 with the aim of compiling a structural-formation map of South Kamchatka on a scale of 1: 500 000. Elizovo: EGFE, 303 p. (In Russ.)

Aprelkov S.E., Olshanskaya O.N. (1989). Tectonic zoning of central and southern Kamchatka according to geological and geophysical data. *Tikhookeanskaya geologiya = Russian Journal of Pacific Geology*, 1, pp. 53-65. (In Russ.)

Balesta S.T., Gontovaya L.I. (1985). Seismic model of the Earth's crust of the Asia-Pacific transition zone in the Kamchatka region. *Vulkanologiya i seysmologiya = Journal of Volcanology and Seismology*, 4, pp. 83-90. (In Russ.)

Geological structure, the latest volcanism and the modern structure of South Kamchatka. The long-lived center of endogenous activity of South Kamchatka. (1980). Ed. Masurenko Yu.P. Moscow: Nauka, pp. 7-78. (In Russ.)

Kola superdeep well. Scientific results and research experience. (1998). Ed. V.P. Orlov, N.P. Laverov. Moscow: Tekhnoneftegaz, 260 p. (In Russ.)

Kononov V.I., Polyak B.G. (1964). Big Bath springs in Kamchatka. Hydrogeothermal conditions of the upper parts of the Earth's crust. Moscow: Nauka, pp. 52-71. (In Russ.) https://doi.org/10.1016/B978-0-08-010003-6.50009-2

Kosminskaya I.P. (1958). The structure of the Earth's crust according to seismic data. *Byul. MOIP,* 4, pp. 145-147.(In Russ.)

Kraevoy Yu.A., Okhapkin V.G., Serezhnikov A.I. (1976). The results of hydrogeological and geothermal studies of the Bolshebannaya and Karymchinsky hydrothermal systems. Hydrothermal systems and thermal fields of Kamchatka. Vladivostok: DVNTs AN SSSR, pp. 179-211. (In Russ.)

Moroz Yu.F., Nurmukhamedov A.G., Loshchinskaya T.A. (1995). Magnetotelluric sounding of the Earth's crust of South Kamchatka. *Vulkanologiya i seysmologiya = Journal of Volcanology and Seismology*, 4-5, pp. 127-138. (In Russ.)

Mishin V.V. (1996). The deep structure and types of the Earth's crust in Southern Kamchatka. *Tikhookeanskaya geologiya = Russian Journal of Pacific Geology*, 1, pp. 110-119. (In Russ.)

Mishin V.V. (1997). Geological and geophysical structure of the South Kamchatka. *Tikhookeanskaya geologiya = Russian Journal of Pacific Geology*, 4, pp. 64-70. (In Russ.)

Moroz Yu.F., Moroz T.A. (2011). Numerical three-dimensional modeling of the magnetotelluric field of Kamchatka. *Fizika Zemli*, 2, pp. 64-73. (In Russ.) https://doi.org/10.1134/S1069351311010071

Nurmukhamedov A.G., Smirnov V.S. (1985). The results of in-depth electromagnetic research in South Kamchatka. *Proc. V Kamchatka Geological Conf.: Geology and minerals of the Koryak-Kamchatka folded region*. Petropavlovsk-Kamchatsky: KPGO Kamchatgeologiya, pp. 69-82. (In Russ.)

Nurmukhamedov A.G., Moroz Yu.F. (2008). Features of the geological structure of the northeastern part of the Koryak-Kamchatka folded region according to deep geophysical studies. *Vestnik KRAUNTs. Nauki o Zemle = Bulletin of Kamchatka Regional Association «Educational-Scientific Center». Earth Sciences*, 11(1), pp. 125-133. (In Russ.)

Nurmukhamedov A.G., Moroz Yu.F. (2009). The deep structure of the north-eastern part of the Koryak-Kamchatka folded region according to regional geophysical studies. *Geofizicheskiy zhurnal*, 31(3), pp. 74-83. (In Russ.)

Nurmukhamedov A.G. (2013). Creating a scheme of seismotectonic zoning of the Koryak-Kamchatka folded region based on a synthesis of deep geological and geophysical work. Report. Petropavlovsk-Kamchatsky: OAO «Kamchatgeologiya», 511 p. (In Russ.)

Nurmukhamedov A.G., Nedyad'ko V.V., Rakitov V.A., Lipat'ev M.S. (2016). The boundaries of the lithosphere in Kamchatka according to the method of exchange waves of earthquakes. *Vestnik KRAUNTs. Nauki o Zemle = Bulletin of Kamchatka Regional Association «Educational-Scientific Center». Earth Sciences*, 29(1), pp. 35-52. (In Russ.)

Nurmukhamedov A.G. (2017). Bath and Karymchinsk hydrothermal systems are energy sources in the south of Kamchatka. *Gornyy informatsionno-analiticheskiy byulleten = Mining informational and analytical bulletin*, spec. is. 32, pp. 347-367. (In Russ.) https://doi.org/10.25018/0236-1493-2017-12-32-347-367

Nurmukhamedov A.G., Sidorov M.D. (2019). Deep structure and geothermal potential along the regional profile set from Opala Mountain to Vakhil' River (Southern Kamchatka). *IOP Conf. Ser.: Earth Environ. Sci.,* 249, 012041. https://doi.org/10.1088/1755-1315/249/1/012041

Pak G., Smirnov V.S., Aprelkov S.E. (1989). Results of geophysical surveys at the Petropavlovsk-Shipunsky prognostic testing ground and regional geophysical profile of the bay Mutnaya-p. Apache. Report of the Kamchatka Integrated Geophysical Party for regional studies conducted in South Kamchatka under the program for forecasting earthquakes and volcanic eruptions in 1987-1989. EGFE PGO "Kamchatgeologiya", 236 p. (In Russ.)

Pomerantseva I.V., Mozzhenko A.N. (1977). Seismic surveys with the equipment «Earth». Moscow: Nedra, 256 p. (In Russ.)

Ringwood A.E. (1972). Composition and evolution of the upper mantle. *Earth's crust and upper mantle*, 43, pp. 7-26. (In Russ.)

Seliverstov N.I. (2009). Geodynamics of the junction zone of the Kuril-Kamchatka and Aleutian island arcs. Petropavlovsk-Kamchatskiy: KamGU, 191 p. (In Russ.)

Sidorov M.D., Novakov R.M. (2014). Density model of the junction zone of Kamchatka and Aleutian island arcs. *Regional'naya geologiya i metallogeniya*, 58, pp. 59-65. (In Russ.)

Sidorov M. D. (2015). Density modeling of magmatic structures in the Kolpakovsky promising nickel-bearing region (Sredinny massif, Kamchatka). *Tikhookeanskaya geologiya = Russian Journal of Pacific Geology*, 34(3), pp. 31-41. (In Russ.) https://doi.org/10.1134/S1819714015030070

Shapiro M.N., Solov'ev A.V. (2009). Formation of the Olyutorsky-Kamchatka foldbelt: A kinematic model. *Geologiya i geofizika = Russian Geology and Geophysics*, 50(8), pp. 668-681. https://doi.org/10.1016/j.rgg.2008.10.006

Sharov N.V. (2017). Lithosphere of Northern Europe according to seismic data. Petrozavodsk: Karel'skiy nauchnyy tsentr RAN, 173 p. (In Russ.)

Yudin M.N., Kazantsev V.V. (1977). The program for calculating the

magnetotelluric field in two-dimensional layered media containing local inhomogeneities (E and H polarization). Library of programs for processing geophysical data on a computer. Electric prospecting. Moscow: VNII Geophysics, 3 p. (In Russ.)

Zobin V.M. (1979). The dynamics of volcanic earthquakes origin. Moscow: Nauka, 92 p. (In Russ.)

About the Authors

Alexandr G. Nurmukhamedov – Cand. Sci. (Geology and Mineralogy), Leading Researcher

Scientific Research Geotechnological Centre of the Far Eastern Branch of the Russian Academy of Sciences

30, Severo-Vostochnoe highway, Petropavlovsk-Kamchatsky, 683002, Russian Federation

E-mail: nurmuxamedov1949@mail.ru

Mikhail D. Sidorov – Cand. Sci. (Geology and Mineralogy), Leading Researcher

Scientific Research Geotechnological Centre of the Far Eastern Branch of the Russian Academy of Sciences

30, Severo-Vostochnoe highway, Petropavlovsk-Kamchatsky, 683002, Russian Federation

Yury F. Moroz – Dr. Sci. (Geology and Mineralogy), Chief Researcher of the Laboratory of seismology and geophysics

Institute of Volcanology and Seismology of the Far Eastern Branch of the Russian Academy of Sciences

9, Piip boul., Petropavlovsk-Kamchatsky, 683006, Russian Federation

Manuscript received 3 June, 2019;
Accepted 19 September, 2019; Published 30 March 2020

ISSN 1608-5043 (Print)
ISSN 1608-5078 (Online)

Key title: «Georesursy»
Parallel title: «Georesources»

GEORESURSY

A peer-reviewed scientific and technical journal published since 1999

The journal is included/indexed in:

- Web of Science Group — Web of Science Core Collection, Emerging Sources Citation Index (ESCI)
- Scopus — Scopus
- CAS, A DIVISION OF THE AMERICAN CHEMICAL SOCIETY — CAS (Chemical Abstracts Service) databases
- GeoRef — GeoRef database
- EBSCOhost — EBSCOhost™ databases
- DOAJ DIRECTORY OF OPEN ACCESS JOURNALS — Directory of Open Access Journals (DOAJ)

The full-text electronic versions of the articles published in the Journal are freely available to the public on our website: **www.geors.ru**

Contacts:
Deputy Chief Editor - Daria Khristoforova
E-mail: mail@geors.ru
Tel: +7 (843) 239-05-30